UNIVERSITY OF CALIFORNIA,
IRVINE

Spatiotemporal Dynamics of the Cystic Fibrosis Airway Microbiome

DISSERTATION

submitted in partial satisfaction of the requirements
for the degree of

DOCTOR OF PHILOSOPHY

in Computational Science

by

Peter Muarice Uhl

Dissertation Committee:
Professor Naveen K. Vaidya, Chair
Professor Dominik Wodarz
Professor Forest Rohwer
Professor Eric Mjolsness
Professor Katrine L. Whiteson

2023

DEDICATION

To my wife Caity and parents Terry and Mary.

TABLE OF CONTENTS

LIST OF FIGURES

LIST OF TABLES

ACKNOWLEDGMENTS

I was able to complete this work only with the guidance and support of dozens of friends, colleagues, and mentors. First, I would like to thank my committee members Dr. Naveen Vaidya, Dr. Dominik Wodarz, Dr. Forest Rohwer, Dr. Eric Mjolsness, and Dr. Katrine Whiteson for their feedback and guidance throughout my degree. I would especially like to thank my co-advisor Dominik Wodarz for his tutelage during my time at UCI which introduced me to many new areas of research, and my advisor Naveen Vaidya, whom I first met as an undergraduate student at UMKC and whose mentorship has taken my career in directions I couldn't otherwise have imagined.

Further thanks are in order to Forest Rohwer and my colleague Greg Burkeen for the data used in Chapter 3 as well as their biological insights which were critical to the modeling work in this dissertation. I would also like to thank my collaborators and co-authors Dr. Cynthia Silveira and Dr. Douglas Conrad for providing the clinical data used in Chapter 4.

I am grateful to several additional faculty members at SDSU. Among them, I would like to thank Dr. Mary Pilgrim and Dr. Ricardo Carretero for their sage advice and personal support throughout the years, as well as Dr. Christopher Curtis and Dr. Antoni Luque for their invaluable technical insights on several projects. I am also grateful to the director of the CSRC Dr. Jose Castillo for his leadership and administration of the computational science doctoral program.

I would also give my thanks to my colleagues from the UAW Lark Winner and Anke Schennick. I deeply enjoyed my work there, and my time with them was formative to my experience in the CSU and UC systems and has made me a more effective scientist.

Funding for this work was provided in part by NSF grants DUE-1259951, DMS-1951793, DMS-1836647, as well as start-up funds and the University Grant Program of San Diego State University.

VITA

Peter Muarice Uhl

EDUCATION

Doctor of Philosophy in Computational Science — **2023**
University of California, Irvine — *Irvine, California*

Master of Science in Mathematics — **2017**
University of Missouri-Kansas City — *Kansas City, Missouri*

Bachelor of Science in Mathematics and Statistics — **2015**
University of Missouri-Kansas City — *Kansas City, Missouri*

RESEARCH EXPERIENCE

Research Specialist I — **2023**
SDSU Research Foundation — *San Diego, California*

Summer Student Assistant — **2019**
San Diego State University — *San Diego, California*

TEACHING EXPERIENCE

Teaching Associate — **2018–2022**
San Diego State University — *San Diego, California*

Teaching Associate — **2019**
University of California, Irvine — *Irvine, California*

PROFESSIONAL EXPERIENCE

Executive Board Member — **2021 – 2022**
United Auto Workers Local 4123 — *Long Beach, California*

Intern–Drug Metabolism Pharmacokinetics — **2021**
Vertex Pharmaceuticals, Inc. — *Boston, Massachusetts*

Logistics Analyst — **2016–2018**
InterCity Direct, LLC — *Lenexa, Kansas*

REFEREED JOURNAL PUBLICATIONS

Modeling the Effects of Drugs of Abuse on Within-host Dynamics of Two HIV Species **2023**
Journal of Theoretical Biology

Spatial dynamics of feedback and feedforward regulation in cell lineages **2022**
PLOS Computational Biology

ABSTRACT OF THE DISSERTATION

Spatiotemporal Dynamics of the Cystic Fibrosis Airway Microbiome

By

Peter Muarice Uhl

Doctor of Philosophy in Computational Science

University of California, Irvine, 2023

Professor Naveen K. Vaidya, Chair

Increased understanding of the ecology of the cystic fibrosis (CF) lung microbiome has improved treatment options for CF lung infections by allowing clinicians to target microbes known to be associated with acute disease. The microbial community responsible for CF lung infections is a complex collection of bacteria, viruses, and fungi with varying nutritional sources and metabolisms. Oxygen is a key resources in this environment, however it has different effects on the various microbial species with some species requiring it for respiration and others inhibited by it. Episodes of acute disease known as cystic fibrosis pulmonary exacerbations (CFPEs) are now known to be associated with higher abundances of fermentative anaerobes which can propagate in low oxygen conditions. The goal of this dissertation is to characterize the CF lung microbiome quantitatively, specifically the interaction between anaerobic and aerobic microbes, the role of oxygen, and the potential for oxygen-based therapies and optimized antibiotic usage. We begin by developing a model for the *in vitro* growth of CF pathogens and estimating basic growth parameters for individual pathogens. We use these parameterizations to model the competition between aerobic and anaerobic communities inside of a CF airway and to predict antibiotic treatments and oxygen conditions that maintain a low anaerobic population. Next, we extend our modeling of aerobic-anaerobic competition to include spatial effects and stochasticity to investigate how oxygen gradients affect community dynamics within aggregated mucus. We use our spatial

models to predict physical properties such as the minimum mucus plug diameter necessary to support anaerobic growth and show that an antibiotic with a high permeability into mucus is the most effective for controlling the anaerobic community. The results from this dissertation will aid the clinical treatment of CF lung infections by predicting antibiotic treatments and oxygen therapies which can be tested in laboratory conditions and eventually be applied clinically.

Chapter 1

Introduction

Cystic fibrosis (CF) is an inherited genetic disorder caused by mutations in the gene responsible for regulating the cystic fibrosis transmembrane conductance regulator (CFTR) protein [22, 29]. The CFTR regulates anion transport across epithelial cell boundaries and mutations to the CFTR gene can cause dehydration of mucins which interferes with a number of physiological functions [11]. CF can be diagnosed at birth, with most cases identified by age ten and diseases of the pancreas, liver, and lungs can be present from a young age [11, 77]. Chronic lung infections leading to bronchiectasis and eventual pulmonary failure are the leading cause of death in people with CF. Improved therapies and, more recently, CFTR modulators have greatly improved the prognosis for treating CF, however, lung infections remain a serious concern for managing CF [11, 51, 81, 107].

Improper transport of chloride ions and water across cell membranes causes a build-up of thick, sticky mucus in the lung and respiratory system in CF patients [57, 71]. The accumulated mucus in the airways is vulnerable to colonization by opportunistic pathogens, and long-term infections are established in the airways early in life [22]. The presence of bacteria and other microbes elicits a strong immune response, including increased mucus

production, leading to epithelial scarring and remodeling of the airway [26, 57]. Over a patient's lifetime, scarring, inflammation, and chronic infections cause a gradual decrease in pulmonary function and dramatically shortens the life expectancy of people with CF [51]. Treatment of CF lung infections has historically been done via airway-clearing techniques and broad-spectrum antibiotics, however, antibiotic resistance is common in many CF pathogens and limits the effectiveness of such therapies [26, 64].

While it was once thought that CF lung infections were a result of colonization dominated by single pathogens, such as *P. aeruginosa, S. aureus*, and *A. xylosoxidans*, studies of the CF microbial community have determined that it is chemically complex, structured, and diverse ecological system [20, 26, 87]. *P. aeruginosa* is considered the classic CF pathogen and antibiotic therapies have been devised specifically to treat it, however, due to high genetic variability and a propensity to form biofilms, it is naturally resistant to many antibiotics and difficult to treat [23, 115]. These resistance characteristics are shared by many gram-negative bacteria common in CF, therefore, the focus of treatment is shifting from targeting individual pathogens to considering how community dynamics are functionally responsible for illness [14, 26].

Cystic fibrosis pulmonary exacerbations (CFPEs) are periods of acute disease associated with rapid decline in pulmonary function and are the leading cause of death in CF patients [33, 38]. CFPEs are commonly treated with broad-spectrum antibiotics, percussive therapies, and anti-inflammatory agents, however, practices are emerging that aim to quickly sample and obtain multi-omic data from patients undergoing an exacerbation and identify pathogens to target on an individualized basis [25, 97]. The goal of this strategy is to identify and develop treatments for the pathogens responsible for causing CFPEs, rather than treating with broad-spectrum antibiotics for which some microbes have developed resistance. Although much remains unknown about their exact causes, CFPEs have been associated with increased abundances of fermentative anaerobes, which are consistently found in CF sputum samples

despite the oxygen-rich conditions of the airway and lungs [19, 59, 84, 87]. Accumulated mucus and aerobic respiration create a steep oxygen gradient which creates hypoxic regions in which anaerobes can propagate [23, 28].

Mathematical modeling has been used to study disease dynamics and there is a growing body of literature on modeling bacterial growth [3, 49, 101]; previously, mathematical models related to CF have been used to study mucus distribution, airflow, and community dynamics driven by chemical gradients [28, 41, 84, 120, 121]. In this work, we develop a collection of mathematical models to investigate the role oxygen plays in the interaction between aerobic and anaerobic microbial species in CF airways. While our focus is on infections caused by CF, the ecological aspects are also applicable to polymicrobial infections at large.

The remainder of this dissertation is organized as follows: in Chapter 2 we introduce the requisite mathematical and statistical techniques used for modeling microbial dynamics in CF airways. In Chapter 3, we develop and validate a model for oxygen- and nutrient-dependent microbial growth and use it to quantify basic growth characteristics of several CF pathogens. In Chapter 4, we extend this model to include populations of anaerobic and aerobic communities growing in a CF airway. We validate this model against a clinical data set and use it to hypothesize novel antibiotic and oxygen based therapies for CFPEs. The model discussed in Chapter 5 further extends this framework to include spatially dependent dynamics which we use to study the effects of oxygen gradients in accumulated mucus and desirable pharmacodynamic properties for antibiotics. Chapter 6 continues the discussion of spatial dynamics and introduces random effects with a stochastic agent-based model. In Chapter 7, we conclude our work and discuss possible directions for future research.

Chapter 2

Preliminaries

This chapter contains the mathematical and computational techniques we use for modeling the cystic fibrosis lung microbiome, as well as procedures for data fitting and evaluating model performance. Throughout this chapter, bold faced variables represent vector quantities.

2.1 Nutrient dependent growth

Throughout the dissertation, we use E-max functions to model nutrient-dependent growth rates. The E-max model is based on pharmacological properties and is commonly used to measure dose-response rates of drugs. Microbial communities rely on nutrients from their surroundings to grow and we expect microbes to grow more quickly when nutrients are more abundant. However, we also expect the growth rate to saturate if nutrient is excessively abundant, i.e., providing infinite nutrient should not result in infinitely fast growth. The

E-max model describes this mathematically with the response function

$$f(x) = \frac{rx^n}{K_s^n + x^n}, \tag{2.1}$$

where x is the density of the nutrient, r is the saturation level, K_s is the concentration of nutrient that gives exactly half the saturation level, and n is the slope factor (also called a Hill coefficient) which determines how sensitive the response is to changes in nutrient concentration. A larger value of n results in a steeper curve, Figure 2.1 depicts the nutrient-dependent growth rate function with several values of n. Similar functions are used throughout biochemistry (Michaelis-Menten kinetics), pharmacology, and ecology [3, 27, 60, 65].

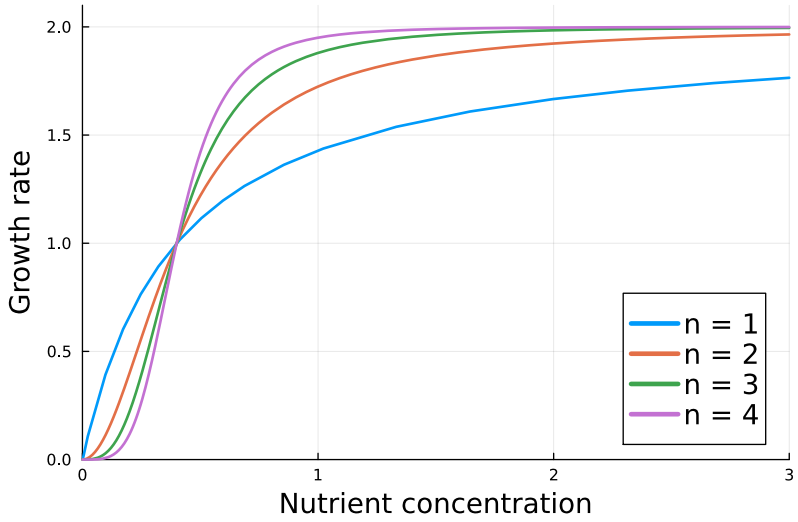

Figure 2.1: E-max functions for several different Hill coefficients.

2.2 Ordinary differential equations

Systems of ordinary differential equations (ODEs) are the primary tools we use to model microbial growth and ODEs have previously been used to investigate diseases such as HIV,

influenza, and dengue [74, 95, 110, 112, 111]. An ODE is an equation of the form

$$\frac{d\mathbf{y}}{dt} = \mathbf{f}(t, \mathbf{y}) \tag{2.2}$$

where $\mathbf{y} = (y_1, y_2, ..., y_n)$ is an unknown state variable that we are interested in tracking over time t, the derivative $\frac{d}{dt}$ is the rate of change with respect to time, and the function $\mathbf{f}$ describes how y changes over time. This work is concerned with modeling the dynamics of several populations and the nutrients they need for growth, so the state variable $\mathbf{y}$ represents a vector with components corresponding to population densities and nutrient concentrations. Solutions of Equation 2.2 are functions $\mathbf{y}(t)$ which describe the amounts of the components of $\mathbf{y}$ over time. Systems of ODEs typically cannot be solved analytically so numerical methods must be used. Consequently, there is a vast body of literature concerning numerical solutions to ODEs, see e.g., [15, 44, 45] and many software packages which utilize such methods, e.g., [67, 89].

2.3 Local stability analysis

Although we generally cannot obtain closed-form solutions to systems of ODEs, there are other analytical techniques available for investigating properties of solutions. Linear stability analysis is one such technique that, for our purposes of modeling microbial populations, involves determining the final state that a model will evolve to over a long period of time. In this dissertation, we consider autonomous equations, i.e., equations for which the function $\mathbf{f}$ on the right-hand side of Equation 2.2 does not depend explicitly on the time variable t [48, 80]. A *steady-state solution* (also called an equilibrium, or critical point) to a system of ODEs is attained when the system is no longer changing with respect to time, i.e., when $d\mathbf{y}/dt = 0$. Therefore we can find the steady-states of Equation 2.2 by solving the algebraic

system

$$\mathbf{f}(\mathbf{y}) = \mathbf{0}. \tag{2.3}$$

Denote solutions to Equation 2.3 by $\mathbf{y}^*$. We say that $\mathbf{y}^*$ is *locally asymptotically stable* if the eigenvalues of the Jacobian matrix

$$\mathbf{J} = \begin{bmatrix} \frac{\partial f_1}{\partial y_1} & \cdots & \frac{\partial f_1}{\partial y_n} \\ \vdots & \ddots & \vdots \\ \frac{\partial f_n}{\partial y_1} & \cdots & \frac{\partial f_n}{\partial y_n} \end{bmatrix} \tag{2.4}$$

each has real part less than zero when $\mathbf{J}$ is evaluated at $\mathbf{y}^*$ and unstable otherwise [48, 80, 117]. Intuitively, if $\mathbf{y}^*$ is stable then the system will evolve toward it over a long enough length of time, whereas if $\mathbf{y}^*$ is unstable then the system will move away from it. The function $\mathbf{f}$ typically also depends on parameters, i.e., $\mathbf{f} = \mathbf{f}(\mathbf{y}, \mathbf{p})$, giving

$$\frac{d\mathbf{y}}{dt} = \mathbf{f}(\mathbf{y}, \mathbf{p}) \tag{2.5}$$

and the stability of the equilibria of Equation 2.5 can change depending on the values of $\mathbf{p}$. Changes in the stability of the equilibria of Equation 2.5 can occur depending on the value of $\mathbf{p}$ and are called *bifurcations* [48, 80, 117]. These bifurcations are of interest because they represent ecological shifts in the steady state of the microbial community [26].

2.4 Parameter estimation

The models we develop in this dissertation are meant to be representative of biological processes. Therefore, we would like for our models to be able to capture and be validated against real data sets. As discussed in the previous section, the output of a model often

depends on the value of certain parameters $\mathbf{p}$, so we desire values of $\mathbf{p}$ which minimize the difference between an observed data set $\widehat{y}$ and a model output $y(t, \mathbf{p})$. Such a $\mathbf{p}$ is called the best-fitting parameter set and is found by minimizing the *sum of square residuals* [10] given by

$$SSR(\mathbf{p}) = \sum_{i=1}^{M} \left(y(t_i, \mathbf{p}) - \widehat{y}_i\right)^2, \tag{2.6}$$

where M is the number of data points available, and $y(t_i, \mathbf{p})$ and $\widehat{y}_i$ are the model prediction and observed data at the i^{th} time point, respectively. Packages are available in, e.g., MATLAB and Julia to solve this optimization problem for the best-fitting values of $\mathbf{p}$ [12, 67].

2.5 Model selection

In Chapter 3 we compare a collection of nested models, aiming to improve a model's goodness-of-fit at the expense of adding additional parameters. We measure the performance of the models with the Akaike Information Criterion and by performing an F-test for nested models.

2.5.1 Akaike Information Criterion

The Akaike Information Criterion (AIC) is a quantitative measure to compare the performance of different models based on the SSE, number of available data points, and number of fitted parameters [2, 74]. To determine the best choice of model, we compute the AIC as

$$AIC = M \ln\left(\frac{J}{M}\right) + \frac{2M\,(N+1)}{M-N-2}, \tag{2.7}$$

where J is the SSE of the best fitting parameter set, M, is the number of available data points, and N is the number of estimated parameters. We take the model with the lowest AIC to be the best choice.

2.5.2 F-test for nested models

When comparing models, we can conduct an F-test to determine if the performance of one model is a statistically significant improvement over another. To compare two nested models, we compute the F-ratio as s_e^2/s_f^2, where s_e is the difference between the residual mean square (RSS) of the models being compared divided by the difference in the number of parameters and s_f is the RSS of the best-fit model divided by the number of data points minus the number of free parameters of that model. We then determine the statistical improvement by comparing this ratio with an F distribution with the corresponding number of degrees of freedom [10].

2.6 Sensitivity analysis

In addition to having a model which is able to capture observed data, we are also interested in identifying individual parameters which have large effects on model output relative to other parameters. Two techniques we employ to determine the model sensitivity to parameters are calculating Sobol indices from repeated samples of parameter values and differential sensitivity analysis.

2.6.1 Local sensitivity analysis

One method to measure the sensitivity of a model to a change in a parameter is to simple differentiate the model output with respect to the parameter. Because we do not typically have closed-forms of our model outputs we require numerical methods to compute these derivatives and we describe a method to do so using a complex-step perturbation [6, 69, 90]. Let $y_{t_k}(\mathbf{p}) = y(t_k, \mathbf{p})$ be the model output at time t_k, $k = (1, 2, ..., m)$ dependent on a parameter vector $\mathbf{p} = (p_1, p_2, ..., p_n)$. For a small, complex valued step-size ih where $i = \sqrt{-1}$ is the imaginary unit, the Taylor expansion of $y_{t_k}(\mathbf{p})$ is

$$y_{t_k}(\mathbf{p} + ih\mathbf{e}_j) = y_{t_k}(\mathbf{p}) + ihy'_{t_k}(\mathbf{p}) - \frac{h^2}{2}y''_{t_k}(\mathbf{p}) + \cdots \tag{2.8}$$

where $\mathbf{e}_j$ is the unit vector with a 1 in the j^{th} position and 0's elsewhere. Taking the imaginary part of Equation 2.8 and dividing by h, we obtain

$$y'_{t_k}(\mathbf{p}) = \frac{Im\left(y_{t_k}(\mathbf{p} + ih\mathbf{e}_j)\right)}{h} + O(h^2), \tag{2.9}$$

where $O(h^2)$ represents terms of order 2 and higher. Thus, we can compute the partial derivatives with the approximation

$$\frac{\partial y_{t_k}}{\partial p_j} = y'_{t_k}(\mathbf{p}) \approx \frac{Im\left(y_{t_k}(\mathbf{p} + ih\mathbf{e}_j)\right)}{h}, \tag{2.10}$$

for a small value of h.

If we have estimated our parameters by fitting the model to a data set, then we can use these sensitivities to compute the standard errors of our estimated values [6]. To do so, we

construct the sensitivity matrix $\widehat{\Psi}$ given by

$$\widehat{\Psi} = \begin{bmatrix} \frac{\partial y_{t_1}}{\partial p_1} & \dots & \frac{\partial y_{t_1}}{\partial p_n} \\ \dots & \ddots & \dots \\ \frac{\partial y_{t_m}}{\partial p_1} & \dots & \frac{\partial y_{t_m}}{\partial p_n} \end{bmatrix}, \tag{2.11}$$

and can compute the standard error or parameter j using

$$\sqrt{\left(\sigma^2 \left(\widehat{\Psi}^T \widehat{\Psi}\right)^{-1}\right)_{jj}}, \tag{2.12}$$

where

$$\sigma^2 \approx \widehat{\sigma}^2 = \frac{SSR(\mathbf{p})}{n-m}. \tag{2.13}$$

We also desire for our estimated parameter values to be uniquely identifiable, which will be the case provided the matrix $\widehat{\Psi}^T \widehat{\Psi}$ possesses full rank [24].

2.6.2 Global sensitivity analysis

The complex-step perturbation method is an example of a technique for performing *local* sensitivity analysis, in the sense that it determines the effect of varying each individual parameter in turn while holding all others fixed. We are also interested in *global* sensitivity, i.e., the effect of individual parameters when all other parameters are simultaneously varied. In Chapter 4, we investigate the global sensitivity of a model by calculating the Sobol indices of several parameters from repeated samples of parameter values [42, 94, 99, 123].

Let $y = f(\mathbf{p})$ be the output of a model based on a set of input parameters $\mathbf{p}$, and let $\mathbf{Y}$ be a collection of such outputs formed from repeatedly sampling the input vector $\mathbf{p}$ from an appropriate probability distribution. Sobol's method is a way of decomposing the variance

of $\mathbf{Y}$ as a sum of the variances caused by changes in the components p_i of $\mathbf{p}$. Changes in model outputs are often caused as a result of interactions between various inputs, and an advantage of Sobol indices is that they are able to quantify these interactive effects [94, 99].

A typical procedure when analyzing a model with Sobol's method is to compute the *first-order index* and *total-effect index* for each parameter [42]. The first-order index for parameter p_i of the model is given by

$$S_i = \frac{Var(E(\mathbf{Y}|p_i)}{Var(\mathbf{Y})}, \tag{2.14}$$

where the numerator represents the variance of the model caused by varying p_i alone, and $E(\cdot)$ and $Var(\cdot)$ are the expected value and variance operators, respectively. The total-effect index represents the variance of the model caused by p_i as well as the interaction between p_i with the set of remaining parameters, denoted by $p_{\sim i}$, and is given by

$$S_{T_i} = 1 - \frac{Var(E(\mathbf{Y}|p_{\sim i})}{Var(\mathbf{Y})}. \tag{2.15}$$

Therefore, the values of the first-order and total-effect indices represent the percent of the output variance induced by changes in a parameter, including changes caused by the parameters interaction with all other parameters. Some characteristics of Sobol indices are that $\sum S_i \leq 1$ and $\sum S_{T_i} > 1$ in general, and $\sum S_i = \sum S_{T_i} = 1$ in the event that there are no interactions between parameters [42].

2.7 Reaction diffusion equations

In Chapter 5 we discuss a spatially dependent partial differential equation (PDE) model. PDEs are often used to model phenomena in which location plays a role in the dynamics, and the particular type of PDE we use is a *reaction-diffusion system*. Reaction-diffusion

systems were developed to model chemical reactions in a specified spatial domain and have also been used to model ecological systems of organisms interacting in an environment [17]. A typical reaction-diffusion model is a system of PDEs of the form

$$\frac{\partial \mathbf{u}}{\partial t} = \mathbf{D}\Delta\mathbf{u} + \mathbf{f}(\mathbf{u}), \tag{2.16}$$

where $\mathbf{u}$ is the vector of state variables of interest, $\partial/\partial t$ is the partial derivative with respect to time, Δ is the Laplace operator which models diffusion throughout the domain, $\mathbf{D}$ is a vector of coefficients which determines the rate of diffusion, and the function $\mathbf{f}$ determines local dynamics.

The solutions of Equation 2.16 are functions $\mathbf{u}(t, \mathbf{x})$ which specify concentrations or densities at time t and location $\mathbf{x}$. We also must specify the spatial domain that a PDE is solved on, including the number of spatial dimensions. In this work, we consider one- and two-dimensional domains. In one dimension, the Laplace operator is $\Delta = \partial^2/\partial x^2$ and in two dimensions $\Delta = \partial^2/\partial x^2 + \partial^2/\partial y^2$. The short-hands $\partial u/\partial t = u_t = u'$ and $\partial u/\partial x = u_x$ are often used.

PDEs typically require that the values of $\mathbf{u}$ or its derivatives be specified at the boundaries of the domain via *boundary conditions* (BCs). The two types of boundary conditions we consider are Dirichlet boundary conditions and (homogeneous) Neumann boundary conditions. Dirichlet BCs are of the form

$$\mathbf{u}(\mathbf{x}) = \mathbf{g}(\mathbf{x}), \tag{2.17}$$

where $\mathbf{g}(\mathbf{x})$ is a pre-specified position function, and homogeneous Neumann of the form

$$\frac{\partial \mathbf{u}}{\partial \mathbf{n}} = \mathbf{0}, \tag{2.18}$$

where $\mathbf{n}$ is a unit normal vector to the boundary. Homogeneous Neumann BCs are also refereed to as no-flux or no-flow BCs. For modeling populations, no-flow BCs can intuitively be thought of as saying that all of the organisms stay inside the environment and are not able to cross the boundary and exit it. Dirichlet BCs simply specify a fixed value at the boundary, and in this work we exclusively use constant functions for the right-hand side of Equation 2.17.

As with ODEs, analytical solutions seldom exist for reaction-diffusion systems but there are many software packages available for obtaining numerical solutions. We use the pdepe MATLAB function for solving one-dimensional systems and the FEniCS Python package for two dimensions [5, 67]

2.8 Agent-based modeling

Agent-based modeling is a computational framework for considering a multitude of individuals interacting within an environment [1, 109, 118]. An agent-based model (ABM) considers a domain in which a collection of individual "agents" act according to a set of pre-determined rules and are allowed to interact with each other over time. This type of modeling is often used to model systems with spatial heterogeneity because the computational domain necessarily involves some type of spatial structure. In Chapter 6, we consider a population of individual anaerobic and aerobic microbes acting as agents interacting in the presence of a diffusible oxygen concentration. The birth and death processes of individual microbes are also inherently random, and agent-based modeling is a natural way to introduce stochasticity into the system. Some drawbacks to ABMs are that they are simulation-based, tend to be computationally expensive, and lack the analytical tractability of deterministic ODE and PDE models.

Chapter 3

Modeling Growth Dynamics of Cystic Fibrosis Pathogens in Aerobic and Anaerobic Conditions

This chapter aims to quantify and characterize basic growth properties of several CF pathogens. Because growth can occur by different mechanisms, we describe microbial growth dynamics using systems of ODEs with several choices of nutrient-dependent growth functions. We then fit our models to *in vitro* growth curves of four CF pathogens and select the model with the most likely mechanism. The available growth curve data is reported in optical density measurements, so our modeling includes terms to account for dead cells and nutrient recycling in the closed system of the optical density capsule. The results in this chapter provide quantification of basic microbial growth dynamics and also increase the utility of optical density measurements by estimating the density of living microbes over longer periods of time than are currently possible.

3.1 Introduction

The cystic fibrosis airway microbiome is a complex ecosystem [26, 87]. It was previously thought that the CF lung was dominated by single pathogens, most commonly *Pseudomonas aeruginosa* [100, 13], however, it is now understood that the CF lung is inhabited by a diverse community of bacteria, viruses, and fungi [26, 87]. Consequently, treatment of CF lung infections has shifted to a multi-omics approach in which specific pathogens are identified and targeted for treatment [25, 97]. Therefore, more detailed characterizations of individual pathogens that inhabit the CF airway are critical for designing better treatment strategies for CF lung infections.

While *P. aeruginosa* is one of the most common pathogens, the CF airway also contains bacteria and fungi that are normally found in healthy human microbiomes and which can cause infections [13, 30, 104]. Pathogens can exhibit a wide variety in their metabolisms, nutritional sources, and responses to treatment [23, 39] but there is not a widespread method of quantifying their growth characteristics. Anaerobic bacteria are routinely found in sputum samples of CF patients, and many classic CF pathogens, including *P. aeruginosa*, are facultatively anaerobic and can survive with or without oxygen [36, 79, 83]. Quantifying the growth behavior of individual pathogens under different conditions is therefore useful clinically for the treatment of CF lung infections and for the broader study of microbial ecology. Recent strategies for treating acute CF infections rely on quickly sequencing and identifying potential targets for treatments, and having basic understanding of the growth mechanisms of individual pathogens is beneficial for such treatments [25].

Optical density (OD) measurements are used frequently by microbiologists to measure microbial growth. These measurements are useful, e.g., for observing relative growth rates between different strains of bacteria, or the growth of a single bacteria under different nutritional conditions. OD machines do not directly count growing microbes, rather, population

density is measured indirectly by passing light through a capsule containing microbes in a nutrient media, and the machine measures the diffraction due to microbial density. A drawback to this technique is that OD machines cannot distinguish between living and dead cells, so OD measurements are only reliable during the exponential phase of microbial growth when little cell death occurs [52, 78, 102]. A further complication is that as microbes die, autolysis can occur and a portion of the nutrients contained by dead cells can be recovered by the remaining live microbes [61, 91].

While individual microbes can function as their own separate organisms, bacteria and other single-cell entities greatly benefit from forming biofilms, colonies, and other organized structures [4, 116]. By organizing into a single, larger entity, microbes are more protected from external stress, can promote genetic diversity, and clear damaged or defective cells [61]. Programmed death has been observed in some bacteria in response to starvation, in which some cells die altruistically and undergo lysis, which releases the nutrients within their cell walls into the intra-cellular matrix where it can be utilized by the remaining community [4, 116]. These mechanisms can be observed in *in vitro* experiments, but it remains difficult to quantify the dynamics inside of microbial communities because cell counts cannot be directly measured. In this chapter, we quantify the behavior of four facultatively anaerobic CF pathogens by estimating several growth-related parameters from *in vitro* measurements. The pathogens, three bacteria and one fungus, were cultured from sputum samples taken from a patient at the University of California, San Diego Cystic Fibrosis Clinic and their growth measured via optical density [102].

The goal of this chapter is to quantify the growth mechanisms and parameters of the several CF pathogens under anaerobic and aerobic conditions using mathematical modeling. The models we develop in this chapter are systems of ODEs with several choices of resource-dependent growth rates. By fitting our models to experimental growth data, we are able to estimate parameters that characterize the growth of the pathogens and identify the most

likely mechanisms of action using the Akaike Information Criterion and perform statistical and sensitivity analysis on the estimated parameter values we obtain [2, 6]. Our results may be useful in understanding the basic ecology of the CF lung microbiome, identifying possible treatment strategies for CF lung infections, and microbial ecology in general. This work may also increase the utility of OD measurements by allowing microbiologists to estimate the amount of living cells present over long periods of growth rather than during the exponential phase alone.

3.2 Experimental data

3.2.1 Aerobic growth curves

All strains were grown using brain and heart infusion (BHI) media in a clear polystyrene float bottom 96 well plate. Strains were grown overnight while shaking at 37 degrees Celsius, then diluted 1:200 before loading into the 96 well plate for the growth curve in a 96 well plate OD reader. OD readings were taken every 20 minutes at 600 nm wavelength light. The OD reader maintained 37 degrees Celsius and medium-intensity orbital shaking throughout the experiment.

3.2.2 Anaerobic growth curves

Anaerobic growth curves were conducted using BHI supplemented with 0.1% KNO_3. Strains were grown overnight in anaerobic conditions and diluted 1:200 under anaerobic conditions before loading into a 96-well plate and sealed using an airtight plastic film. Once sealed, the plate was removed from the anaerobic chamber and loaded into the 96-well plate OD reader with the same settings as for the aerobic growth curves.

3.2.3 Microbial growth profiles

The three bacteria *E. faecalis*, *P. aeruginosa*, and *S. odorifera* and the pathogenic yeast *C. albicans* were grown in aerobic and anaerobic conditions over 48 hours, producing eight total growth curves. The bar graphs in Figure 3.1 show the observed mean optical density for the four microbes. In anaerobic conditions (blue bars in Figure 3.1), each microbe reached peak density between 0.4 and 0.5 OD. *P. aeruginosa* and *C. albicans* saw slight increases in OD at approximately 1.2 days. *E. faecalis* and *S. odorifera* enter the death phase by the end of the data collection, while the curves for *P. aeruginosa* and *C. albicans* are still in the stationary phase after two days.

Each of the four microbes in the experiment are facultative anaerobes and can grow with or without oxygen. However, many facultative anaerobes survive anaerobic conditions by drastically slowing their metabolisms and growing faster when oxygen is available. The red bars in Figure 3.1 demonstrate each of the four species' faster metabolism in aerobic conditions. *E. faecalis* and *P. aeruginosa* have similar profiles during the exponential growth phase in both oxygen scenarios but reach higher peak concentrations when grown aerobically. *P. aeruginosa* and *S. odorifera* both grow beyond ODs of 1 where the measurements become unreliable; however *P. aeruginosa* is still growing at 2 days while *S. odorifera* is in the stationary phase. *E. faecalis* and *C. albicans*, on the other hand, are clearly in the death phase after 2 days and their populations are in decline. This is likely because these populations have depleted their supply of nutrient to the point that they are not reproducing enough to replace the dead cells. Other than *S. odorifera*, each microbe showed a longer lag phase in the aerobic case than in the anaerobic case. This may be due to differences in initial densities when the aerobic experiment began, resulting in a longer time before exponential growth begins.

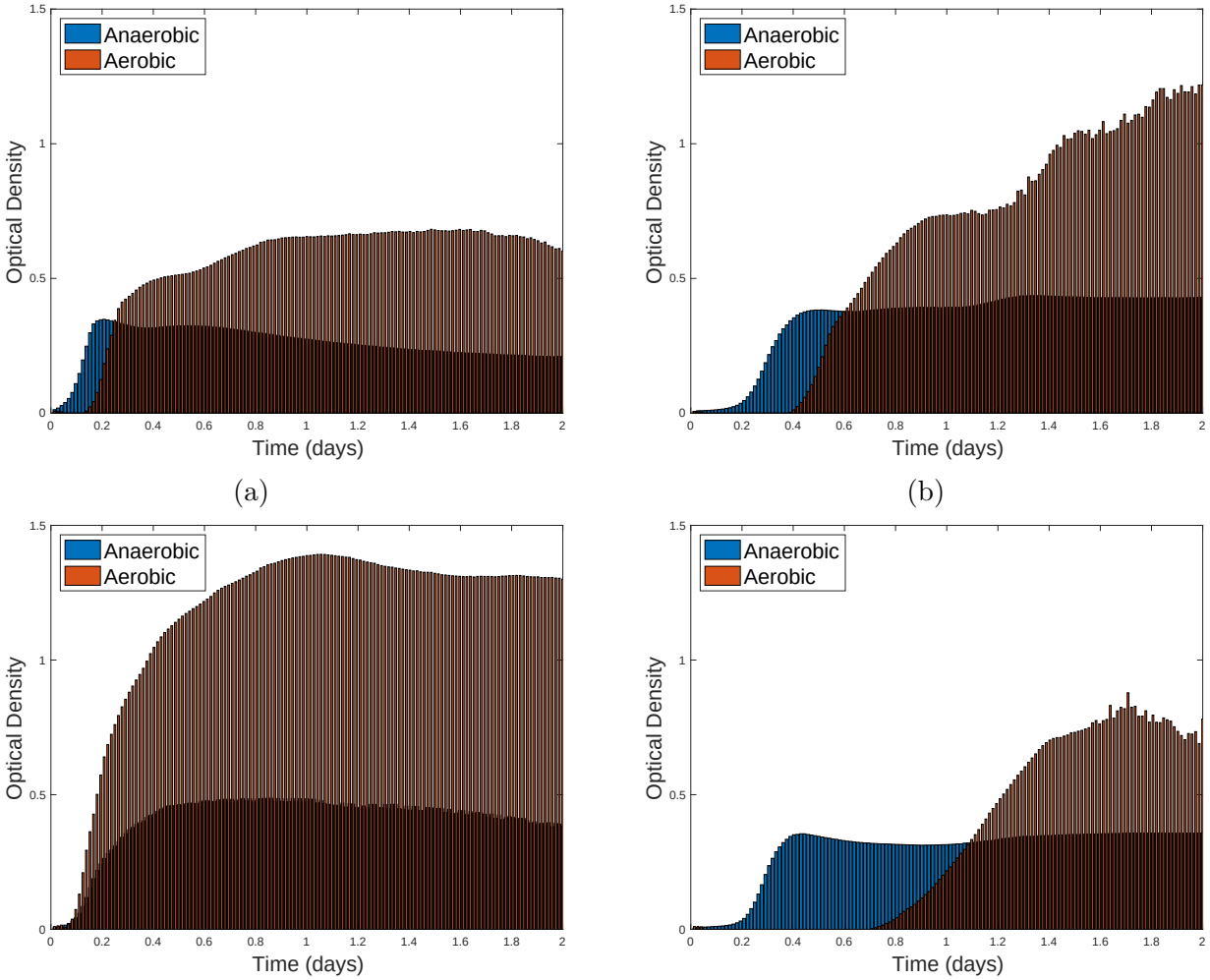

Figure 3.1: Observed optical densities of *E. faecalis* (a), *P. aeruginosa* (b), *S. odorifera* (c), and *C. albicans* (d) grown anaerobically (blue bars) and aerobically (red bars) over 48 hours.

3.3 Model development

We develop a mathematical model for microbial growth inside an optical density capsule with a limited amount of nutrient, and for either aerobic or anaerobic oxygen concentrations. Our model describes microbial growth in a nutritional media inside capsules which are periodically agitated to ensure homogenization, and there is no nutrient entering the capsule during the experiment. Microbial growth follows a four-phase progression: lag, exponential, stationary, and death. During the lag phase, the microbes become metabolically active and adapt to the environment before growing rapidly in the exponential phase. In the stationary phase, the microbes have consumed much of the available nutrient and begin to die off with new cells replacing the dead ones. When there is too little nutrient to sustain the community any longer, the microbes enter the death phase and gradually die off. As microbes die during the stationary and death phases, they may undergo autolysis. When this occurs, the dead microbe's cell wall breaks up, releasing unmetabolized nutrient back into the media where it can be utilized by the remaining population [4, 91, 102].

Our model consists of a three-component system of ODEs. The three components correspond to living microbes, denoted by x, dead microbes, denoted by y, and nutrient concentration, denoted by z. We assume microbes grow in a density-dependent manner, which we model with a logistic proliferation term where the growth rate is a function of both the nutrient concentration and amount of available oxygen, denoted by w.

Since both living and dead microbes occupy space inside the capsule, we assume both contribute to the competition term of the logistic growth function. Cells die at per capita rate d, which can occur due to starvation, programmed death, or genetic factors [4, 61, 116]. When microbes die, they transition to the dead cell compartment y at rate d and lyse at rate γ. Nutrient z is consumed by living microbes at rate δ and recovered from dead cells at rate μ. To be consistent with the experimental data, we assume that oxygen concentrations in the

capsules are constant with $w = 0$ for the anaerobic data and $w = w_0$ for the aerobic data, where the value of w_0 corresponds to the atmospheric oxygen concentration.

The microbial growth rate is nutrient-dependent [3] and nutrient can be recovered from dead cells after lysis occurs [4, 61], but the OD capsule is a closed system and no new nutrient can enter from the outside. We assume that no dead cells are initially present, denote the nutrient- and oxygen-dependent growth function by $f(w, z)$, and write the full model as

$$\frac{dx}{dt} = f(w,z)x\left(1 - \frac{x+y}{K}\right) - dx, \qquad x(0) = x_0 \tag{3.1}$$

$$\frac{dy}{dt} = dx - \gamma y, \qquad y(0) = 0 \tag{3.2}$$

$$\frac{dz}{dt} = -\delta xz + \mu y, \qquad z(0) = z_0 \tag{3.3}$$

where K represents the carrying capacity inside the capsule. We use E-max functions to model the nutrient- and oxygen-dependent growth rate $f(w, z)$. Because growth in our model is a function of two distinct resources, we take $f(w, z)$ as the product of two component functions corresponding to nutrient and oxygen. The oxygen-dependent growth rate for aerobic or facultative microbes is given by

$$g(w) = \beta_0 + \frac{\beta w^{n'}}{b^{n'} + w^{n'}}, \tag{3.4}$$

where β corresponds to the maximum achievable growth rate under high-oxygen conditions, b and n' are the half-saturation constant and slope factor for the E-max function, respectively, and β_0 is the growth rate that occurs in low-oxygen conditions and accounts for facultative anaerobic growth [3, 60, 65].

The function $g(w)$ is the component of $f(w, z)$ which accounts for increased growth in highly oxygenated conditions. To incorporate nutrient dependence into $f(w, z)$, we introduce an additional E-max function and consider three cases for the slope-factor n corresponding to

different nutrient-dependent mechanisms: $n = 0$ (constant growth with respect to nutrient), $n = 1$, and $n \neq 0, 1$. The total growth functions for the three potential mechanisms can be written

$$(1)\ \ f(w,z) = g(w) \tag{3.5}$$

$$(2)\ \ f(w,z) = g(w)\frac{z}{K_s + z} \tag{3.6}$$

$$(3)\ \ f(w,z) = g(w)\frac{z^n}{K_s^n + z^n}, \tag{3.7}$$

where K_s is the half-saturation concentration of nutrient and the Hill-coefficient n determine how sensitive the growth rate curve is to changes in nutrient concentration. The hill-coefficient is also a measure of cooperativity between microbes and nutrient and is a function of the amount of particles of nutrient needed for a microbe to accumulate enough mass to undergo binary fission and produce offspring [3]. Our experimental data contains two scenarios for oxygen availability, with $w = 0$ for the anaerobic data and $w = w_0 > 0$ for the aerobic data, in both cases the growth function $f(w, z)$ is constant with respect to oxygen. Then without loss of generality, we can denote $g(w) = r$ and write the nutrient-only dependent growth functions as

$$(1)\ \ f(z) = r \tag{3.8}$$

$$(2)\ \ f(z) = \frac{rz}{K_s + z} \tag{3.9}$$

$$(3)\ \ f(z) = \frac{rz^n}{K_s^n + z^n}. \tag{3.10}$$

Throughout this chapter, we will refer to the three models with the above growth functions as Model 1, Model 2, and Model 3, respectively.

3.4 Parameter estimation

Our experimental data is reported in optical density, a ratio of the proportion of light that passes through a transparent material [122], and both living and dead cells contribute to the OD measurement [4, 116]. We assume that optical density is proportional to cell density, i.e., that $OD = \alpha(x+y)$, where α is a linear scaling factor relating cell count to OD [75]. For data fitting purposes and to reduce the total number of parameters, we nondimensionalize the model by introducing the scaled variables $\bar{x} = x/K$, $\bar{y} = y/K$, $\bar{z} = z/z_0$ and rewrite the scaled model as

$$\frac{d\bar{x}}{dt} = f(\bar{z})\bar{x}\,(1-\bar{x}-\bar{y}) - d\bar{x}, \qquad \bar{x}(0) = \bar{x_0} \tag{3.11}$$

$$\frac{d\bar{y}}{dt} = d\bar{x} - \gamma\bar{y}, \qquad \bar{y}(0) = 0 \tag{3.12}$$

$$\frac{d\bar{z}}{dt} = -\bar{\delta}\bar{x}\bar{z} + \bar{\mu}\bar{y}, \qquad \bar{z}(0) = z_0 \tag{3.13}$$

where $\bar{\delta} = \delta K$, $\bar{\mu} = \mu K/z_0$, and $\bar{x_0} = x_0/K$. Note that scaling by z_0 allows us to set the initial nutrient concentration to 1. E-max functions are often scaled by the half-saturation concentration; however, we expect this value to be different for each microbe so scaling by the initial concentration allows us to eliminate a parameter while comparing the different half-saturation values between species. The growth rate functions therefore scale to

$$(1)\ \ f(\bar{z}) = r \tag{3.14}$$

$$(2)\ \ f(\bar{z}) = \frac{r\bar{z}}{\bar{K_s} + \bar{z}} \tag{3.15}$$

$$(3)\ \ f(\bar{z}) = \frac{r\bar{z}^n}{\bar{K_s}^n + \bar{z}^n}, \tag{3.16}$$

where $\bar{K_s} = K_s/z_0$. The relation between the non-dimensionalized microbial density and OD is then given by $OD = \bar{\alpha}(\bar{x}+\bar{y})$, where $\bar{\alpha} = \alpha K$. For Model 1, we estimate the five parameters r, d, γ, $\bar{\alpha}$, and $\bar{x}_0$, for Model 2 the eight parameters r, $\bar{K_s}$, d, γ, $\bar{\delta}$, $\bar{\mu}$, $\bar{\alpha}$, and

$\bar{x}_0$, and for Model 3 the nine parameters r, $\bar{K}_s$, n, d, γ, $\bar{\delta}$, $\bar{\mu}$, $\bar{\alpha}$, and $\bar{x_0}$. We performed computations in MATLAB using the ode15s, fminsearch, and fmincon functions [67]. For each model, we obtained parameter estimates by solving the system of ODEs and selecting values that minimize the sum of square errors (SSE) given by

$$J(p) = \sum_{i=1}^{M} \left(OD(t_i) - \widehat{OD}(t_i, p) \right)^2, \tag{3.17}$$

where $OD(t_i)$ is the observed optical density at time point i, $\widehat{OD}(t_i, p) = \bar{\alpha}\left(\bar{x}(t_i, p) + \bar{y}(t_i, p)\right)$ is the model predicted optical density, $p = (r, d, \gamma, \bar{\alpha}, \bar{x}_0)$ for Model 1, $p = (r, \bar{K}_s, d, \gamma, \bar{\delta}, \bar{\mu}, \bar{\alpha}, \bar{x}_0)$ for Model 2, and $p = (r, \bar{K}_s, n, d, \gamma, \bar{\delta}, \bar{\mu}, \bar{\alpha}, \bar{x}_0)$ for Model 3, and M is the number of available data points. For each estimated parameter value, we also computed standard errors using a complex-step derivative approximation [7, 8, 9, 69, 90]. These best-fitting values and standard errors are shown in Tables 3.2 and 3.3. Figures 3.2 and 3.3 show simulations with best-fit parameters for each microbe and each of the three models. These figures are plotted with their observed standard deviations of each measurement.

Maximal aerobic growth rates r were larger than the anaerobic values for each species, which is expected given the larger densities observed in the aerobic measurements. Similarly, the estimated nutrient consumption rates $\bar{\delta}$ also tended to be larger in the aerobic case indicating higher metabolic activity than we see in anaerobic conditions. On the other hand, the lysis rate γ was higher in the anaerobic data sets. This may be a survival mechanism in which microbes are recycling nutrients more rapidly due to the less favorable anaerobic conditions.

3.5 Model selection

For each growth curve, we used the AIC to select the best-fit model in both anaerobic and aerobic conditions. In Tables 3.2 and 3.3 we list the SSE and AIC for each microbe

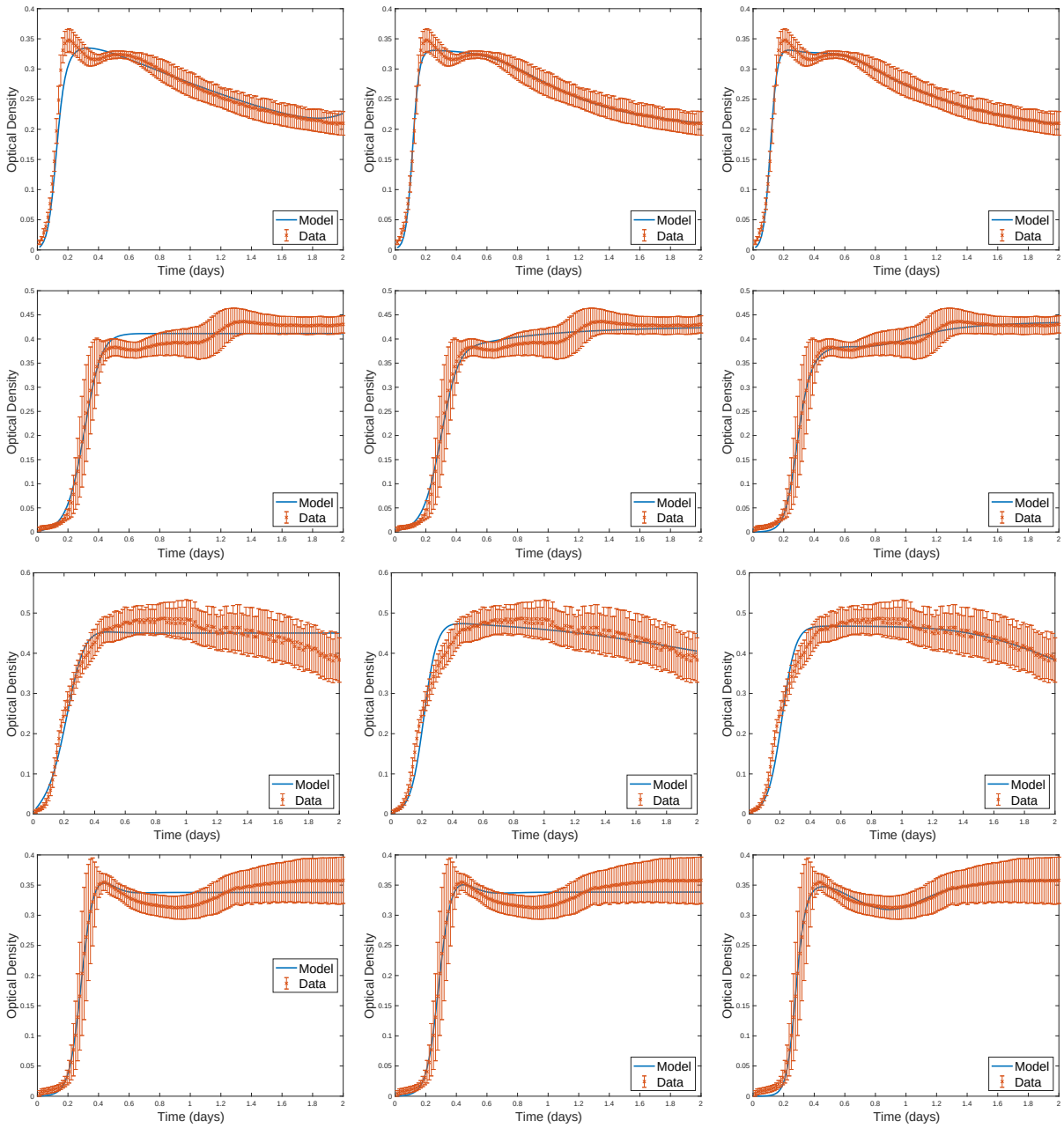

Figure 3.2: Anaerobic growth curves and solutions with best fitting parameters for *E. faecalis* (top row), *P. aeruginosa* (second row), *S. odorifera* (third row), and *C. albicans* (bottom row). The left column shows simulations for Model 1, the middle column for Model 2, and the left column for Model 3.

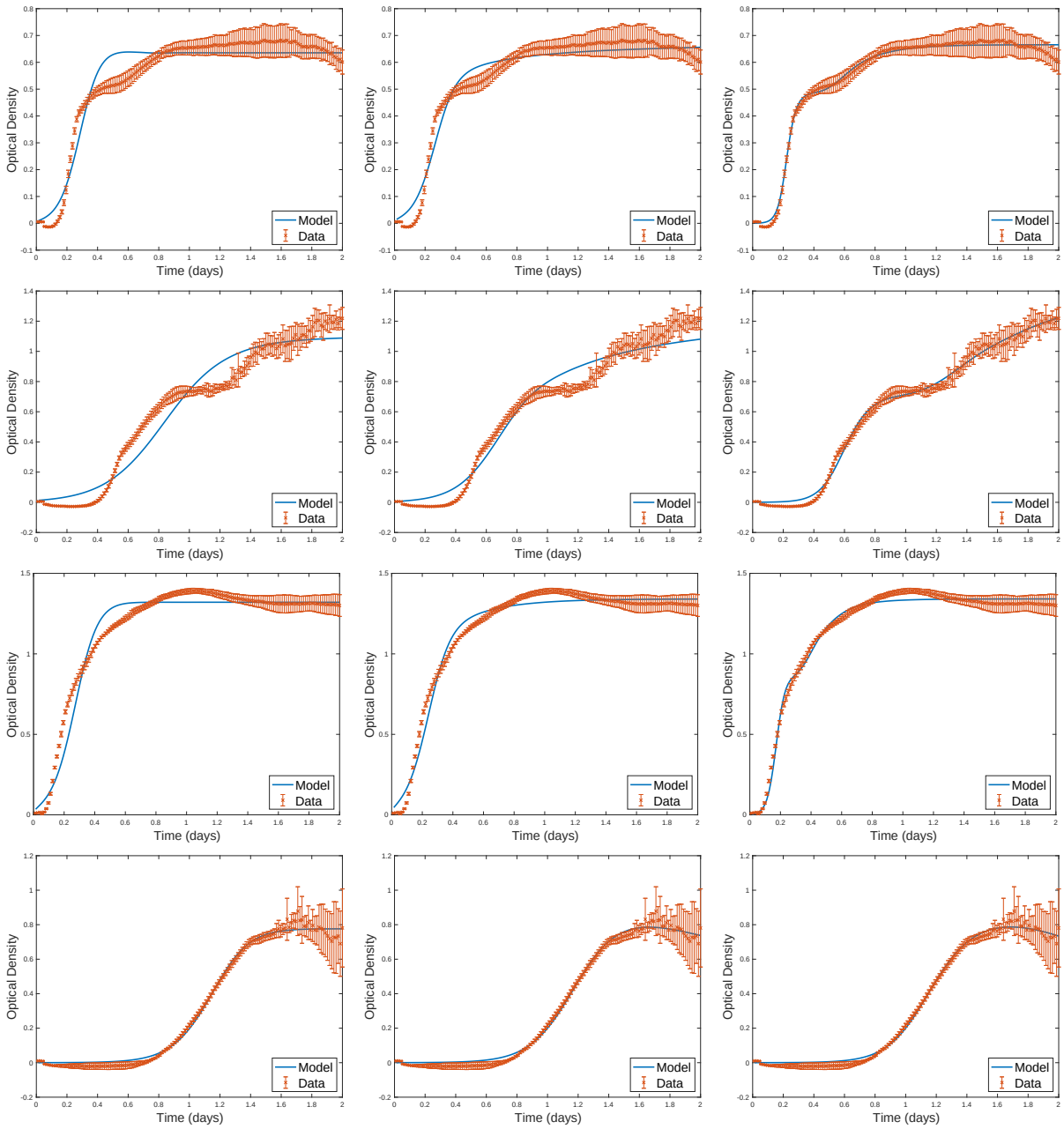

Figure 3.3: Aerobic growth curves and solutions with best fitting parameters for *E. faecalis* (top row), *P. aeruginosa* (second row), *S. odorifera* (third row), and *C. albicans* (bottom row). The left column shows simulations for Model 1, the middle column for Model 2, and the left column for Model 3.

Table 3.1: Model 3 best-fit parameters

	E. faecalis		*P. aeruginosa*		*S. odorifera*		*C. albicans*	
	An.	Aer.	An.	Aer.	An.	Aer.	An.	Aer.
r (day^{-1})	48.65	53.96	45.56	48.39	25.92	57.55	39.24	42.68
(st. err.)	(0.22)	(4.92)	(4.21)	(14.49)	(4.01)	(3.21)	(0.66)	(660.96)
K_s	0.25	0.85	0.96	1.05	0.18	0.93	0.87	1.49
(st. err.)	(0.022)	(0.053)	(0.013)	(0.034)	(0.66)	(0.014)	(0.040)	(91.77)
n	12.84	4.89	9.32	11.87	5.11	17.19	14.51	3.35
(st. err.)	(1.07)	(2.77)	(6.12)	(6.81)	(12.98)	(3.22)	(4.86)	(493.83)
d (day^{-1})	3.57	2.63	0.72	4.21	4.06	9.91	1.19	1.14
(st. err.)	(0.30)	(0.65)	(0.056)	(0.48)	(4.18)	(1.02)	(0.057)	(28.72)
γ (day^{-1})	14.02	7.46	5.10	4.43	27.39	18.49	3.00	1.51
(st. err.)	(1.14)	(2.62)	(0.69)	(0.34)	(12.75)	(1.07)	(0.20)	(32.79)
$\bar{\delta}$ (day^{-1})	6.54	15.05	3.04	3.23	2.33	8.88	2.30	1.87
(st. err.)	(0.12)	(7.45)	(1.84)	(2.26)	(2.57)	(1.60)	(0.80)	(276.17)
$\bar{\mu}$ (day^{-1})	5.60	34.82	20.07	4.16	2.01	18.31	5.76	0.01
(st. err.)	(0.57)	(8.16)	(5.65)	(2.67)	(6.40)	(4.07)	(1.34)	(46.34)
$\bar{\alpha}$	0.35	0.75	0.45	1.53	0.55	1.64	0.37	1.23
(st. err.)	(0.0023)	(0.028)	(0.0096)	(0.091)	(0.090)	(0.024)	(0.0018)	(2.77)
$\bar{x}_0$	0.010	5.0×10^{-4}	6.2×10^{-4}	1.9×10^{-4}	0.0098	0.020	1.1×10^{-4}	9.2×10^{-5}
(st. err.)	(1.2×10^{-4})	(4.3×10^{-5})	(2.9×10^{-5})	(1.3×10^{-5})	(0.0020)	(9.3×10^{-5})	(3.8×10^{-6})	(3.8×10^{-4})

and choice of model for the anaerobic and aerobic data, respectively. For each of the four microbes, Model 3 provides the lowest AIC for both oxygen conditions suggesting a higher degree of cooperativity between individual microbes and nutrient than is present in Monod equation-type dynamics [3]. The estimated value for n for each microbe (Table 3.1) for each microbe is then a result of different mechanisms being utilized for nutrient consumption for each species.

In every case, Model 1 performed poorly compared to Models 2 and 3. This is to be expected because of Model 1's constant growth term, which does not account for diminishing nutrient availability affecting the proliferation rate. Since Model 1 does not track the nutrient concentration, it also does not consider nutrient recycling which further limits the dynamics it can describe. For several of the data sets, Model 2 had similar performance to Model 3, however, Model 3 was better able to capture some of the transient behavior for some microbes, e.g., the anaerobic *C. albicans* curve. This indicates that the higher-order reaction kinetics possible in Model 3 are best suited for modeling microbial dynamics.

We performed F-tests to determine if the additional parameters significantly improved the performance of Model 3 over Models 1 and 2. The calculated p-values are shown in Tables 3.4 and 3.5 for the aerobic and anaerobic data, respectively. For each of the eight data sets, the calculated p-value was less than 0.001, indicating that Model 3 is significantly better at

capturing the growth curve data. The OD measurements provide a relatively large number of data points which offsets the penalty of adding a small number of additional parameters, four and one for Models 1 and 2, respectively.

Table 3.2: Anaerobic growth SSE and AIC

	Model 1		Model 2		Model 3	
	SSE	AIC	SSE	AIC	SSE	AIC
E. faecalis	0.0274	-1221.1	0.0057	-1440.1	0.0047	-1465.6
P. aeruginosa	0.0506	-1132.7	0.0254	-1225.3	0.0060	-1431.3
S. odorifera	0.1061	-1026.1	0.0777	-1064.3	0.0540	-1114.3
C. albicans	0.0315	-1200.8	0.0309	-1197.0	0.0030	-1529.7

Table 3.3: Aerobic growth SSE and AIC

	Model 1		Model 2		Model 3	
	SSE	AIC	SSE	AIC	SSE	AIC
E. faecalis	0.3696	-846.37	0.2016	-926.91	0.0321	-1189.3
P. aeruginosa	1.4111	-653.45	0.8617	-717.47	0.1131	-1007.9
S. odorifera	0.7335	-747.66	0.3797	-835.75	0.2913	-871.59
C. albicans	0.0907	-1048.6	0.0728	-1073.5	0.0631	-1092.0

Table 3.4: Anaerobic p-values

	p-value	
	Model 1 vs Model 3	Model 2 vs Model 3
E. faecalis	6.9×10^{-55}	3.5×10^{-7}
P. aeruginosa	2.2×10^{-61}	3.9×10^{-44}
S. odorifera	5.2×10^{-30}	2.6×10^{-12}
C. albicans	3.2×10^{-3}	7.0×10^{-14}

Table 3.5: Aerobic p-values

	p-value	
	Model 1 vs Model 3	Model 2 vs Model 3
E. faecalis	1.4×10^{-70}	1.2×10^{-50}
P. aeruginosa	6.0×10^{-73}	2.3×10^{-61}
S. odorifera	1.7×10^{-46}	5.2×10^{-19}
C. albicans	9.3×10^{-5}	9.3×10^{-12}

3.6 Sensitivity analysis

To determine the sensitivities of the model output to changes in parameter values and compute confidence intervals, we construct the sensitivity matrix Ψ given by

$$\Psi = \begin{bmatrix} \frac{\partial \widehat{OD}_{t_1}}{\partial p_1} & \cdots & \frac{\partial \widehat{OD}_{t_1}}{\partial p_{N_p}} \\ \vdots & \ddots & \vdots \\ \frac{\partial \widehat{OD}_{t_M}}{\partial p_1} & \cdots & \frac{\partial \widehat{OD}_{t_M}}{\partial p_{N_p}} \end{bmatrix}, \tag{3.18}$$

where $\widehat{OD}$ is the model predicted optical density, and $\frac{\partial \widehat{OD}_{t_i}}{\partial p_j} = \frac{\partial \widehat{OD}(t_i,p)}{\partial p_j}$ is the partial derivative of the predicted optical density at the i^{th} time point with respect to the best-fit j^{th} parameter value, $i = 1, 2, ..., M$, $j = 1, 2, ..., N_p$, and $N_p = 5, 8$ and 9 for Models 1, 2, and 3, respectively. Because we do not have closed-form expressions for the OD curves, we use a complex-step approximation as described in [7, 8, 9, 69, 90] to approximate each derivative. The complex-step procedure begins by taking the Taylor series expansion of $\widehat{OD}_{t_i}$ with complex step ih, where i is the imaginary unit and h is a small positive constant. The Taylor expansion is given by

$$\widehat{OD}(t_i, p + ihe_j) = \widehat{OD}(t_i, p) + ih\frac{\partial \widehat{OD}(t_i,p)}{\partial p_j} - \frac{h^2}{2}\frac{\partial^2 \widehat{OD}(t_i,p)}{\partial p_j^2} + \cdots, \tag{3.19}$$

where e_j is the unit vector with 1 in the j^{th} position and 0's elsewhere. After taking the imaginary part of both sides and dividing by h, we can rearrange to obtain

$$\frac{\partial \widehat{OD}(t_i, p)}{\partial p_j} \approx \frac{Im\left(\widehat{OD}(t_i, p + ihe_j)\right)}{h}, \tag{3.20}$$

where we discard terms of order 2 and higher on the right-hand side. We do not have an analytical expression for Ψ, so we construct an approximation $\widehat{\Psi}$ to computing the $M \times N_p$ partial derivatives using Equation 3.20 for each time point and estimated parameter. We then compute the standard deviation of parameter i using

$$\sqrt{\left(\sigma^2 \left(\widehat{\Psi}^T \widehat{\Psi}\right)^{-1}\right)_{ii}}, \tag{3.21}$$

where

$$\sigma^2 \approx \widehat{\sigma}^2 = \frac{J(p)}{N_p - M}. \tag{3.22}$$

We are estimating a relatively large number of parameters, so we are concerned whether each estimated value is uniquely identifiable. Using results from Banks et al, our estimated parameter values are identifiable if the matrix $\widehat{\Psi}^T \widehat{\Psi}$ above possesses full rank [24].

The model sensitivities are shown as the curves in Figure 3.4 for the anaerobic data and Figure 3.5 for the aerobic. In all cases, the initial density of live microbes $\bar{x}_0$ was the most sensitive parameter by 1-2 orders of magnitude, followed by the OD scaling factor $\bar{\alpha}$. These parameters are a by-product of the OD measurement itself and not directly related to mechanisms of growth, so the other parameters are of more interest.

Notwithstanding $\bar{\alpha}$ and $\bar{x}_0$, the half-saturation constant $\bar{K}_s$ was the most sensitive parameter related to growth dynamic mechanisms, being roughly an order of magnitude larger than the other parameters. Additionally, the maximal growth rate r tended to be less sensitive

as the microbes are not necessarily likely to be near the maximum rate most of the time, but the value $\bar{K}_s$ does determine the nutrient concentration where growth rates change most rapidly. The Hill coefficients and nutrient depletion rate were also relatively sensitive to various degrees, which speaks to the differing characteristics of the four species.

We would like to know if the estimated parameter values are identifiable, which we determine based on the rank of the matrix $\widehat{\Psi}^T\widehat{\Psi}$. We found $\widehat{\Psi}^T\widehat{\Psi}$ to be full rank for seven of the eight data sets, indicating identifiable parameters in those seven cases. For the aerobic *C. albicans* data set, $\widehat{\Psi}^T\widehat{\Psi}$ was nearly singular and consequently had very large standard errors. This is likely a result of the long lag phase in that data set where little death occurs and the full model dynamics do not take place until a long time into the experiment, so the estimated parameters may not be identifiable for this single growth curve [24].

3.7 Cell death

Optical density measurements cannot distinguish between living and dead cells, so measurements taken via OD are only reliable in terms of live cell counts during the lag and exponential phases when it is reasonably certain that very little cell death occurs. Because we fit the sum of living and dead cells when fitting to OD data, we can use our model to predict the percent of cells still alive as a function of time. Figure 3.6 shows plots of the percent of living cells predicted by the best-fitting parameter values, i.e., the percent $x(t)/(x(t)+y(t))$, where $x(t)$ and $y(t)$ are the densities of living and dead microbes predicted by the model over time. Curves for anaerobic growth are plotted in Figure 3.6a, and aerobic growth in Figure 3.6b. The model predicted that living cells were above 70% of the OD measurement of anaerobic conditions, this could be a result of slower metabolic activity and higher rates of autolysis expected under these conditions. The percent living curves have each leveled off by the end of the data collection period. *E. faecalis* had a similar profile in aerobic conditions, while *S.*

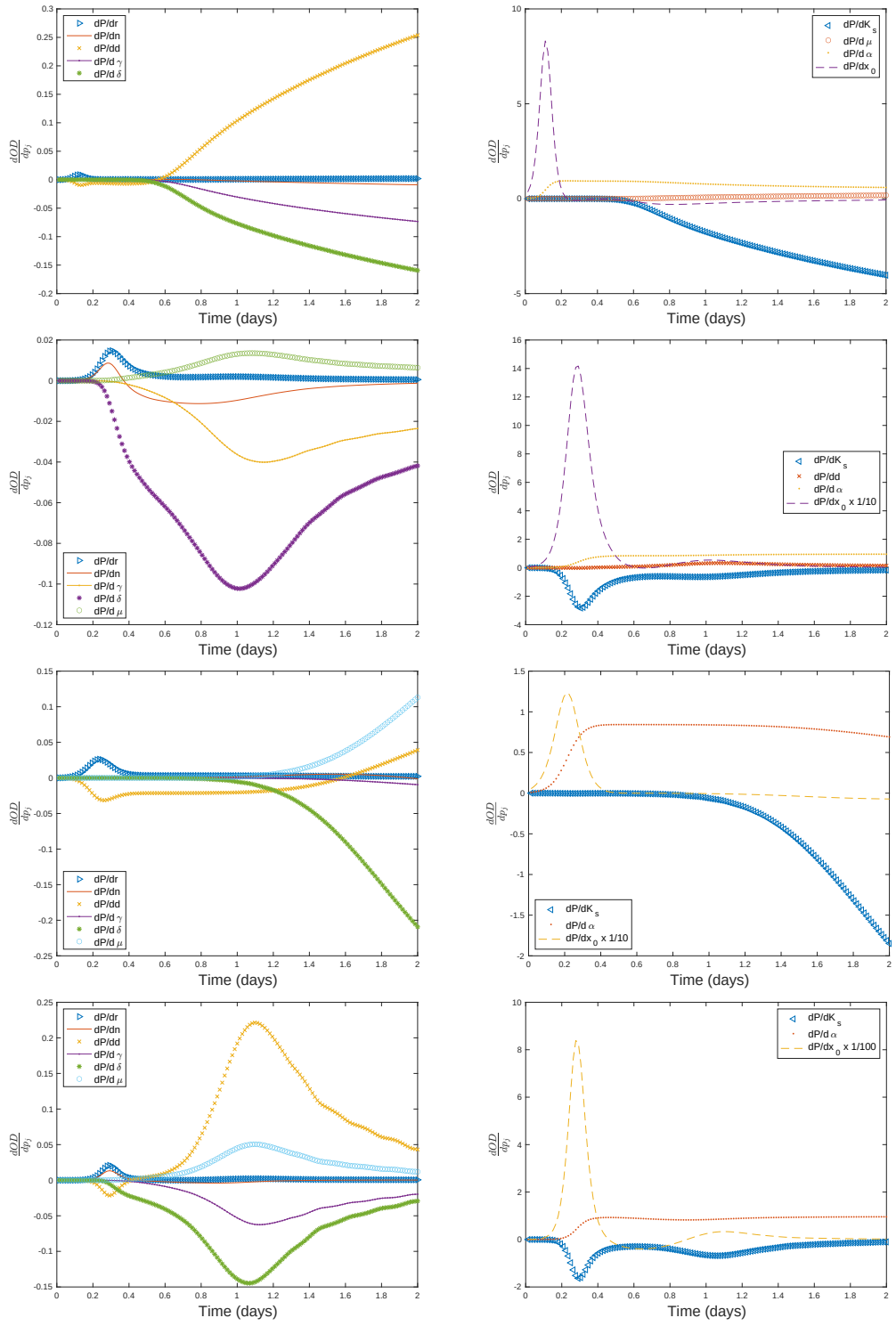

Figure 3.4: Anaerobic sensitivity curves. Rows represent (from top to bottom) *E. faecalis*, *P. aeruginosa*, *S. odorifera*, and *C. albicans*. Each curve is the partial derivative $\frac{\partial \widehat{OD}(t_i,p)}{\partial p_j}$ for the various parameters with more sensitive parameters having larger magnitudes. For visualization purposes, lower magnitude sensitivity are in the left column and larger ones in the right.

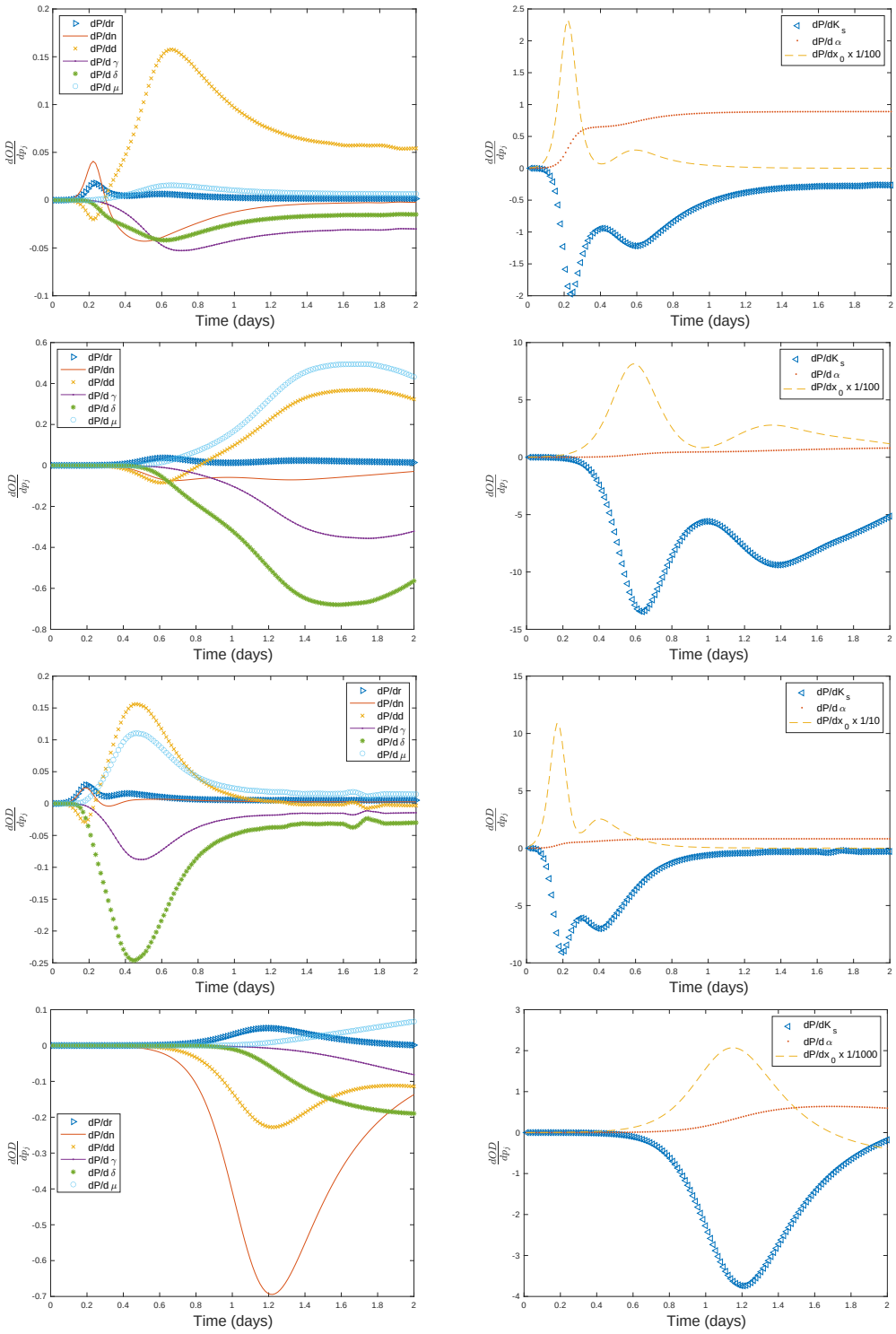

Figure 3.5: Aerobic sensitivity curves. Rows represent (from top to bottom) *E. faecalis*, *P. aeruginosa*, *S. odorifera*, and *C. albicans*. Each curve is the partial derivative $\frac{\partial \widehat{OD}(t_i,p)}{\partial p_j}$ for the various parameters with more sensitive parameters having larger magnitudes. For visualization purposes, lower magnitude sensitivity are in the left column and larger ones in the right.

odorifera was stable after two days but had a lower percent living cells. *P. aeruginosa* also had a lower percent living in aerobic conditions which may or may not be decreasing at the end of the data set, however, *P. aeruginosa* was not at steady-state, so a longer observation period is needed to be certain of its dynamics. Living *C. albicans* is clearly declining after two days.

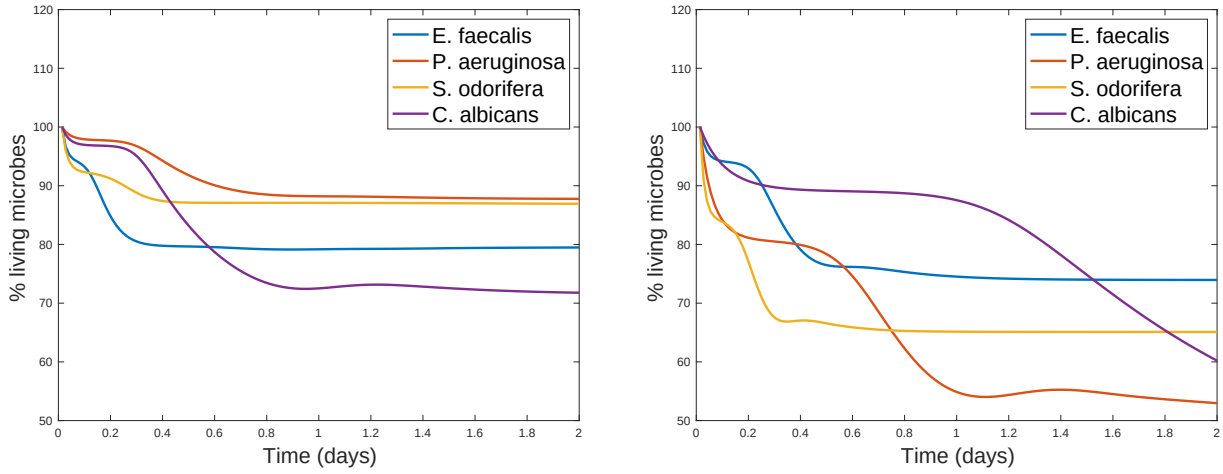

(a) (b)

Figure 3.6: Model predicted percent of living cells over time for anaerobic conditions (a) and aerobic conditions (b).

3.8 Long-term growth dynamics

We can predict long-term outcomes of microbial dynamics by examining the steady-state solutions of our model [48, 80]. The steady-states of the model are found by solving the non-linear system

$$0 = \frac{rz^n}{K_s^n + z^n} x(1 - x - y) - dx \tag{3.23}$$

$$0 = dx - \gamma y \tag{3.24}$$

$$0 = -\delta xz + \mu y. \tag{3.25}$$

Note that we have dropped the bars over the scaled quantities. This system has two categories of solutions. First, there is a positive steady-state given by

$$x^* = \frac{\gamma\left((r-d) - d\left(\frac{K_s\delta\gamma}{d\mu}\right)^n\right)}{r(d+\gamma)} \tag{3.26}$$

$$y^* = \frac{d\left((r-d) - d\left(\frac{K_s\delta\gamma}{d\mu}\right)^n\right)}{r(d+\gamma)} \tag{3.27}$$

$$z^* = \frac{d\mu}{\delta\gamma}. \tag{3.28}$$

Extinction in the model corresponds to solutions with $x = y = 0$, however, the model does not permit a unique value of z in this case so there are an infinite number of steady-states depending on the initial nutrient concentration z_0. This is not entirely unexpected, because if the population is prone to extinction then microbes will consume food until the population reaches zero and any remaining nutrient will remain in the capsule indefinitely. The model then exhibits a form of bi-stability in which the population will crash if there is not enough nutrient initially but otherwise will evolve to the positive steady-state.

The Jacobian of the model when $x = y = 0$ is of the form

$$J = \begin{bmatrix} \frac{rz^n}{K_s^n+z^n} - d & 0 & 0 \\ d & -\gamma & 0 \\ -\delta z & \mu & 0 \end{bmatrix}, \tag{3.29}$$

which has a zero eigenvalue and corresponding eigenvector $(0, 0, 1)^T$, indicating the model has a one-dimensional center manifold along the z-axis [117]. The phase portraits in Figure 3.7 show trajectories of the system for various initial nutrient concentrations for both sets of *P. aeruginosa* parameters. In these phase portraits, blue dots represent initial conditions and red terminal positions. For sufficiently high nutrient, the model moves to the positive steady-state in which the microbial population persists in the long term. Figure 3.7b is a

zoomed-in view of the low z_0 curves showing the range where the change in dynamics occurs. These curves show that with low z_0, the amount of living cells decreases monotonically while the dead cell density initially increases before diminishing as the cells lyse. The curves end along the z-axis with a z value representing however much nutrient is leftover after all the cells have died.

The two categories of steady-state represent extinction and long-term persistence. The long-term persistence solution is of interest because it represents scenarios in which the microbial community utilizes programmed cell death and autolysis, or slower metabolic activity in response to limited resources for group survival. The nutrient depletion rate δ and re-absorption rate μ are key parameters in determining the long-term outcome, so we performed parameter sweeps of them along with the initial condition z_0. Figure 3.7 shows stability diagrams for the range of δ (c, g) and μ (d, h), yellow regions represent the positive steady-state, and blue represents extinction. We see that consuming nutrient too quickly or recycling it too slowly causes the population to crash. Both sets of figures have straight-line segments separating the two regions, these represent bifurcation values where the stability of the steady-state changes.

3.9 Dynamic oxygen and nutrient concentrations

The model we have developed in this chapter considers a growing microbial population whose growth rate depends on the availability of oxygen and nutrient. So far, we have considered the case where nutrient is a limited resource and oxygen is constant but either at concentration zero or essentially infinite. A more realistic scenario is one in which oxygen and nutrient are both depletable and dynamic, rather than fixed. To consider this, we can extend the current model to include terms for in-flow and metabolization of nutrient and oxygen. This model

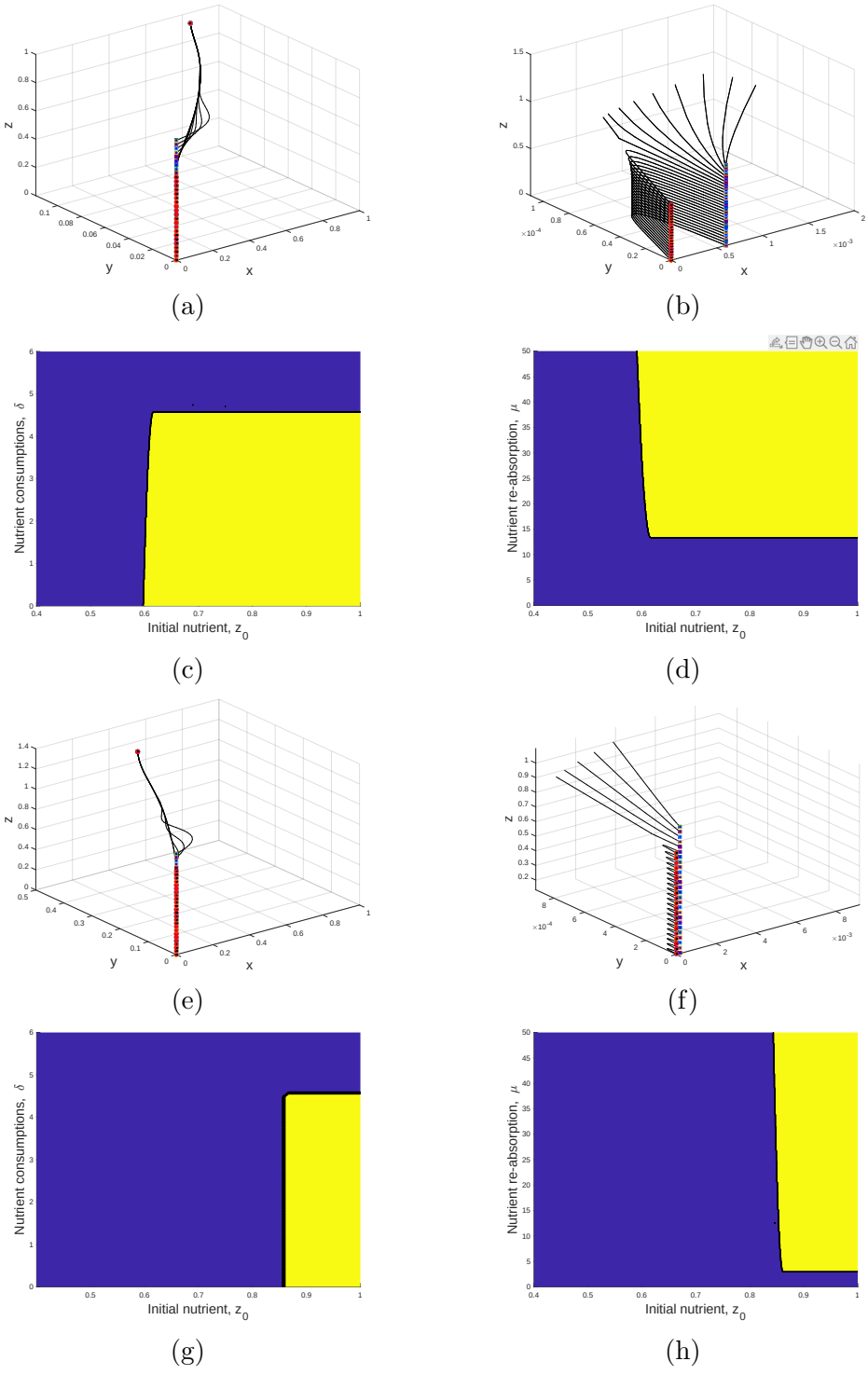

Figure 3.7: Phase portraits and stability diagrams for anaerobic (a-d) and aerobic (e-h) *P. aeruginosa* simulations. The phase portraits show trajectories of the model for a range of initial nutrient concentrations, blue dots are initial conditions, and red dots are steady-state solutions. The phase portraits in (b) and (f) are zoomed in to show where trajectories move from the z-axis to the positive steady state. Blue regions in the stability diagrams represent parameter values that cause extinction, yellow regions correspond to the positive steady-sate. These diagrams represent stability in the $z_0 - \delta$ and $z_0 - \mu$ space.

can be written

$$\frac{dx}{dt} = f(w,z)x(1-x-y) - dx \tag{3.30}$$
$$\frac{dy}{dt} = dx - \gamma y \tag{3.31}$$
$$\frac{dw}{dt} = \lambda_w - g_w w - \eta x w \tag{3.32}$$
$$\frac{dz}{dt} = \lambda_z - g_z z - \delta x z + \mu y \tag{3.33}$$

where λ_w, λ_z, g_w, g_z are the recruitment and per capita decay rates for oxygen and nutrient, respectively, and η is the microbial consumption rate of oxygen. Figure 3.8 shows a comparison between simulations with constant and dynamic oxygen concentrations, using the best-fitting *P. aeruginosa* parameter values. The depletable oxygen resulted in less overall growth, as lower oxygen caused a decrease in the oxygen-dependent function $f(w,z)$.

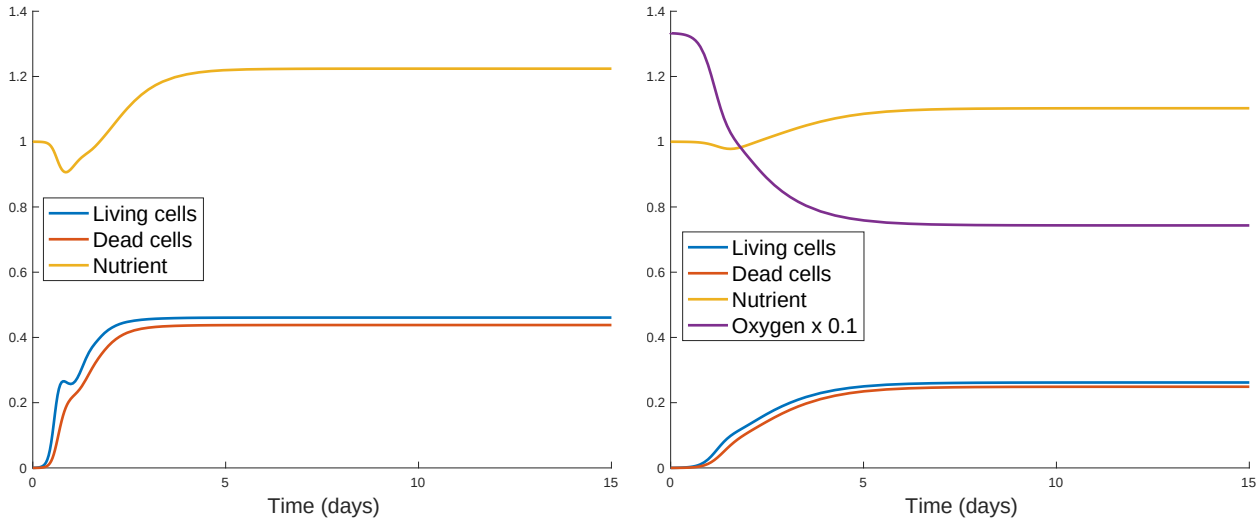

(a) (b)

Figure 3.8: Simulation of *P. aeruginosa* with constant (a) and depletable (b) oxygen concentrations. Having a depletable oxygen concentration resulted in less growth overall.

3.10 Conclusion

In summary, the goal of this chapter was to develop a mathematical model capable of quantifying growth characteristics of several pathogenic microbes found in cystic fibrosis airways. We modeled microbial growth as a function of available nutrient, considered three different nutrient-dependent growth functions to identify the most likely mechanisms of action of the microbial dynamics, and used the Akaike Information Criterion to select the best fitting growth function. While Michaelis-Menten mechanics have previously been used to model nutrient-dependent growth, our results here show that the use of Hill coefficients can better describe microbial growth dynamics [3, 101]. By fitting our model to *in vitro* data, we were able to estimate growth parameters for several CF pathogens in aerobic and anaerobic conditions. These data were collected via optical density measurements and because OD measurements only estimate total cell density, we included compartments corresponding to living and dead cells. By also including terms accounting for autolysis and nutrient recycling, our model may increase the utility of OD measurements by providing a more complete picture of the dynamics taking place.

One drawback of this study is the assumption that OD is directly proportional to cell density. There are scenarios where this assumptions holds, but in general this relationship is only linear in certain conditions and varies between species. Calibration curves that relate OD to cell density can be constructed on a case-by-case basis, but this is a laborious process itself and these curves are only useful for the species they were constructed for [102]. Some related issues are the OD measurements are less reliable above OD = 1, which occurred for two out of our eight data sets, and that the sizes of individual cells can change based on environmental factors. While the measurements are less reliable, very high OD values indicate high cell densities which were captured by our modeling. The large number of parameters we fit is another possible limitation. While our estimates were identifiable in most cases (seven out of eight), experimental estimates for parameters such as the per capita death rate, lysis rate,

or rate of nutrient consumption would decrease uncertainty in the remaining parameters.

To conclude, the mathematical model presented in this chapter allowed us to quantify and parameterize basic growth characteristics of four CF pathogens. The parameters estimated from experimental growth curves can now be incorporated into more complicated models of the CF lung ecosystem, as well as to catalog basic characteristics of the microbes we investigated in a quantitative manner. Since much of the treatment for CF lung infections involves the use of antibiotics, these results could also potentially be used to investigate treatment options to be used clinically.

Chapter 4

Modeling Aerobic and Anaerobic Communities in Cystic Fibrosis Airways

In this chapter, we extend the ideas of nutrient and oxygen-dependent growth from Chapter 3 to include aerobic and anaerobic communities inside of a CF airway. We validate this model against a longitudinal data set of microbial abundances collected from a patient undergoing a CF pulmonary exacerbation and treatment with antibiotics. There is evidence that CFPEs are associated with high abundances of fermentative anaerobes, so we explore oxygen effects and targeted antibiotics with the aim to prevent the anaerobes from becoming the majority community.

4.1 Introduction

Cystic fibrosis results from mutations in the CF transmembrane conductance regulator gene that regulates anion transport and, thus, mucus hydration and function associated with epithelia. Mucus accumulation in the airways interferes with gas exchange and respiratory function [25, 57]. Viscous mucus results in poor mucociliary clearance and eventual long-term polymicrobial biofilm airway infection. Over time, host inflammatory responses to these infections cause airway remodeling, progressive bronchiectasis, and eventually respiratory failure [26, 51, 54].

Numerous microbes colonize CF airways, and a greater diversity of microbes has been associated with better health in people with CF [19]. Ecological theory has been used to categorize the various bacteria, viruses, and fungi that cause illness in CF [26, 87]. Some microbes adapt to the airway environment and consume resources, such as oxygen, creating favorable conditions for other microbes to reproduce [84]. Such resource-altered conditions may create a complex community dynamic wherein some species disproportionately affect the environment, creating opportunities for other pathogens to thrive [86]. In this regard, oxygen, in particular, serves as a vital resource altering the environment through its inhibitory effects on some species while being favorable for others [28].

Current ecological models and evidence support the existence of two functional classes of microbes colonizing the CF airway: aerobic and anaerobic communities. The aerobic community comprises facultative and obligate aerobic bacteria and is relatively slow-growing. In contrast, the anaerobic community comprises primarily facultatively anaerobic, faster-growing, and pathogenic bacteria [26]. The anaerobic community is only transiently abundant but produces waste products associated with acute episodes of severe illness, known as cystic fibrosis pulmonary exacerbations (CFPEs) [87, 88]. CFPEs are marked by significant declines in pulmonary function and increased respiratory symptoms, and require intravenous

antibiotics and frequent hospitalization to reduce microbial density and improve overall condition [33, 38]. In some cases, microbes may activate the immune system to destroy lung tissue, creating a larger spatial niche for the anaerobic community. In addition, anaerobes produce fermentation products that support the growth of an anaerobic biofilm [39].

Here, we use mathematical modeling to track the ecological dynamics of the aerobic and anaerobic communities and determine how oxygen availability and antibiotic use affect each community's abundance. While there has been some modeling work related to CF airways [41, 70, 84, 86, 120, 121], these models have not considered polymicrobial communities, functional classes such as aerobic or anaerobic, nor how microbes in CF airways are influenced by oxygen availability. We develop an ODE model of the two communities and a depletable oxygen concentration to gain basic insight into the ecological dynamics and validate it with data from a patient undergoing treatment for a CFPE. We then perform analysis and numerical simulations to determine optimal strategies for treating the anaerobic community with targeted antibiotics. The data fitting we employ offers essential tools for designing treatment protocols according to patient-specific parameters.

4.2 Patient data

The data used in this chapter were obtained via sputum samples from a patient at the University of California, San Diego Adult Cystic Fibrosis Clinic over thirty-nine days [97]. this timeframe was divided into three periods: Period A - the first 25 days during which the patient was treated with broad-spectrum antibiotics, Period B - the next 8 days when the patient was off antibiotics, and Period C - the remaining 4 days in which the patient was treated with the antibiotic clindamycin targeting the anaerobic community [98]. The patient experienced a rapid decline in lung function at day 0 when the cystic fibrosis rapid response (CFRR) was initiated [97], and lung function improved during the period of hospitalization in

Period A. Six days after discharge (Period B), the individual's lung function again declined, leading to the clindamycin treatment in Period C. Sputum samples were collected on days 0, 14, 19, 26, 28, 31, 33, 35, and 38. At each time point, relative abundances of eight genera from two communities were available based on previous ecological classifications [26]: the climax community (*Rothia, Pseudomonas, Haemophilus, Neisseria,* and *Prevotella*) and the attack community (*Veillonella, Staphylococcus,* and *Streptococcus*), which we use as proxies for the aerobic and anaerobic communities.

4.3 Ordinary differential equation model

We model two microbial communities, one aerobic and one anaerobic using generalized Lotka-Volterra equations. The aerobic community is denoted by C and the anaerobic community by F, with respective growth rates r_c and r_f and common carrying capacity K. The two communities' growth rates depend on the amount of available oxygen, so their growth rates are functions of oxygen and are denoted by $r_c(W)$ and $r_f(W)$, where W is the concentration of oxygen. To model the aerobic and anaerobic nature of the two communities, we assume that $r_c(W)$ and $r_f(W)$ are increasing and decreasing functions of W, respectively. The aerobic and anaerobic communities are cleared at per capita rates d_c and d_f, respectively, resulting from mucociliary clearance, intrinsic death, immune responses, and treatment with antibiotics [16, 43, 66, 72, 93]. Since oxygen is toxic to anaerobic, F can also be killed at rate q due to oxygen toxicity [47]. Oxygen dynamics are governed by flow-in at rate λ, metabolization by the lung at per capita rate μ, and consumption by aerobic microbes at rate η.

The aerobic community grows slowly in low oxygen conditions and more quickly as the oxygen concentration increases. However, the aerobic growth rate does not increase indefinitely, even with a very high oxygen concentration. We describe this phenomenon using an E-max model,

which increases as oxygen increases up to a saturating level [49, 60, 65]. The E-max model is parameterized by a maximum possible growth rate, β, the concentration of oxygen which corresponds to half of the maximum rate, b, and a Hill's coefficient, n, which determines the sensitivity of the growth rate to changes in oxygen. The two communities also contain facultatively anaerobic microbes which can grow with or without oxygen. We account for the presence of facultative anaerobes by including an oxygen-independent term, β_{min}, in both growth functions. The aerobic and anaerobic growth rate functions are can be written as

$$r_c(W) = \beta \frac{W^n}{b^n + W^n} + \beta_{min} \tag{4.1}$$

and

$$r_f(W) = \beta \left(1 - \frac{W^n}{b^n + W^n}\right) + \beta_{min}, \tag{4.2}$$

respectively. The patient data set we use to validate the model consists of three time periods, denoted A, B, and C. No antibiotics were used in Period B. In Period A, the patient was given broad-spectrum antibiotics (colistin, vancomycin, piperacillin, and ceftazidime) which killed both types of microbes but moreso the aerobic community [55, 68]. During Period C, clindamycin was used to kill the anaerobic community only [98]. To capture the treatment protocol implemented for this patient, we consider both broad-spectrum and anaerobic-specific antibiotics. Death due to broad-spectrum antibiotics is denoted by d_{BS}, death due to clindamycin by d_{clin}, and natural death by d_N. Then the total death rates of each community under antibiotic treatment become

$$d_c = d_n + d_{BS} \tag{4.3}$$

$$d_f = d_n + \gamma d_{BS} + d_{clin} \tag{4.4}$$

where $\gamma \in [0, 1]$ measures the extent to which the broad-spectrum antibiotics are less effective

in killing anaerobic microbes. According to the patient's treatment schedule, $d_{BS} > 0$ in Period A and $d_{BS} = 0$ in Periods B and C. Likewise, $d_{clin} = 0$ in Periods A and B and $d_{clin} > 0$ in Period C. The full model can be written as

$$\frac{dC}{dt} = r_c(W)C\left(1 - \frac{C+F}{K}\right) - d_cC \tag{4.5}$$

$$\frac{dF}{dt} = r_f(W)C\left(1 - \frac{C+F}{K}\right) - d_fF - qFW \tag{4.6}$$

$$\frac{dW}{dt} = \lambda - \mu W - \eta CW. \tag{4.7}$$

A schematic diagram of the model is shown in Figure 4.1.

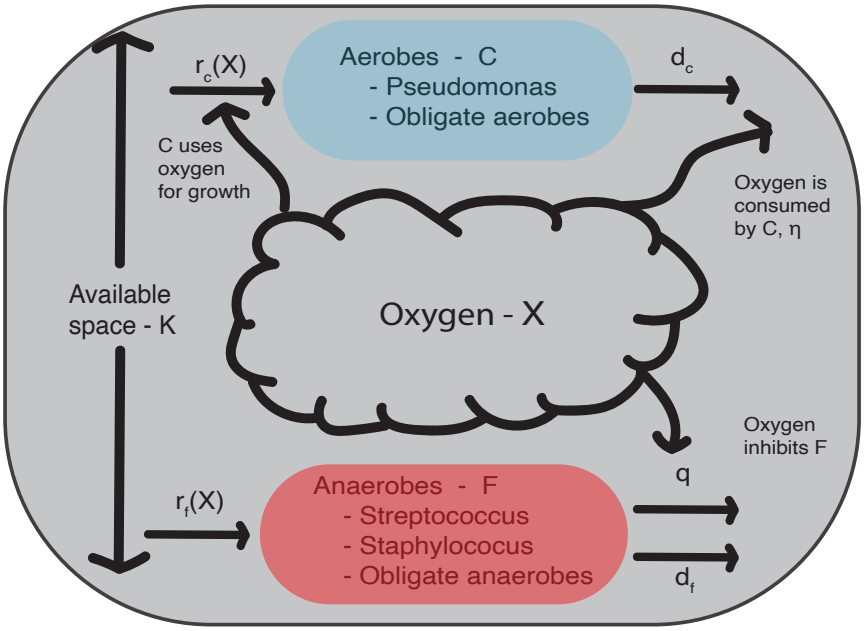

Figure 4.1: Schematic diagram of the oxygen-based community dynamics model. Aerobes and anaerobes compete for a common carrying capacity, K. Aerobes grow faster in high oxygen concentrations and anaerobes in lower oxygen concentrations. Oxygen is depleted by aerobes and is toxic to anaerobes.

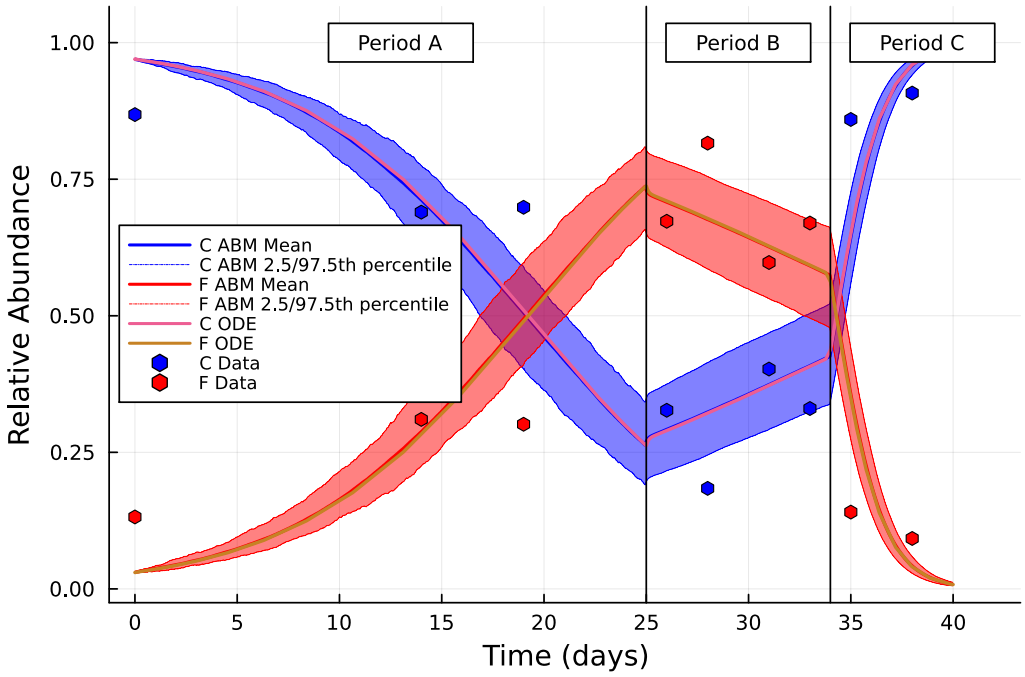

Figure 4.2: Patient data and fit of models to patient data. Sampling time is shown on the x-axis and the relative abundances of aerobic (blue) and anaerobic (red) communities are plotted on the y-axis. Mean, 2.5^{th} and 97.5^{th} percentiles of 500 agent-based simulations are shown for comparison to best-fitting ODE solution and patient data. In Period A, the patient was receiving broad-spectrum antibiotics. In Period B, the patient was released from the hospital and off antibiotics. In Period C, the patient was receiving the antibiotic clindamycin. Lung function declined around day 30 [97], indicating onset of exacerbation.

4.4 Parameter estimation

Cowley et al. used oxygen microsensors to obtain oxygen profiles in CF sputum samples and found nearly all samples to be anoxic with steep oxygen oxygen gradients at the air-mucus interface [28]. They showed areas free of mucus to have concentrations of 200-300 μM O_2 and the mucus interior to have concentrations of 1 - 3 μM O_2 with a steep gradient between the two regions. Cystic fibrosis is known to increase patients' respiratory rates, i.e., the number of breaths taken per minute. Perpati et al. observed a mean resting respiratory rate of 23 breaths per minute in a cohort of 18 adults with CF. Therefore, we take the per capita

decay rate of oxygen as $\mu = 23 \times 60 \times 24 = 3.3 \times 10^4\ day^{-1}$ [81]. We estimated the initial concentration, W_0, from the available data and take the oxygen inflow rate as $\lambda = \mu W_0$.

In vitro microbial densities of $10^8\ CFU\ ml^{-1}$ have been observed in aerobic conditions; however, densities as high as $10^12\ CFU\ ml^{-1}$ have been observed in CF sputum samples so we chose $K = 10^9$ as the carrying capacity [92, 103]. The patient data had a microbial density of $6.7 \times 10^8\ CFU\ ml^{-1}$ which we take as the initial population density, denoted by N_0, and use this value to estimate the initial relative abundances, C_0 and F_0 by fitting the model to the data. We obtain values for C_0 and F_0 by taking $C_0 = \alpha N_0$ and $F_0 = (1-\alpha)N_0$ and estimating the fraction $\alpha \in [0, 1]$ from the data.

Note that the clinical data were reported in relative abundances of the microbial communities. From the model, the corresponding relative abundances can be computed using $\frac{C(t)}{C(t)+F(t)}$ and $\frac{F(t)}{C(t)+F(t)}$ for the aerobic and anaerobic communities, respectively. Broad-spectrum antibiotics were in use and killed cells from both communities during the 25 days of Period A. Thus, for Period A, $d_c = d_N + d_{BS}$ and $d_f = d_N + \gamma d_{BS}$ with $d_{BS} > 0$ and $0 < \gamma < 1$. For Period B, the patient was off antibiotics, and thus $d_c = d_f = d_N$. In Period C, clindamycin was killing the anaerobic community, so $d_f = d_N + d_{clin}$ [97].

We performed computations in MATLAB [67] - we obtained numerical solutions for the system of ODEs and used the solutions to obtain parameter values which minimized the sum of squared residuals given by

$$J(p) = \sum_{i=1}^{m} \left(\left(\frac{C(t_i)}{C(t_i) + F(t_i)} - C_i \right)^2 + \left(\frac{F(t_i)}{C(t_i) + F(t_i)} - F_i \right)^2 \right), \tag{4.8}$$

where $p = (W_0, \alpha, \beta, \beta_{min}, \eta, d_N, d_{BS}, \gamma, d_{clin}, q, b, n)$ and m is the number of data points collected over the 38 days of observation. C_i and F_i are the i^{th} data points for the aerobic and anaerobic communities, respectively, and $C(t_i)$, $F(t_i)$ are the corresponding values predicted by the model. Best-fitting parameter estimations are shown in Table 4.1. For each estimate,

we obtained 95% confidence intervals by bootstrapping the residuals 500 times [10, 34]. Figure 4.2 shows a simulation of the model with the best-fitting parameter values. The bands surrounding the ODE solution curves represent the 2.5^{th} and 97.5^{th} percentiles of an ensemble of 500 runs of an analogous agent-based model, discussed in Chapter 6.

The estimated oxygen consumption rate η (1.8×10^{-7} day^{-1}) is similar to what has been previously observed [92]. *Staphylococcus, Streptococcus,* and *Pseudomonas* have doubling times between 20 minutes and 1.5 hours in laboratory conditions [32, 58, 40]. These doubling times correspond to exponential growth rates of 10 - 50 day^{-1}, which is consistent with our estimated maximal growth rate $\beta = 26.12$ day^{-1}. The estimated half-saturation value of oxygen, b, was 12.13 μM, higher than what had previously been measured for *P. aeruginosa* alone [49]. The estimated value represents an average of the two microbial communities, however, so a higher value is expected in the model. Similarly, the estimated slope-factor n was 1.72. The death rate due to broad-spectrum antibiotics, d_{BS}, for the aerobic community was an order of magnitude larger than the natural death rate d_N. Broad-spectrum antibiotics were 18% less effective against the anaerobic community ($\gamma = 0.82$) than the aerobic community. In Period A, antibiotics were suppressing both communities, but more so the aerobes, which allowed the anaerobic community to reach approximately 75% abundance. Period B saw a slight downward trend in the anaerobic community, but it remained significantly more abundant than the aerobic community. During Period C, we estimated the clindamycin efficacy to be $d_{clin} = 0.76$, which rapidly suppressed the anaerobic community.

Table 4.1: Parameter descriptions and best-fitting values for the oxygen-based microbial dynamics model

Parameter	Value (95% confidence interval)	Description	Source
β	26.21 day^{-1} (25.95 - 27.94)	Maximal microbial growth rate	Estimated
b	12.13 μM (12.11 - 12.18)	Oxygen-half saturation constant	Estimated
n	1.72 (1.64 - 1.76)	Growth rate slope factor	Estimated
β_{min}	3.22×10^{-5} day^{-1} (3.16×10^{-5} - 3.36×10^{-5})	Minimum microbial growth rate	Estimated
d_n	0.52 day^{-1} (0.51 - 0.53)	Natural microbial death rate	Estimated
d_{BS}	4.94 day^{-1} (4.68 - 5.01)	Broad-spectrum antibiotic death rate	Estimated
γ	8.20×10^{-1} (8.16 - 8.26×10^{-5})	Anaerobic antibiotic resistance coefficient	Estimated
q	1.12×10^{-7} μM day^{-1} (1.10 - 1.14×10^{-7})	Oxygen toxicity rate	Estimated
K	10^9	Carrying capacity	[92, 103]
d_{clin}	7.64×10^{-1} day^{-1} (7.61×10^{-1} - 7.77×10^{-1})	Clindamycin efficacy	Estimated
μ	3.3×10^4 μM day^{-1}	Oxygen decay rate	[28, 81]
λ	4.4×10^5 μM day^{-1}	Oxygen in-flow rate	[28, 81]
η	1.8×10^{-7} day^{-1} (1.64×10^{-7} - 1.83×10^{-7})	Oxygen consumption rate	Estimated
α	0.97 (0.94 - 0.98)	Fraction of initial population in aerobic community	Estimated
N_0	6.7×10^8	Initial population size	[97]
C_0	6.5×10^8	Initial aerobic population	Estimated
F_0	2.0×10^7	Initial anaerobic population	Estimated
W_0	13.18 μM (13.14 - 13.24)	Initial oxygen concentration	Estimated

4.5 Long-term dynamics: Aerobic and anaerobic communities under constant oxygen

To analyze out model, we first consider the case when the oxygen concentration is constant, say $W = W_0$, then the oxygen dependent growth rates r_c and r_f become fixed depending on the value of W_0. The larger of the two growth rates is determined by the value of W_0 relative to the half-saturation value b, i.e., $r_c > r_f$ when $W_0 > b$ and $r_f > r_c$ when $W_0 < b$. When considering each community's death rate separately as d_c and d_f, where each can contain separate terms accounting for intrinsic death, antibiotics, and oxygen toxicity, the model becomes

$$\frac{dC}{dt} = r_c C\left(1 - \frac{C+F}{K}\right) - (d_N + d_{BS})C \tag{4.9}$$

$$\frac{dF}{dt} = r_f F\left(1 - \frac{C+F}{K}\right) - (d_N + \gamma d_{BS} + d_{clin} + qW_0)F. \tag{4.10}$$

This model admits three steady-state solutions: the extinction steady-state given by $(0, 0)$, the aerobic-only steady-state given by, $\left(\frac{K(r_c-(d_N+d_{BS}))}{r_c}, 0\right)$, and the anaerobic-only steady-state given by, $\left(0, \frac{K(r_f-(d_N+\gamma d_{BS}+d_{clin}+qW_0))}{r_f}\right)$. We determined which of the three steady-states the model evolves toward via linear stability analysis [48, 80]. Conditions for both communities to go extinct can be written in terms of the inequalities $\frac{r_c}{d_N+d_{BS}} < 1$ and $\frac{r_f}{d_N+\gamma d_{BS}+d_{clin}+qW_0} < 1$, i.e., when each community's death rate is larger than its growth rate. This shows that both communities can be driven to extinction by increasing the death rates via sufficiently strong broad-spectrum antibiotics. The aerobic-only steady-state is achieved if both $\frac{r_c}{d_N+d_{BS}} > 1$ and $\frac{r_c}{d_N+d_{BS}} > \frac{r_f}{d_N+\gamma d_{BS}+d_{clin}+qW_0}$. These conditions indicate that only the aerobic community survives if the growth-death ratio of the aerobic community is larger than unity and larger than that of the anaerobic community. Similarly, the anaerobic-only steady-state is achieved if $\frac{r_f}{d_N+\gamma d_{BS}+d_{clin}+qW0} > 1$ and $\frac{r_f}{d_N+\gamma d_{BS}+d_{clin}+qW0} > \frac{r_c}{d_N+d_BS}$.

This steady-state analysis shows that if a broad-spectrum antibiotic is not strong enough to cause death rates larger than growth rates, the only microbial community that will survive depends on the oxygen concentration and anaerobic-specific antibiotics. Obtaining $r_c > r_f$ for a higher oxygen level (large W_0) causes the anaerobic community to go extinct, and vice-versa for small W_0. For an intermediate oxygen level, the surviving community is determined by the value of the anaerobic-specific antibiotic with the aerobic-only steady-state achieved for a sufficiently strong anaerobic-specific antibiotic strength. Notably, assuming a constant oxygen concentration does not allow for the co-existence of the two communities.

4.6 Long-term dynamics: Aerobic and anaerobic communities under quasi-steady-state oxygen

Oxygen concentrations may not be constant in CF airways [28], thus, we now adjust the model to analyze the long-term dynamics of the two communities when oxygen is at a quasi-steady-state. Introducing the scaled variables $c = C/K$ and $f = F/K$ and taking $\beta_{min} = 0$, the population equations become

$$\frac{dc}{dt} = \left(\frac{\beta W^n}{b^n + W^n}\right) c(1 - c - f) - d_c c \tag{4.11}$$

$$\frac{df}{dt} = \beta \left(1 - \frac{W^n}{b^n + W^n}\right) f(1 - c - f) - d_f f - qfW. \tag{4.12}$$

Because oxygen has a much faster turnover than the two microbial communities we take it to be at a quasi-steady-state, i.e., $\frac{dW}{dt} = 0$, which gives the oxygen concentration as

$$W = \frac{\lambda}{\mu + \eta K c}. \tag{4.13}$$

After some algebraic manipulation, the equations for c and f become

$$\frac{dc}{dt} = \left(\frac{\beta\lambda^n}{\lambda^n + b^n(\mu + \eta Kc)^n}\right) c(1 - c - f) - d_c c \tag{4.14}$$

$$\frac{df}{dt} = \beta\left(1 - \frac{\lambda^n}{\lambda^n + b^n(\mu + \eta Kc)^n}\right) f(1 - c - f) - \frac{q\lambda}{\mu + \eta Kc} f - d_f f. \tag{4.15}$$

In this case, in addition to extinction, aerobic only, and anaerobic-only steady-states, the model also admits a coexistence steady-state in which both communities persist. This indicates that oxygen dynamics play a critical role in the coexistence of the two communities. As in the constant oxygen case, we can derive analytical conditions for the extinction steady-state via linear stability analysis [48, 80]. This analysis shows that the model will evolve to the extinction steady-state if the following three conditions are satisfied:

$$\mu > 0 \tag{4.16}$$

$$d_c > \frac{\beta}{1 + \left(\frac{\mu b}{\lambda}\right)^n} \tag{4.17}$$

$$d_f > \frac{\beta}{1 + \left(\frac{\lambda}{\mu b}\right)^n} - q\frac{\lambda}{\mu}. \tag{4.18}$$

The terms on the right of the second and third inequalities are the minimal death rates needed to drive the aerobic and anaerobic communities to extinction and can be increased via antibiotics.

Due to the highly nonlinear form of the growth rate functions, we did not derive analytical conditions for the three remaining steady-states, and instead examined them using phase plane analysis. The coexistence steady-state exists in the $cf-$plane where the curves given by $\frac{dc}{dt} = 0$ and $\frac{df}{dt} = 0$ intersect in the first quadrant (Figure 4.3a). The location of the intersection point changes depending on parameter values, and local bifurcations occur where the intersection point crosses either the $c-$ or $f-$axes. This represents a change in the long-term behavior of the system as it shifts from a coexistence equilibrium to the extinction of

one (or both) communities.

Since the anaerobic community may be associated with acute illness, parameter values for which the anaerobes are in the minority are desirable clinically [87]. Thus, we are interested in parameter values that cause the anaerobic community to be less than 50% abundant at equilibrium. The steady-state values for c and/or f are shown in Figure 4.3. These simulations where performed with an intrinsic death rate $d_N = 0.52$ while varying a broad-spectrum antibiotic response d_{BS}, giving $d_c = d_f = d_N + d_{BS}$. Figure 4.3b shows the scaled populations at steady-state as d_{BS} is varied. For $d_{BS} < 10\ day^{-1}$, the anaerobes were the majority community. Only for $d_{BS} > 10\ day^{-1}$ did the aerobic community become more abundant, and as d_{BS} continued to increases both communities became extinct at equilibrium. Similarly, the heatmaps in Figure 4.3c and Figure 4.3d show the value of f at steady-state for ranges of q (oxygen toxicity) and η (oxygen consumption) and Hill function parameters b and n. Lighter regions correspond to parameter values with higher densities of f at equilibrium and, therefore, a more severe disease state. Exacerbated and non-exacerbated states are separated by the curves given by $\frac{f}{c+f} = 0.5$. These simulations show that exacerbations occur when oxygen consumption is high and toxicity is low, which depends on the makeup of the microbial community, as well as for smaller values of b and n.

4.7 Transient dynamics: Time to exacerbation

We can use our ODE model to observe short-term dynamics of the aerobic and anaerobic communities. In the available single patient data set, the anaerobic community went from 12% to 70% relative abundance in $\sim$ 26 days under broad-spectrum antibiotics. We used the best fitting parameters as a baseline to examine the amount of time necessary for the anaerobes to grow to become the dominant community, i.e., 50% relative abundance [85, 87], which we refer to as the "switch time". This length of time can be interpreted as the time

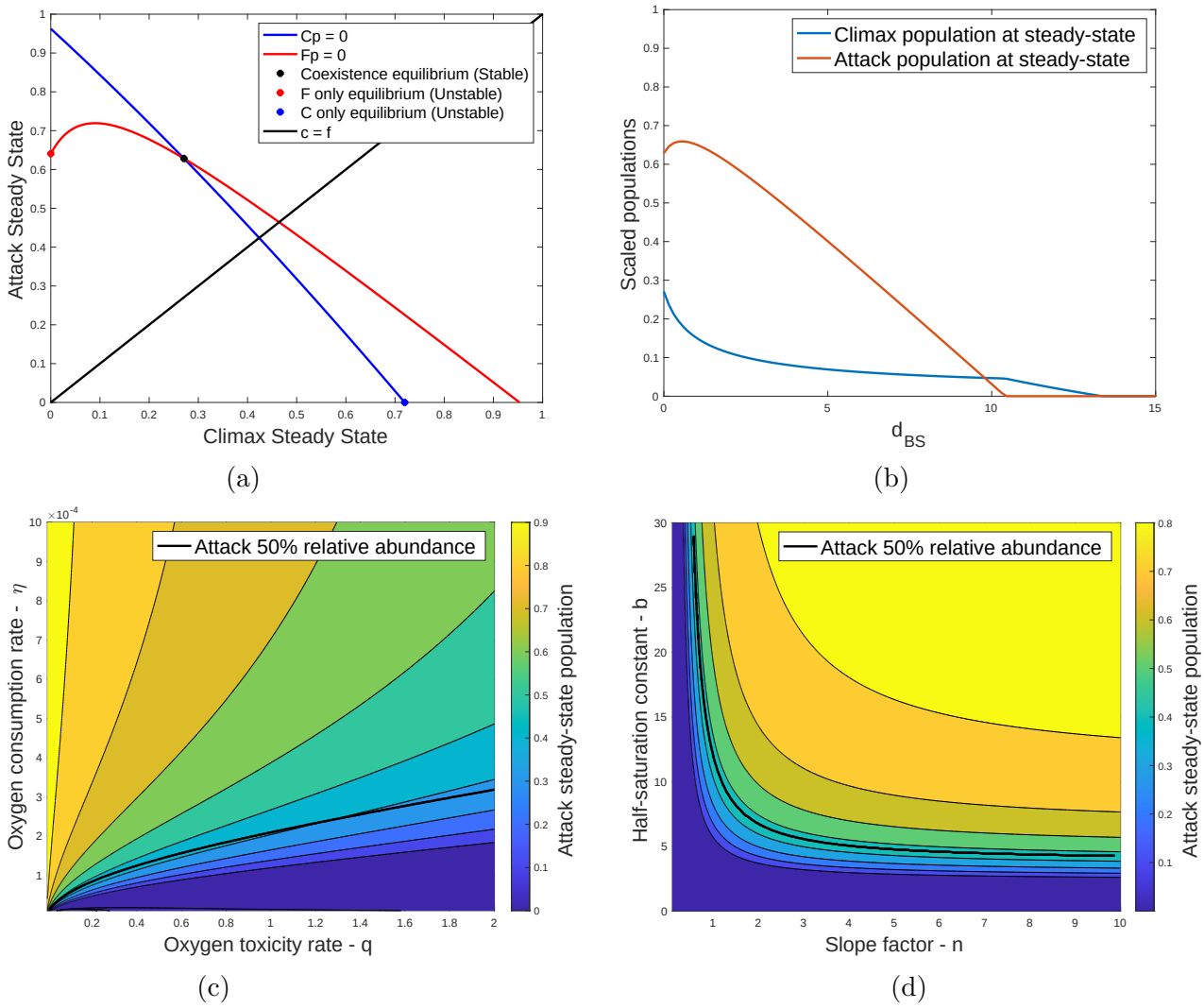

Figure 4.3: Coexistence steady-state densities fo aerobic and anaerobic communities. (a) The nullclines $\frac{dc}{dt} = 0$ and $\frac{df}{dt} = 0$ in the first quadrant with best fitting parameters, $\eta = 1.8 \times 10^{-4}$ and $q = 0.3$. (b) Equilibrium population densities for $d_{BS} \in [0, 15]$. (c) Coexistence level of f for a range of q and η values, the region above and to the left of the black line is exacerbated at equilibrium. (d) Coexistence levels of f for a range of n and b values, the region in the top right is exacerbated at equilibrium.

it takes a CF patient to transition from a stable state to a CFPE and we can use it to investigate how increased oxygen and antibiotics can delay or prevent CFPEs. This switch time may be useful in designing suitable protocols for antibiotic administration based on patient-specific parameters.

We simulated the model from the initial base conditions and obtained switch times for varying oxygen flow rates λ and antibiotic strengths d_{BS} and d_{clin}, shown in Figure 4.4. In general, increasing λ gave an advantage to the aerobic community and increased the population switch time. Increasing λ sufficiently can prevent the anaerobic community from ever reaching 50% relative abundance, and therefore, prevent a CFPE (represented by the white regions in Figures 4.4a and 4.4b). Figure 4.4b shows the switch time whilst varying λ and the anaerobic-targeting treatment d_{clin} and demonstrates that a targeted drug can prevent exacerbation with a much smaller dose than compared to a broad-spectrum antibiotic.

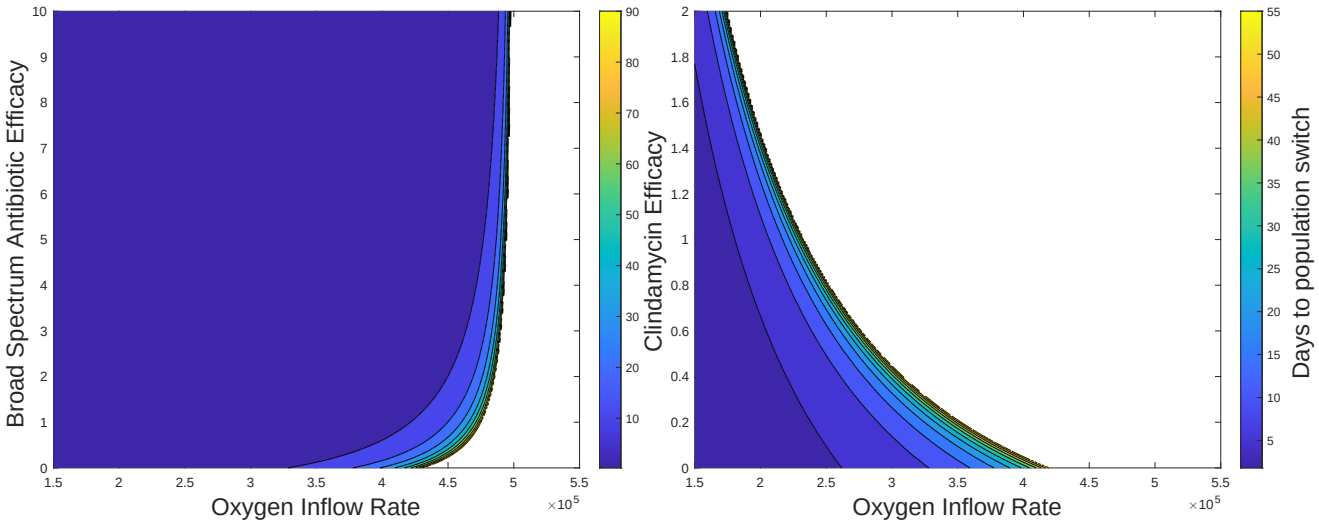

(a) (b)

Figure 4.4: Time to population switch for a range of oxygen flow rates and antibiotic responses. (a) Population switch time as a function of d_{BS} and λ. (b) Population switch time as a function of d_{clin} and λ. Color indicates the time necessary for the anaerobic community to reach majority. White regions are parameter values in which the anaerobic community never reaches majority and exacerbation does not take place.

4.8 Sensitivity analysis

We determined the sensitivity of the ODE model to changes in parameters values by computing the Sobol indices for nine parameters [42, 94, 99, 123]. For each of the nine parameters, we calculated the first-order and total-effect indices for the population switch time and anaerobic equilibrium level. We performed the computation using the GlobalSensitivity.jl Julia package with $n = 1024$ Sobol samples [31], these indices are shown in Figure 4.5. In the parameter space we search, the slope-factor n, oxygen in-flow rate λ, and oxygen consumption rate η had the largest effect on population switch time variance, while the maximal growth rate β, oxygen toxicity rate q, n, λ, and μ all had similar total effects on the anaerobic equilibrium level.

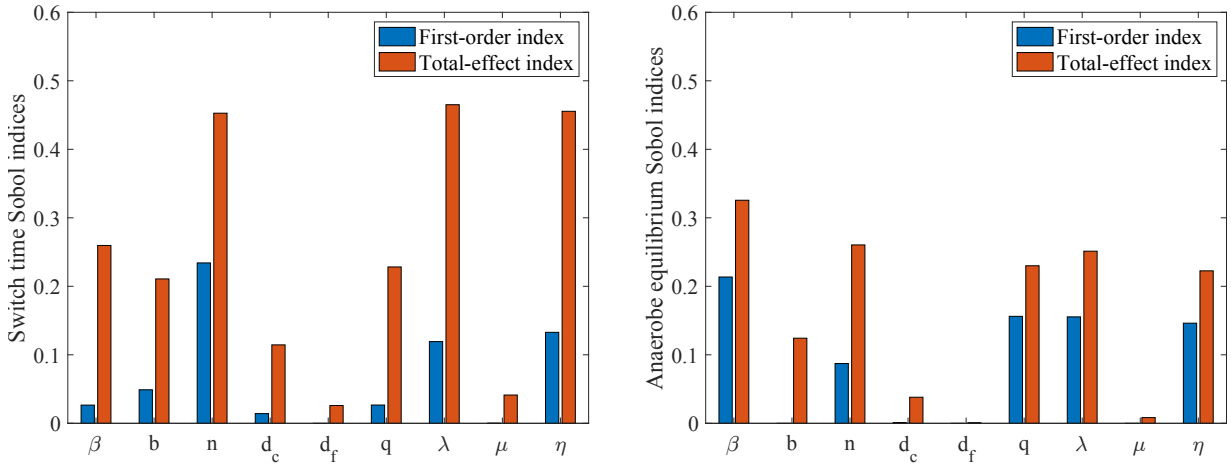

Figure 4.5: First-order and total-effect Sobol indices for population switch time (a) and anaerobic population at equilibrium (b).

4.9 Strategies for controlling the anaerobic community with antibiotics

Pulmonary exacerbations may be associated with higher abundances or metabolic activity of anaerobic microbes [87]. We used our model to investigate ways to keep the anaerobic population low via antibiotics, starting in a parameter regime in which a population switch occurs in eleven days with no treatment. To determine antibiotic strategies to keep the anaerobes in the minority, we solved the model with an anaerobe-targeted antibiotic for a number of days, followed by a number of days with no treatment. The top row of Figure 4.6 shows two simulations with different treatment timings, anaerobe-targeting antibiotics begin at the solid vertical lines and end at the dashed lines. In the simulation on the left, antibiotics are in use for three days, followed by fourteen days with no treatment; this schedule allows the anaerobic community to reach majority. The simulation on the right has the time on treatment increased from three to seven days and is able to prevent a population switch. The second row of Figure 4.6 shows simulations performed for a range of treatment and off-treatment times for antibiotic strength $d_f = 0.4$ (left) and $d_f = 0.8$ (right); yellow regions indicate that the anaerobic community never reaches 50% relative abundance for that timing, and blue regions indicate that a population switch occurs.

We also tested alternative strategies for treating the anaerobic community by exploring the model in different parameter spaces. The third row of Figure 4.6 shows a potential option to reduce the anaerobic community by using aerobe-targeted antibiotics. In Figure 4.6e, the aerobic community is killed with antibiotics beginning after five days and the resulting increase in oxygen concentration causes the anaerobic community to crash. Figure 4.6f shows the three possible outcomes of treating the aerobic community based on the antibiotic strength d_c. Low values of d_c still allow the anaerobic community to persist and achieve a majority. And intermediate d_c allows aerobes to persist and anaerobes to go extinct due

to increased oxygen, and a large d_c causes the aerobes to also go extinct. These three scenarios are separated by critical values of d_c, which we can determine via linear stability analysis [48, 80]. We numerically found the minimum antibiotic efficacy required to eliminate the anaerobic community to be $d_c = 4.61\ day^{-1}$, the minimum strength to eliminate both communities we found analytically as

$$d_c = \frac{\beta\lambda - d_n\lambda - bd_n\mu}{\lambda + b\mu}. \tag{4.19}$$

These two critical values are shown as vertical lines in Figure 4.6f.

4.10 Conclusion

Loss of pulmonary function is the predominant health concern associated with cystic fibrosis. Acute pulmonary exacerbations cause irreversible damage to the airways, and represent a leading cause of shortened lifespan for people with CF. In this chapter, we develop a quantitative framework for studying the interactions of the two major functional groups in the cystic fibrosis airway ecosystem. We developed an ODE model of the two communities in the presence of a depletable oxygen concentration and validated it against a clinical data set of microbial abundances.

We analyzed our model to obtain analytical results that show that a dynamic oxygen concentration is necessary for the coexistence of the two communities. Sensitivity analysis of the model parameters determined quantitative conditions showing that pulmonary exacerbations occur when oxygen inflow and toxicity are low, or oxygen consumption by aerobic bacteria is high. Stability analysis of the ODE model informed possible strategies for treating CF lung infections. These results quantify the advantage the aerobic bacteria have when oxygen flow is increased in the system and shed light on how increasing oxygen can prevent exac-

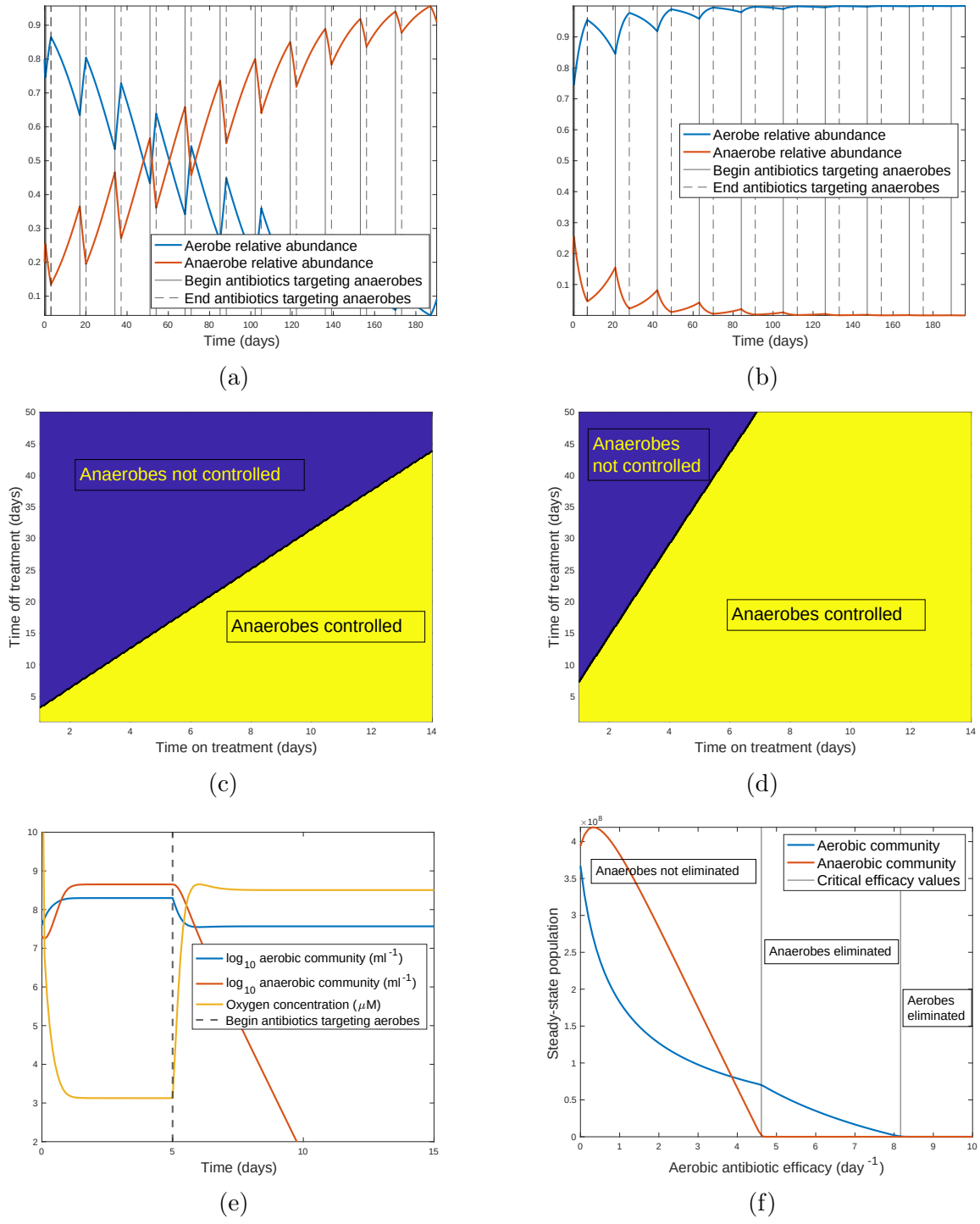

Figure 4.6: Antibiotic strategies for treating the anaerobic community. (a) and (b) Simulations with antibiotics targeting the anaerobic community. (c) and (d) Show treatment timings that allow for control of the anaerobic community with targeted antibiotics with efficacies of 0.4 day^{-1} (c) and 0.8 day^{-1} (d). (e) shows a simulation in which the anaerobic community is driven extinct by treating the aerobic community. The possible scenarios for treating the aerobic community and corresponding critical values are shown in (f).

erbations. We also studied the effects of various antibiotic treatments intended to keep the anaerobic population level low, these results demonstrate that anaerobes may be controlled using targeted antibiotics or by leveraging oxygen-related effects such as consumption and toxicity.

Most of the parameter values used in the model were estimated from data; however, the data set was from a single patient and is thus limited, and the estimated values may not be identifiable. Despite this, most of the estimated values were consistent with values from literature sources and the model was able to capture the multiple features embedded in the data set. The parameter estimates would need to be verified with a larger data set to give more confidence in the estimated values. Future work should also include more microbial species to provide detail into the intra-community dynamics, to investigate, e.g., competition between different aerobic and/or anaerobic microbial species, and to reduce uncertainty in the fitted parameter values. The time to exacerbation metric was based on previous network analysis associating fermentative anaerobes with pulmonary exacerbations [87]. The modeling in this chapter focused on oxygen dynamics and antibiotics; however, other chemical and environmental factors may affect the CF microbiome [41, 86]. The simple nature of the model discussed here clearly demonstrates the effects of oxygen dynamics in the interaction between aerobic and anaerobic microbes and our results can be implemented in future investigations of the CF airway microbiome. Similarly, the models discussed can be used in conjunction with multi-omics to determine optimized antibiotic treatments [18, 25].

In summary, this study developed a mathematical model the the CF airway microbiome and identified several potential strategies for preventing and treating pulmonary exacerbations. Conditions that best prevent the expansion of anaerobic activity were identified which may be beneficial for designing ideal treatment protocols for CF patients.

Chapter 5

Spatiotemporal Modeling of the Cystic Fibrosis Airway Microbiome

Building on the previous chapter, here we extend the oxygen-based community dynamics model to include spatial effects. By adding terms to account for spatial diffusion, we now describe aerobic-anaerobic dynamics with a reaction-diffusion partial differential equation system. We use this model to simulate microbial dynamics in three different scenarios of mucus aggregation in airways and perform analytical techniques to determine the minimum size for a mucus plug to support anaerobic growth. We also discuss a traveling wave solution to the model and examine the effect of pharmacodynamic properties of an anaerobe-targeting antibiotic.

5.1 Introduction

The ODE models discussed so far have all been spatially homogeneous, i.e., the model does not impose any kind of spatial structure and assumes that all of the dynamics take

place in a well-mixed environment. This is appropriate for some situations, e.g. bacteria growing in a test tube that is periodically being shaken, but this is not the case for modeling microbial community dynamics in a human airway. In fact, the CF airway is a geometrically complex structure and this spatial heterogeneity likely plays a significant role in the microbial community dynamics. While the spatially homogeneous model in Chapter 4 allowed us to gain basic insights into CF airway dynamics, that model cannot investigate spatially-dependent phenomena such as accumulation or spread.

In this chapter, we develop a spatiotemporal model to investigate the role of spatial dynamics in CF-lung infections and how oxygen effects determine how populations of pathogenic anaerobes accumulate over time. We use this model to determine the amount of hypoxic space needed for anaerobes to survive in aggregated mucus and the speed at which anaerobes can propagate through a mucus-clogged airway, and also show how effectively the anaerobic community is able to spread throughout an airway in various parameter spaces. Finally, we introduce a spatially-dependent anaerobe-targeting antibiotic and show that a drug with a high permeability in mucus may be effective in controlling anaerobic microbes in CF-lung infections.

5.2 Model development

Our model consists of three coupled partial differential equations with state variables corresponding to the aerobic community C, anaerobic community F, and oxygen concentration W, where each variable is a function of time t and location $\mathbf{x} = (x, y)$. Growth of the microbial communities is governed by logistic functions with oxygen-dependent growth rates and carrying capacity K. Microbial death occurs at per capita rates d_c and d_f, and death due to oxygen toxicity at rate q for the anaerobic community [3, 47, 49, 61]. The microbes spread spatially via diffusion with diffusion coefficients D_i, $i = c, f, w$.

We use Michaelis-Menten-like kinetics to model the oxygen-dependent growth rates of the two communities, wherein each community's growth is determined by a maximum growth rate β, half-saturation concentration b, and slope factor n [60, 65]. Since the aerobic community grows faster as the oxygen concentration increases, we take $\frac{\beta W^n}{b^n+W^n}$ as the aerobic growth function. The anaerobic community should grow slower as oxygen increases, hence we take the anaerobic growth function as $\beta\left(1-\frac{W^n}{b^n+W^n}\right)$.

Local oxygen dynamics are governed by an in-flow rate λ representing oxygen coming into the airway via respiration, per capita decay rate μ, and consumption by the aerobic community at rate η. The full model can be written as

$$\frac{dC}{dt} = \frac{\beta W^n}{(b^n+W^n)} C\left(1-\frac{C+F}{K}\right) - d_c C + D_c \Delta C \tag{5.1}$$

$$\frac{dF}{dt} = \beta\left(1-\frac{W^n}{b^n+W^n}\right) F\left(1-\frac{C+F}{K}\right) - d_f F - qFW + D_f \Delta F \tag{5.2}$$

$$\frac{dW}{dt} = \lambda - \mu W - \eta CW + D_w \Delta W. \tag{5.3}$$

5.3 Computational domain and boundary conditions

Cowley et al. investigated three scenarios in which mucus can accumulate inside CF airways and the oxygen gradient within aggregated mucus [28]. The three scenarios they discuss are A) a clogged alveolar sac, B) a mucus-lined airway, and C) a dislodged mucus plug; we represent these three scenarios as computational domains on which to solve our PDE. In each case, the microbial dynamics take place on a fixed, two-dimensional cross-section of the aggregated mucus. To model oxygen dynamics, we assume that oxygen is neither flowing into nor being metabolized within aggregated mucus and take $\lambda = \mu = 0$. Instead, we allow oxygen to flow into the domain by using Dirichlet boundary conditions at the appropriate boundaries, i.e., $w(\mathbf{x}_{boundary}, t) = w_B$, where $\mathbf{x}_{boundary}$ is the air-mucus interface and w_B

is the value of oxygen at the boundary. Inside the domain, oxygen is depleted solely via consumption by the aerobic community, i.e., $\eta > 0$.

We first consider the clogged alveolar sac in Scenario A. Alveolar sacs are small (200-500 um diameter) cavities where oxygen is transferred from the lung into the bloodstream, in CF these sacs can become completely congested with mucus and become non-functioning. In this case, we consider a rectangular cross-section in which the top of the rectangle represents the air-mucus interface, and inside the rectangle is the aggregated mucus. Mathematically we model this as a rectangular domain with a Dirichlet BC for oxygen along the top of the rectangle and no-flux BCs elsewhere. For the mucus-lined airway in scenario B, we consider the airway as a cylindrical column with a layer of mucus spreading inward from the radius of the column toward the center. Taking a cross-section of the column, we can formulate the domain for Scenario B as a donut-shaped region with oxygen penetrating from the inner radius of the donut. In this case, the oxygen Dirichlet BC is along the inner radius and no-flux BCs along the outer radius. In Scenario C, we assume a spherical mucus plug exposed to oxygen from all sides logged in an airway. The cross-section in this case will be a circle with Dirichlet oxygen BCs at the radius. For each case, we assume that microbes can only grow within the mucus matrix and cannot pass the boundary, which we implement with no-flux BCs for both communities. The schematics in Figure 5.1 depict the type of mucus aggregation, corresponding PDE domains, and oxygen conditions for the three scenarios.

5.4 Parameter estimation and nondimensionalization

In Chapter 4, we used a spatially homogeneous model to obtain estimates for the parameters governing local dynamics, i.e., the parameters other than the diffusion coefficients. We estimated those values by fitting a model to a longitudinal data set of microbial abundances obtained from a patient undergoing treatment for CF-lung infection [97]. Those values, and estimates for the diffusion coefficients are listed in Table 5.1.

Table 5.1: PDE parameter descriptions

Parameter	Value	Description	Source
β	26.21 day^{-1}	Maximal microbial growth rate	-
b	12.13 μM	Oxygen-half saturation constant	-
n	1.72	Growth rate slope factor	-
K	10^9	Carrying capacity	-
d_c	0.52 day^{-1}	Aerobic death rate	-
d_f	0.52 day^{-1}	Anaerobic death rate	-
q	1.12 $\mu M\ day^{-1}$	Oxygen toxicity rate	-
λ	4.4×10^5 $\mu M\ day^{-1}$	Oxygen in-flow rate	-
μ	3.3×10^4 day^{-1}	Oxygen decay rate	-
η	1.8×10^{-7} day^{-1}	Oxygen consumption rate	-
D_c	200 - 1900 $\mu m^2 s^{-1}$	Aerobic diffusion rate	[62]
D_f	200 - 1900 $\mu m^2 s^{-1}$	Anaerobic diffusion rate	[62]
D_w	2.4 - 26.8 $\times 10^{-6}$ $cm^2 s^{-1}$	Oxygen diffusion rate	[28]

Several of the parameters have very large values, therefore we nondimensionalize the model to make it more tractable computationally as well as to reduce the overall number of parameters [105, 106]. Introducing the scaled quantities $c = C/K$, $f = F/K$, and $w = W/b$, the

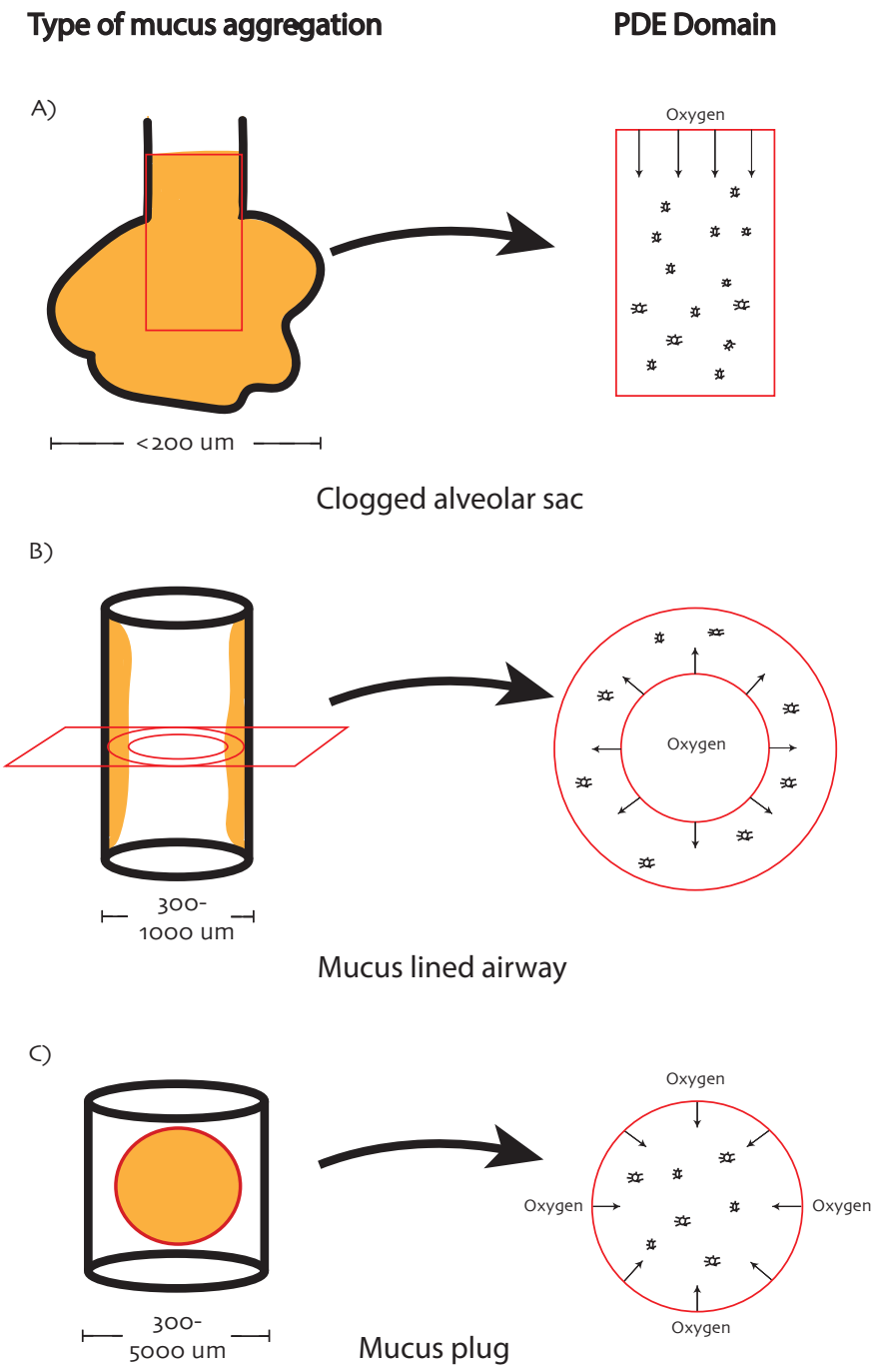

Figure 5.1: Schematic diagram of the three types of mucus accumulation and their corresponding computational domains. Scenario A is a clogged alveolar sac and is represented as a rectangle with oxygen entering from the top side. Scenario B is a mucus-lined airway and is represented as a donut with oxygen entering from the inner radius. Scenario C is a spherical mucus plug lodged in an airway and is represented as a circle with oxygen entering from the radius. Lengths in the left column are taken from [28].

nondimensionalized equations are

$$\frac{dc}{dt} = \frac{\beta^* w}{(1+w)} c\,(1-c-f) - d_c^* c + D_c^* \Delta c \tag{5.4}$$

$$\frac{df}{dt} = \beta^* \left(1 - \frac{w}{1+w}\right) f\,(1-c-f) - d_f^* f - q^* f w + D_f^* \Delta f \tag{5.5}$$

$$\frac{dw}{dt} = -\eta^* c w + \Delta w, \tag{5.6}$$

where we have scaled the time and space by factors $t_{fac} = \beta$ and $x_{fac} = \sqrt{\beta b / D_w}$, and taken $n = 1$ to improve numerical performance. Expressions for the scaled parameters are listed in Table 5.2. For the remainder of the chapter, we will drop the $*'s$ and discuss parameters in terms of the scaled values. We solve the model numerically using the pdepe function in MATLAB, which is based on the method of lines, and the FEniCS finite element package for Python [5, 63, 67].

Table 5.2: Scaled PDE parameter expressions

Parameter	Expression	Description
t_{fac}	β	Temporal scaling factor
x_{fac}	$\sqrt{\beta / D_w}$	Spatial scaling factor
β^*	β / t_{fac}	Scaled maximum growth rate
d_c^*	d_c / t_{fac}	Scaled aerobic death rate
d_f^*	d_f / t_{fac}	Scaled anaerobic death rate
q^*	qb / t_{fac}	Scaled oxygen toxicity rate
η^*	$\eta K / t_{fac} b$	Scaled oxygen consumption rate
D_c^*	D_c / Dw	Aerobe diffusion rate
D_f^*	D_f / Dw	Anaerobe diffusion rate

5.5 Basic dynamics of the aerobic and anaerobic communities

Figure 5.2 shows snapshots of the three mucus scenarios after the model has been simulated to an approximate steady-state. We started the two microbial communities with uniform initial distributions and in each of the three cases, the aerobic community became concentrated near the oxygenated boundary while the anaerobic community was more abundant in low-oxygen regions. Because there is little data available on the spatial distribution of oxygen and microbial species within CF-airways, we performed these simulations with a scaled set of parameters (see Table 5.2) to make the model more tractable numerically and focus on showing qualitative phenomena rather than identifying realistic parameter values, which are likely to vary between individuals.

These simulations show that our model can exhibit the basic dynamics we expect in mucus-clogged CF airways. Scenario A represents an alveolar sac completely clogged with mucus and exposed to oxygen at one end, represented by the top side of the rectangle in Figure 5.2A. Aerobes reach a higher population density at and near this boundary, farther away from top-boundary diffusion and consumption lower the oxygen concentration and allow the anaerobic community to be more abundant. The simulations for Scenarios B and C are similar. In Scenario B oxygen enters the domain from the inner radius of the donut and in Scenario C from the outer radius of the circle. In both cases, aerobes are more prevalent at the oxygenated boundary, and anaerobes more prevalent far away from it. In each scenario, aerobes reached population densities of approximately 1 and 0.3 in high- and low-oxygen regions, respectively, where anaerobes had densities of roughly 0.7 and 0.

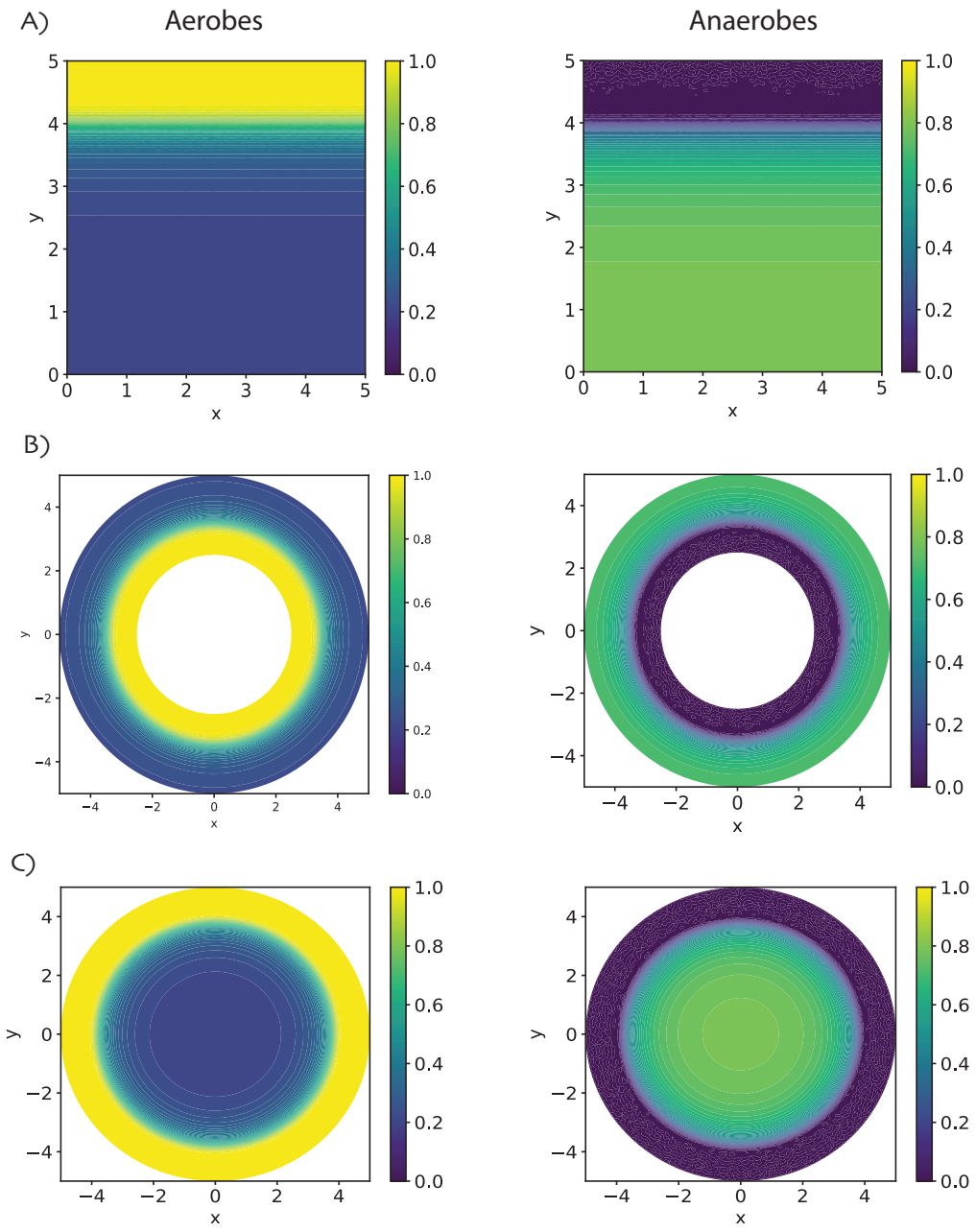

Figure 5.2: Snapshots of the model at approximate steady-state for the three mucus scenarios. Steady-state distributions are shown for the aerobic community in the left column and the anaerobic community in the right column. In each case, the aerobic community is concentrated near the source of oxygen, and the anaerobic community is concentrated in the hypoxic regions.

5.6 Critical domain size

5.6.1 Constant oxygen

We can use our model to predict the minimum size of a mucus plug required for anaerobic microbes to survive [46, 53, 73, 82]. Specifically, we identify how large a mucus plug must be to support a hypoxic region where anaerobic bacteria can survive. We first consider our model with a constant oxygen concentration. Such an estimation can be used, e.g., to determine the minimum mucus plug size on an individualized basis, or the size depending on how deep in an airway the plug is. We can obtain an analytical expression for the critical domain size by making some simplifying assumptions of our model. First, we assume a one-dimensional domain, which we can take as a 1D cross-section of the mucus plug in Scenario C. This domain can be taken as the interval $[0, L]$, and we impose death of the anaerobic community at the boundary with homogeneous Dirichlet BCs at $x = 0$ and $x = L$. Next, because the interior of a mucus plug is a low-oxygen environment and therefore very favorable to the anaerobic community, we assume that anaerobic death is negligible in the interior of the plug and take $q = d_f = 0$. Finally, because we desire an expression for the anaerobic community and to simplify the analysis, we briefly disregard the aerobic community, assuming that the total density of the two communities remains constant. With these assumptions, we can consider the single, one-dimensional PDE

$$\frac{df}{dt} = \beta \left(1 - \frac{w_0}{1 + w_0}\right) f(1 - f) + D_f \frac{d^2 f}{dx^2} f \tag{5.7}$$

for the anaerobic community, where w_0 is the constant oxygen concentration. This is an extension of the Fisher-KPP equation which has a well-known expression for the critical domain size [53, 73]. We desire a non-trivial steady-state solution to this PDE which satisfies the Dirichlet BCs $f(0, t) = f(L, t) = 0$. Steady-state solutions are given by the second-order

ODE

$$\frac{d^2f}{dx^2} = -\frac{\beta}{D_f}\left(1 - \frac{w_0}{1+w_0}\right) f(1-f). \tag{5.8}$$

Through the change of variables $u = f$, $\frac{du}{dx} = v$ we can derive an expression for the minimum mucus plug size via phase plane analysis [35, 53, 119]. The change in variables gives the system

$$\frac{du}{dx} = v \tag{5.9}$$

$$\frac{dv}{dx} = -\frac{\beta}{D_f}\left(1 - \frac{w_0}{1+w_0}\right) u(1-u), \tag{5.10}$$

with $u(0) = u(L) = 0$. This system has steady-state solutions at $P_1 : (u, v) = (0, 0)$ and $P_2 : (u, v) = (1, 0)$, and its Jacobian is given by

$$J = \begin{bmatrix} 0 & 1 \\ \frac{\beta}{D_f}\left(1 - \frac{w_0}{1+w_0}\right)(2u-1) & 0 \end{bmatrix}. \tag{5.11}$$

The eigenvalues for P_1 are $\xi_{1,2} = \pm i\sqrt{\frac{\beta}{D_f}\left(1 - \frac{w_0}{1+w_0}\right)}$ and for P_2 are $\xi_{1,2} = \pm\sqrt{\frac{\beta}{D_f}\left(1 - \frac{w_0}{1+w_0}\right)}$, hence, we see that P_1 is a center and P_2 is a saddle [48, 80]. Note that because P_1 is a center, solutions near the origin are given by the family of circles

$$(u(x), v(x)) = \left(c_1 \cos\left(\sqrt{\frac{\beta}{D_f}\left(1 - \frac{w_0}{1+w_0}\right)}x + \phi\right), c_1 \sin\left(\sqrt{\frac{\beta}{D_f}\left(1 - \frac{w_0}{1+w_0}\right)}x + \phi\right)\right), \tag{5.12}$$

for constant c_1's and where ϕ is a phase-shift to be determined. Solutions satisfying our boundary conditions are represented by half-circles starting from $(0, c_1)$ and terminating at

$(0, -c_1)$. Using the boundary at $x = 0$, we find that

$$0 = c_1 \cos\left(\sqrt{\frac{\beta}{D_f}\left(1 - \frac{w_0}{1+w_0}\right)} \cdot 0 + \phi\right) \tag{5.13}$$

$$0 = \cos(\phi) \tag{5.14}$$

$$\phi = \frac{\pi}{2}. \tag{5.15}$$

From the boundary at $x = L$, we have

$$-c_1 = c_1 \sin\left(\sqrt{\frac{\beta}{D_f}\left(1 - \frac{w_0}{1+w_0}\right)} \cdot L + \frac{\pi}{2}\right) \tag{5.16}$$

$$-1 = \cos\left(\sqrt{\frac{\beta}{D_f}\left(1 - \frac{w_0}{1+w_0}\right)} \cdot L\right) \tag{5.17}$$

$$\pi = \sqrt{\frac{\beta}{D_f}\left(1 - \frac{w_0}{1+w_0}\right)} \cdot L \tag{5.18}$$

$$\pi = \sqrt{\frac{\beta\left(1 - \frac{w_0}{1+w_0}\right)}{D_f}} \cdot L \tag{5.19}$$

$$L^* = \pi \sqrt{\frac{D_f}{\beta\left(1 - \frac{w_0}{1+w_0}\right)}}, \tag{5.20}$$

where L^* represents the minimum mucus plug size necessary for anaerobic growth - mucus plugs smaller than this will have oxygen concentrations high enough to prevent anaerobic growth. Heatmaps with parameter ranges for β, D_w, and w_0 (in dimensionless units) are shown in Figure 5.3. Clinically, a larger critical domain size is favorable, i.e., smaller mucus plugs may not be able to support an anaerobic population, and Figure 5.3 shows that L^* is an increasing function of β and a decreasing function of D_w. In these parameter spaces, the critical domain size ranges from approximately $L = 2$ to $L = 15$.

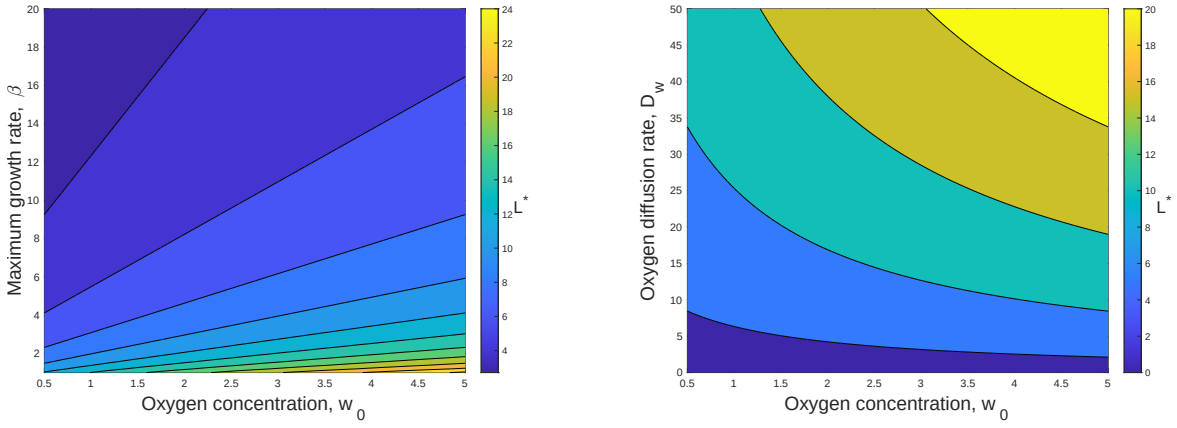

(a) (b)

Figure 5.3: Critical domain size for the anaerobic community under constant oxygen. Plots show the minimum size of a mucus plug that can support anaerobic growth as a function of w_0 and β (a) and w_0 and D_w (b).

5.6.2 Time-dependent oxygen

In the previous section, we neglected the dynamics of the aerobic community and oxygen concentration in order to derive an analytical expression for the minimum mucus plug size L^*. Here, we determine L^* numerically using the full, three-component model. We do this by simulating the model on a large number of domain sizes and parameter values. The computational procedure is as follows: first, we fix a set of parameters for which we want to compute L^*. Next, we fix a (small) domain size and simulate the model until it reaches steady-state and observe the steady-state distribution of the anaerobic community. If the anaerobic community has gone extinct, then we incrementally increase the domain size and repeat; if any anaerobes persist, then we take that domain size as the critical value L^*.

We repeated this procedure for a range of parameters and Figure 5.4 shows the critical domain size L^* as a function of aerobic oxygen consumption, aerobic and oxygen diffusion rates, and anaerobic oxygen toxicity. In each of the plots of Figure 5.4, the blue line represents the minimum mucus plug size for the corresponding parameter value. Domains sizes larger than the values given by the blue lines are large enough to support anaerobic growth while those

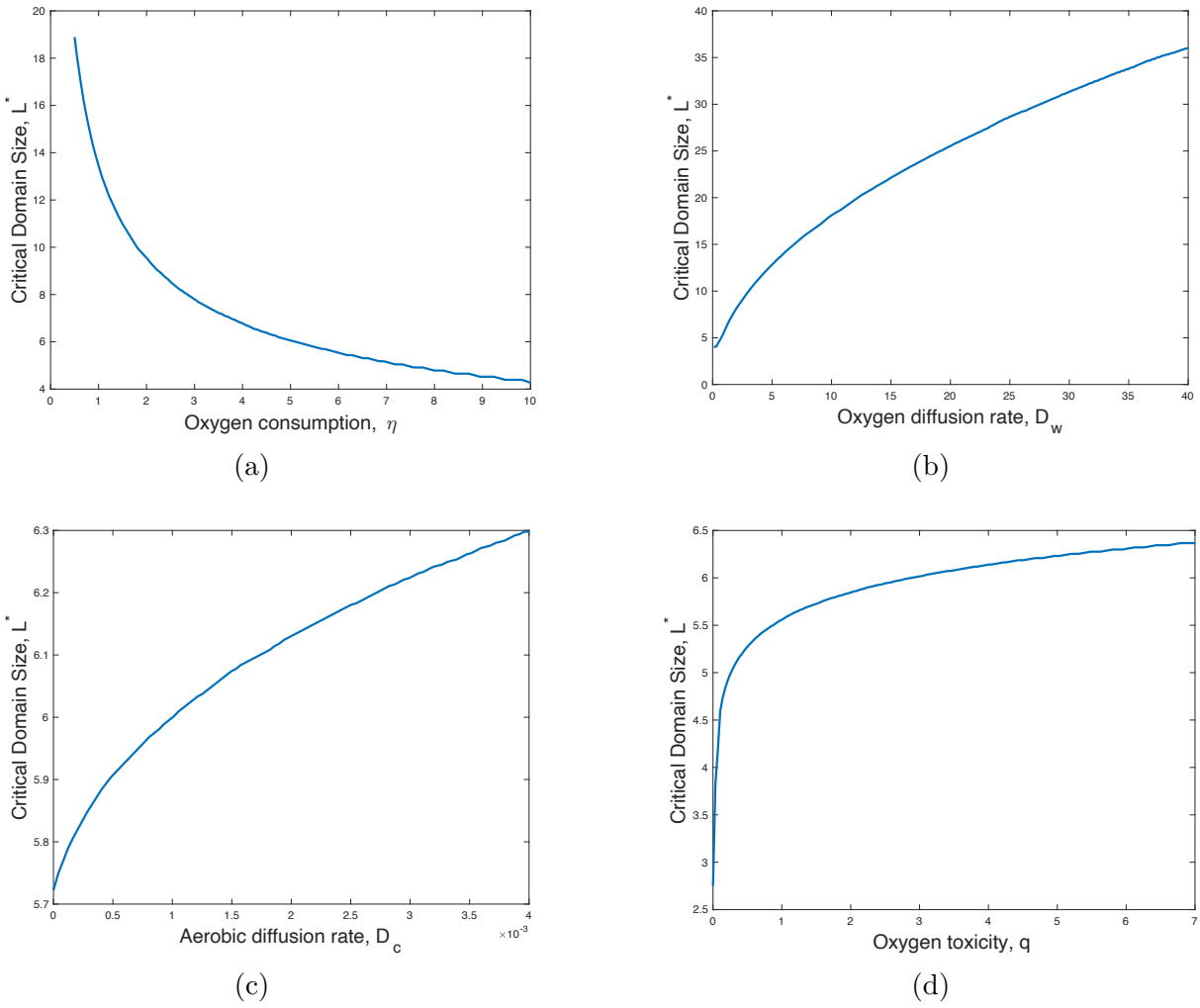

Figure 5.4: Critical domain sizes for various parameter ranges, clockwise from the top-left, oxygen consumption η, oxygen diffusion D_w, aerobic community diffusion D_c, and oxygen toxicity q. In each plot, the region above the blue line represents parameter values that cause the anaerobic community to go extinct but survive for values below the line.

less than the blue lines are small enough to prevent it. Of the parameters we investigated, we observed the consumption rate η and oxygen diffusion rate D_w to have larger effects than the aerobic diffusion rate D_c and oxygen toxicity rate q. We found that L^* is inversely related to η, and ranged between $L^* \approx 19$ for small η's approached $L^* \approx 4$ for larger η's. The largest parameter effect was from D_w, where L^* was $\sim$35 for large values. For D_c and q, L^* was in a much smaller range, between $\sim$2.5 and 6.5 for the values we simulated.

We were also able to observe the minimum mucus plug size phenomena in a two-dimensional

circular domain of radius L. Figure 5.5 shows the anaerobic components of two simulations, the left column with $L = 2$ and the right with $L = 6$. Due to computational costs, we did not determine the critical value L^* for the two-dimensional case, but we can infer that the simulation with radius $L = 2$ is below a threshold domain size and causes the anaerobes to go extinct. Conversely, $L = 6$ is a large enough domain for anaerobes to survive long-term.

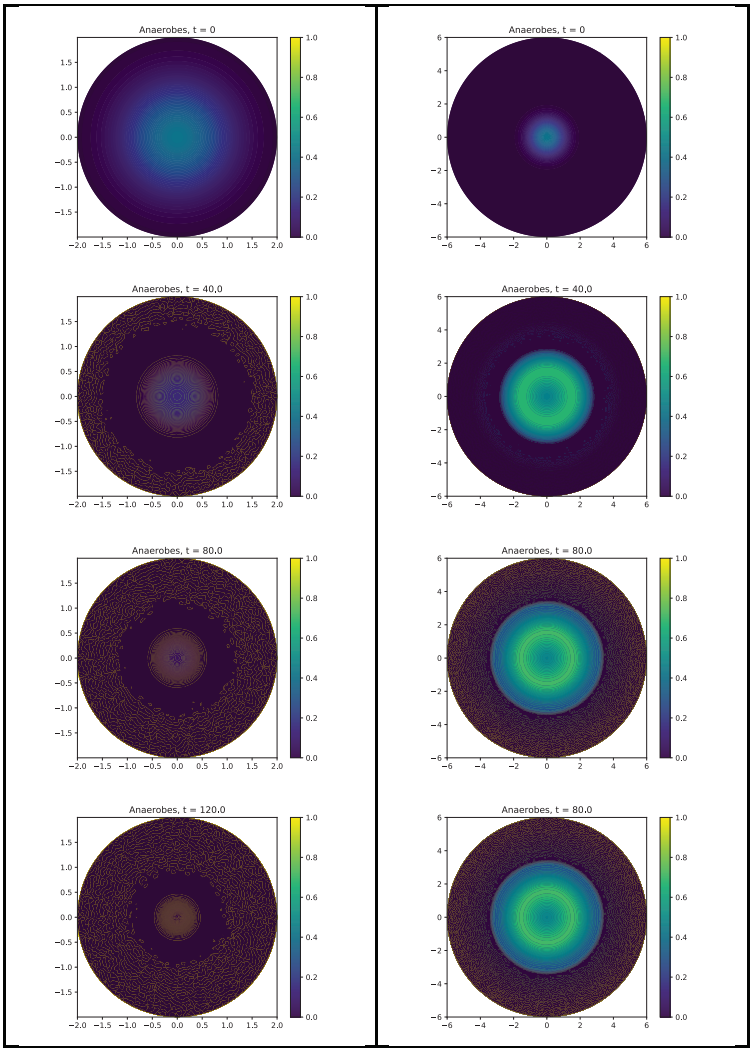

Figure 5.5: Two-dimensional simulation showing the effect of domain size on dynamics. In the left column, the domain is radius 2, and in the right radius 6 (note the different scales on the x- and y-axes between the two columns). The domain size on the left is below the critical value, so the anaerobes go extinct. On the right, the domain is large enough for the anaerobes to survive.

5.7 Maximum anaerobic spread

We are interested in determining how far the anaerobic community can spread throughout the lung and determining parameter spaces that result in low abundances of anaerobes. To observe this we simulated the model until it reached steady-state and recorded the length of the domain which was occupied by anaerobes. To measure this distance, we solved the model on a one-dimensional domain $[-L/2, L/2]$ with oxygen entering from the boundaries at $x = -L/2$ and $x = L/2$ and the anaerobes concentrated at the origin initially. After reaching steady-state, we take the distance from the origin to where there is no longer any anaerobic density (within a tolerance) as the maximum anaerobic spread. The heatmaps in Figure 5.6 show parameter sweeps for the maximum anaerobic spread as a function of β, d_f, D_f, D_w, η, and q, the color represents the distance that the anaerobic community reaches from the origin over a long time.

As seen in the previous section, the size of the domain plays a significant role in the dynamics of the two microbial communities, with a larger domain benefiting the anaerobic community by providing more hypoxic space to propagate. Therefore, we also varied the domain size in addition to the six parameters when plotting the anaerobic radius. Blue regions in each sub-figure of Figure 5.6 represent parameter values for which the anaerobes do not survive and which may be clinically favorable [87]. In the parameter spaces we searched, the largest anaerobic radius was about 8. The parameters D_f, β, and q showed a smaller overall effect on the spread, and for those heatmaps, the maximum spread varies mostly as a function of the domain size L. In contrast, η, D_w, and d_f had larger non-linear effects on the anaerobic spread, with the model predicting that anaerobes can be eliminated (i.e., have a radius of 0) with sufficiently low oxygen consumption, say $\eta \approx 0.05$ or high anaerobic death, say $d_f \approx 0.65$. The death rate d_f is particularly of note, as we can consider it as a control, e.g., with an antibiotic targeting the anaerobic community.

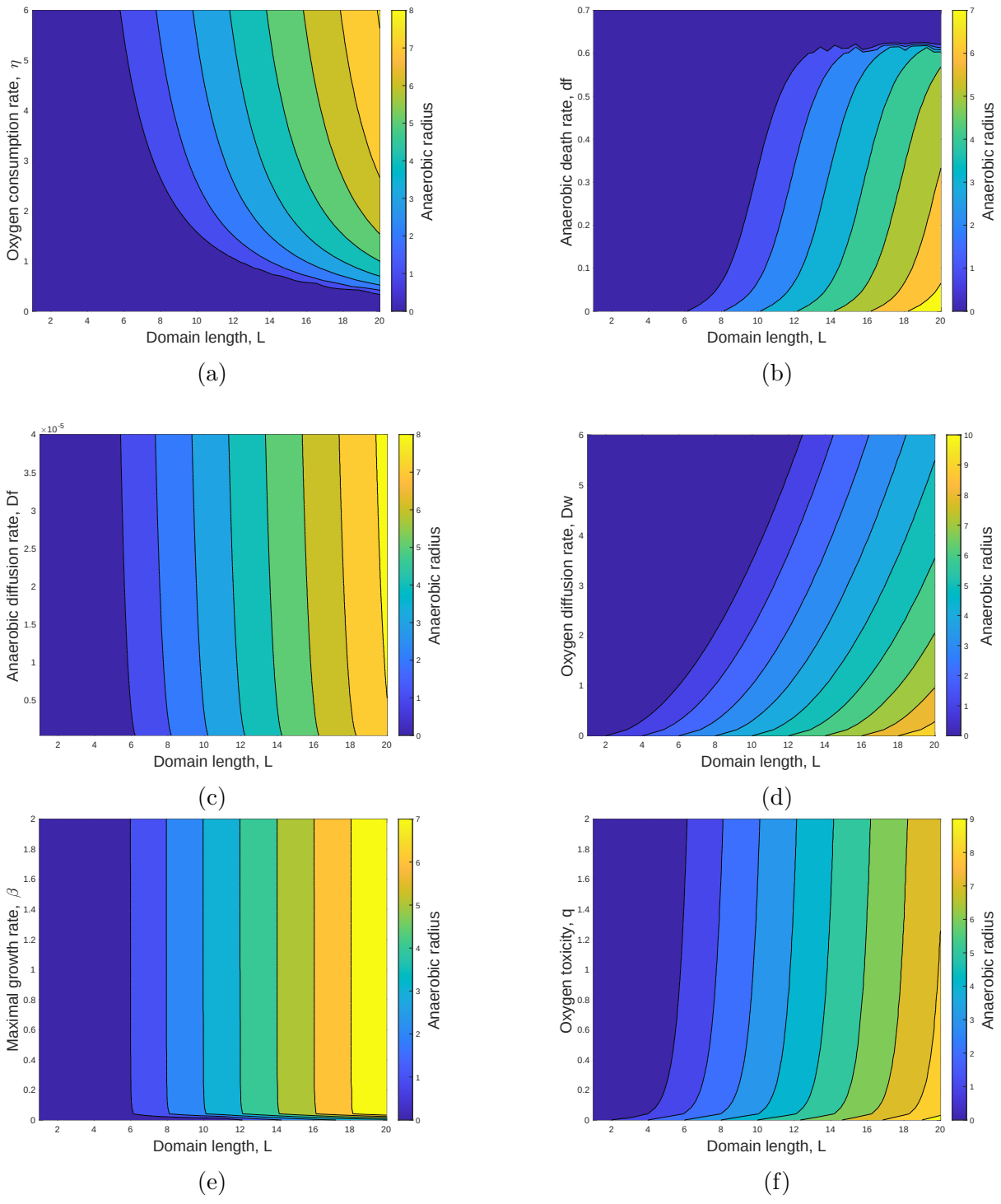

Figure 5.6: Heatmaps depicting the long-term anaerobic density in various parameter spaces. In each plot, the domain size L is on the x-axis, and another parameter on the y-axis. Darker regions represent lower anaerobic density at steady-state, lighter regions represent higher values.

5.8 Traveling wave solution

A traveling wave solution is a solution to a diffusion equation that maintains its shape and speed as it moves throughout the spatial domain [37, 50, 56, 76, 108]. We can use a traveling wave solution of our model to investigate the amount of time anaerobes need to propagate through a mucus-clogged region of an airway [28, 41]. For the simplest case, we consider only the anaerobic equation of the model with oxygen fixed in space, say $w(x) = w_0 e^{-ax}$. As a domain, we consider a mucus-filled airway exposed to oxygen at one end, e.g., a one-dimensional cross-section of the clogged alveolar sac in Scenario A where $x = 0$ corresponds to the air-mucus interface. The parameter a can be used to give a range of oxygen profiles corresponding to different microbial densities with steeper oxygen gradients corresponding to higher microbial densities [28]. A traveling wave solution to the PDE

$$\frac{df}{dt} = \beta \left(1 - \frac{w(x)}{1 + w(x)}\right) f(1 - f) - d_f f - q f w(x) + D_f \Delta f \tag{5.21}$$

is a function of the form $f = \phi(x - kt)$, where k represents the wave speed, i.e., the speed at which anaerobes propagate through the airway. With this solution we have $f' = df/dt = -k\phi'$ and $\Delta f = \phi''$ so the anaerobic PDE becomes the second-order ODE

$$-k\phi = \beta \left(1 - \frac{w(x)}{1 + w(x)}\right) \phi\,(1 - \phi) - d_f \phi - q\phi w(x) + D_f \phi''. \tag{5.22}$$

Note that because of the $w(x)$ terms this ODE is non-autonomous, so we cannot use phase-plane analysis to examine this system in the most general case [48, 80]. However, far away from the mucus-air interface, i.e., when $x \gg 0$, we have $\left(1 - \frac{w(x)}{1+w(x)}\right) \approx 1$. Additionally, $q\phi w(x) \approx 0$ for large x, and if we disregard the term $-d_f\phi$ then we can use phase-plane analysis to find the minimum traveling wave speed $k_{min} = 2\sqrt{D_f \beta}$. The anaerobic community will move in a traveling wave at this speed provided it has some non-zero initial distribution [35].

As for the critical domain size, we can analyze the anaerobic equation in the case of constant oxygen. Constant oxygen corresponds to no consumption of oxygen by microbes, i.e., $a = 0$ so that $w(x) = w_0$. The general reaction-diffusion equation with a traveling wave solution can be written

$$u' = \Delta u + F(u), \tag{5.23}$$

for the unknown function $u(x,t)$, and the minimum wave speed is computed as $k_{min} = 2\sqrt{F'(0)}$ [108]. For the anaerobic PDE with constant oxygen (and neglecting death terms), we have

$$f' = \beta\left(1 - \frac{w_0}{1+w_0}\right) f(1-f) + D_f \Delta f, \tag{5.24}$$

hence we can find the minimum speed of anaerobic propagation as

$$k_{min} = 2\sqrt{\beta\left(1 - \frac{w_0}{1+w_0}\right)}.$$

A high oxygen concentration may cause a non-biologically relevant complex value in this expression, which is expected given that the anaerobic community should not be able to move into a highly oxygenated region. A low oxygen concentration gives $k_{min} \approx 2\sqrt{\beta}$ as the speed at which anaerobes can spread through a clogged airway.

We again use the full model to simulate more realistic dynamics of a traveling wave through a CF airway, demonstrated in Figure 5.7. This simulation takes place on the one-dimensional domain $[0, L]$ with oxygen initially distributed as $w(x) = w_0 e^{-ax}$, Dirichlet BC $w(0) = w_0$ representing the air-mucus interface on the left boundary, and a no-flux condition on the right boundary. Aerobes are initially distributed uniformly with 0.4 density, and anaerobes are concentrated at the right, hypoxic boundary, both with no-flux conditions on both ends of the domain. The heat map on the left of Figure 5.7 shows the time series of the anaerobic

community. Initially concentrated on the far right, the anaerobes move in a wave formation at a constant speed until reaching the left, oxygenated part of the domain when the wavefront stops. The right plot of Figure 5.7 shows several snapshots of the anaerobes taken at equal time intervals showing the wavefront moving at a constant speed.

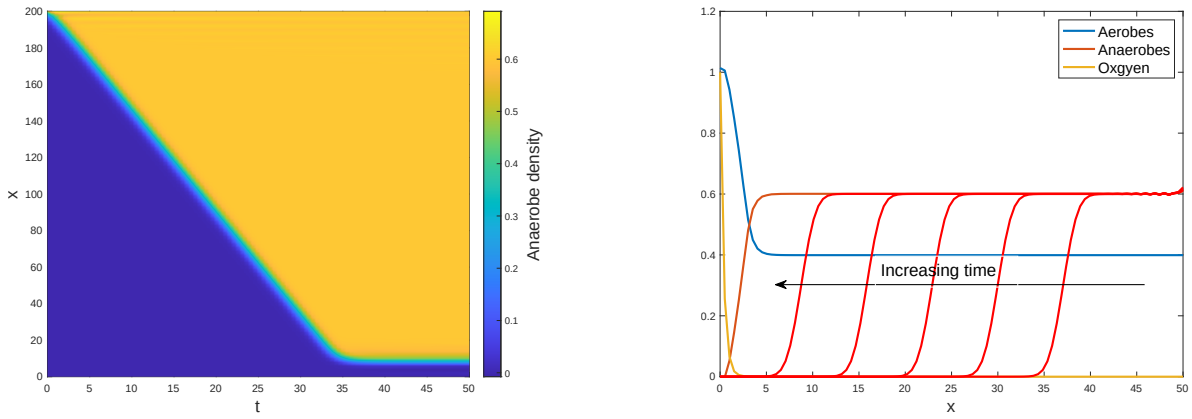

(a) (b)

Figure 5.7: A one-dimensional simulation showing the anaerobic community moving in a traveling wave. The heat map on the left shows the anaerobic wavefront moving through the hypoxic part of the domain until stopping at the oxygenated left boundary. The plot on the right shows several snapshots of this solution as well as the relatively stationary aerobic community and oxygen profiles.

5.9 Targeted antibiotic course

High abundances of anaerobic microbes have been associated with periods of acute disease known as pulmonary exacerbations [87], so using the model to predict a course of antibiotic treatments that minimize the anaerobic population would be clinically beneficial. We can simulate the effectiveness of an antibiotic targeting the anaerobic community by incorporating an anaerobe-targeting antibiotic into our model:

$$\frac{db}{dt} = -\alpha b + D_b \Delta b, \tag{5.25}$$

where $b(t)$ is the concentration of the antibiotic at time t, α is its per capita decay rate, and D_b is its diffusion rate [101]. Introducing another parameter δ for the antibiotic-induced anaerobic death rate, the model becomes

$$\frac{dc}{dt} = \frac{\beta w}{(1+w)} c\,(1-c-f) - d_c C + D_c \Delta c \tag{5.26}$$

$$\frac{df}{dt} = \beta \left(1 - \frac{w}{1+w}\right) f\,(1-c-f) - d_f f - q f w - \delta b f + D_f \Delta f \tag{5.27}$$

$$\frac{dw}{dt} = -\eta c w + \Delta w, \tag{5.28}$$

$$\frac{db}{dt} = -\alpha b + D_b \Delta b. \tag{5.29}$$

Similar to how we handle oxygen, we assume that the antibiotic has to move into the domain via diffusion rather than being generated within the mucus matrix. This can be modeled with Dirichlet BCs where we can consider the value at the boundary as the dose of the antibiotic and investigate how large of a dose is necessary to reduce the anaerobic population. These boundary conditions can be written $b(-L/2, t) = b(L/2, t) = b_B$ for the one-dimensional domain $[-L/2, L/2]$ where b_B is the dose. The antibiotic parameters are listed in Table 5.3.

Table 5.3: Antibiotic Parameters

Parameter	Base value	Description
α	1	Antibiotic clearance rate
D_b	1	Antibiotic diffusion rate
δ	10	Antibiotic efficacy
b_B	1	Dose size

The parameters in Table 5.3 correspond to pharmacological properties of the antibiotic, and we can determine what properties produce desirable effects in terms of treating the anaerobic community. To simulate an antibiotic treatment we first solved the four-equation model without antibiotics (which we can do simply by taking $b_B = 0$) until the system is

approximately at steady-state. Then we increase the does b_B to our base value to simulate the course of treatment. Figure 5.8 shows several snapshots of a treatment course with our base parameter values.

Our base case simulation shows the anaerobic community surviving, so we performed parameter sweeps of the four antibiotic parameters to determine what properties are most effective in eliminating anaerobes. In Figure 5.9, we plot the maximum anaerobic density for ranges of each parameter. Interestingly, the antibiotic-induced death rate δ required a much higher value (an order of magnitude higher) than the other parameters to eliminate the anaerobes. Anaerobes were eliminated more easily with a low clearance or high diffusion rate of the antibiotic, with anaerobes eliminated with $\alpha < 0.5$ or $D_b > 2.2$. Practically, a drug with a high permeability into mucus may be the most desirable for controlling pathogenic anaerobes, as large doses and exposures can lead to complications in treatment.

5.10 Conclusion

In this chapter, we developed a spatially-dependent model the CF airway microbiome in which dynamics are driven by a diffusible oxygen concentration. Our model consists of a coupled system of reaction-diffusion partial differential equations with state variables corresponding to the oxygen concentration, an aerobic community, and an anaerobic community. The setting of our model is in clogged or partially clogged airways; microbes proliferate in mucus-lined epithelial cells and a steep oxygen gradient exists between the air-mucus interface and the deeper mucus. To model this, we considered one- and two-dimensional domains representing the mucus-biofilm matrix with boundaries representing the air-mucus interface through which oxygen diffuses in.

The three kinds of mucus blockages we considered are a mucus lined airway, a spherical

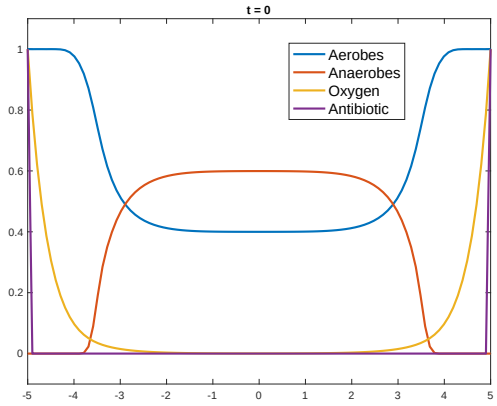

(a)

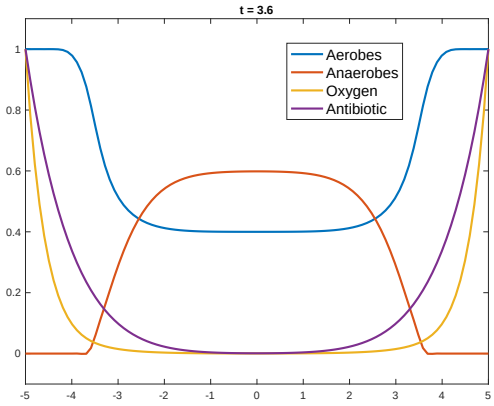

(b)

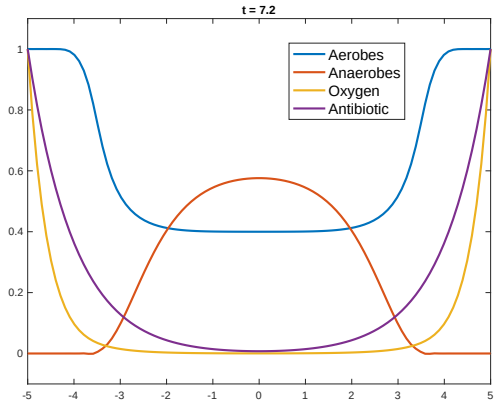

(c)

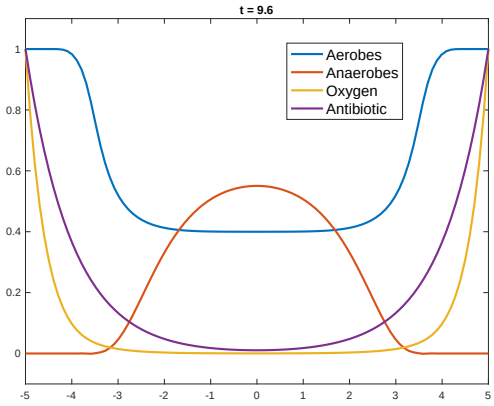

(d)

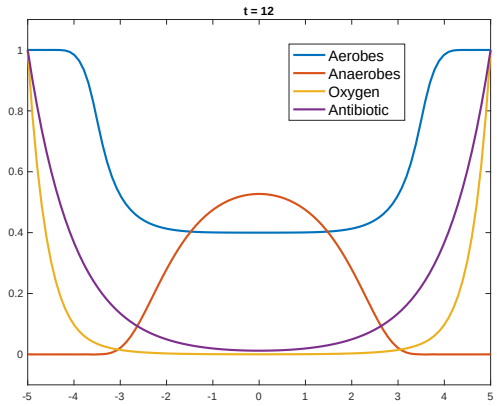

(e)

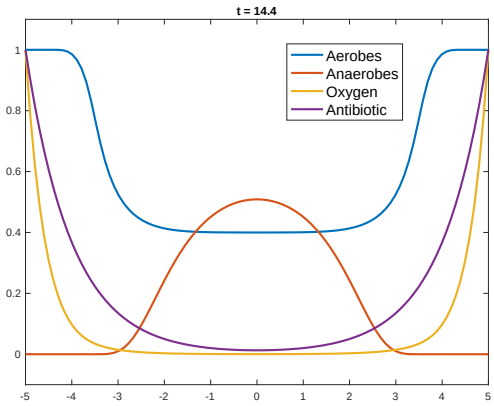

(f)

Figure 5.8: Snapshots of the baseline antibiotic treatment. Images were taken at $t = 0, 3.6, 7.2, 9.6, 12$, and 14.4. The anaerobic community persists with this antibiotic treatment.

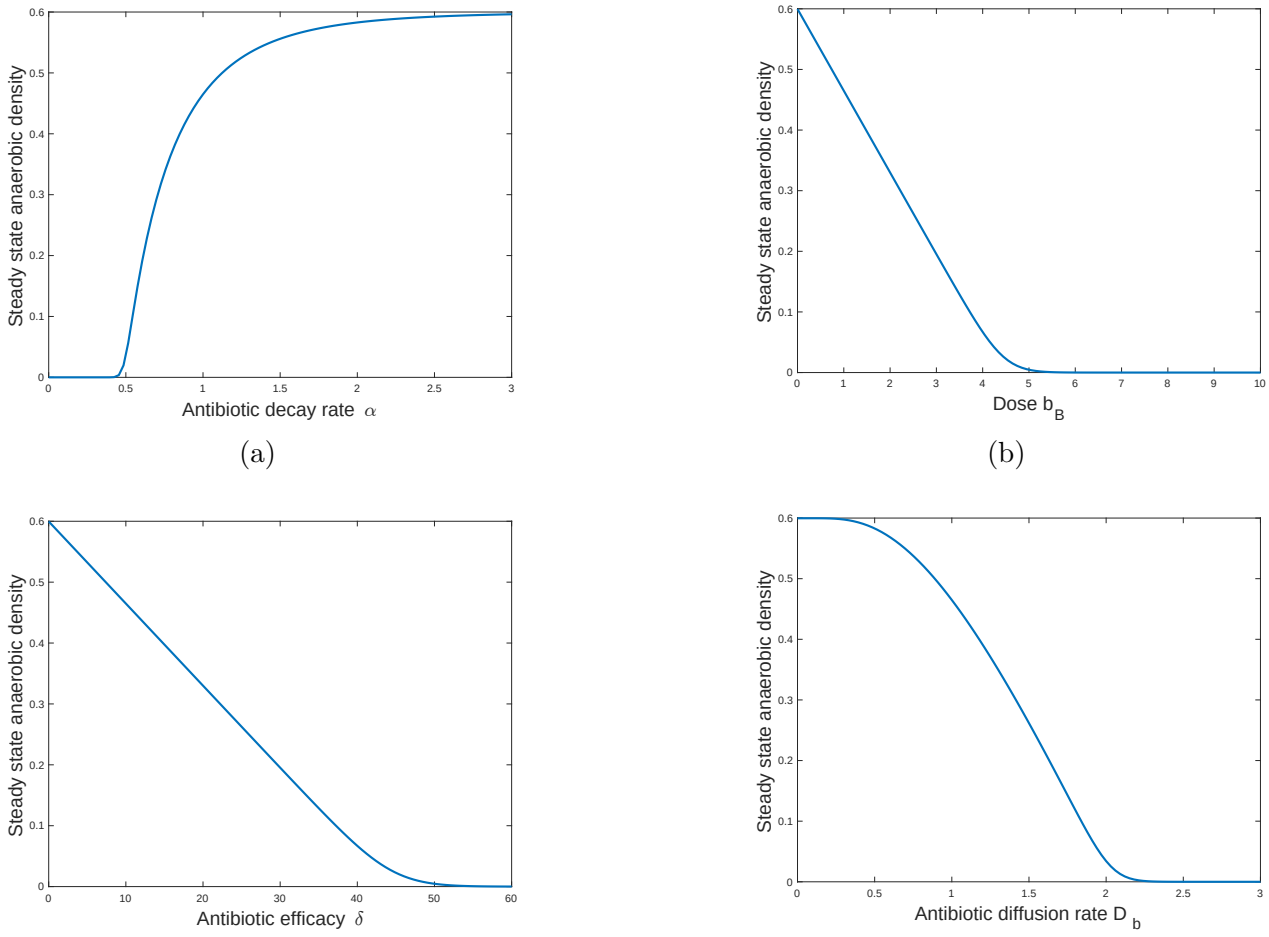

Figure 5.9: Parameter sweeps of the four antibiotic-related parameters. The blue line indicates the maximum density the anaerobic community persists after a course of antibiotic treatment.

plug logged in an airway, and a completely clogged alveolar sac [28]. Using our model, we were able to predict the minimum-size mucus plug necessary for anaerobic survival, and the speed that the anaerobic community can propagate through the clogged airway. In the case of a constant oxygen concentration, which could be found between various individual patients or at varying depths of a single patient's lung, we derived analytical expressions for these quantities in terms of the model parameters. With dynamic oxygen, we were able to perform a large number of simulations and observe the minimal mucus plug size and propagation speed for a wide range of parameter values. We also incorporated an anaerobe-targeted antibiotic component into the model, which, like oxygen, diffuses into the domain

from the boundary. We found that an antibiotic with high diffusivity and slow decay was more effective in lowering the anaerobic population than increasing the dose of a less effective drug.

There are many mathematical models of bacterial growth available in the literature, both spatially homogeneous and dependent [3, 49, 76, 101]. The choice of a spatially dependent PDE model is appropriate in our case due to the physical properties of the mucus-biofilm as well as the inherent spatial complexity of the lung. Anaerobic microbes can only reproduce in low-oxygen environments which strongly depend on gradients created by aerobic respiration and mucus penetration, phenomena which are difficult to capture in a spatially homogeneous model. Moreover, biofilm formation by pathogens such as *P. aeruginosa* contributes to antibiotic resistance by physically preventing the drug from coming in contact with pathogen cells [96]. Using a spatially structured model, we showed that a drug with a higher permeability into mucus could potentially treat anaerobic infections.

We made several simplifying assumptions in this chapter. Our focus with this model was to observe the effects of dynamic oxygen, but the CF microbiome depends on many nutrients that we did not discuss, particularly the role of pH and sulfides [28, 41, 85, 86]. CF pathogens also exhibit a wide range of metabolic properties, of particular importance are facultative anaerobes which can grow with or without oxygen. *P. aeruginosa* is one such facultative anaerobe and exhibits markedly different metabolic behavior depending on the availability of oxygen [79]. We also remark that there is much uncertainty in the causes of CFPEs and that while facultative anaerobes are associated with exacerbations, anaerobic targeting antibiotics have not thus far been shown to be effective in treating them [18]. In our modeling we assumed a mass-action death term due to antibiotics, which would correspond to a bactericidal drug. However, many anaerobe-targeting drugs are bacteriostatic and work by slowing the bacteria's growth rate.

In conclusion, we developed a mathematical model of interacting aerobic and anaerobic

microbes in the CF airway with dynamics driven by diffusible oxygen. Our goal with this model was to determine oxygen-related conditions for anaerobic growth. Via analytical techniques and simulation, we determined conditions for the survival and propagation of the anaerobic community. We also incorporated an anaerobe-targeting antibiotic and found that highly diffusable, slower-decaying drugs can more easily reach hypoxic regions and treat the anaerobic community.

Chapter 6

A Stochastic Agent-based Model of Cystic Fibrosis Microbial Dynamics

We develop an agent-based modeling framework for CF microbial community dynamics. First, we discuss a spatially homogeneous model which behaves as a stochastic analog of the ODE model developed in Chapter 4 and validate it against the patient data set. We then introduce spatially heterogeneity by requiring individual microbes to place offspring in nearby locations and introducing locally oxygen depletion. We compare the population switch time between the spatially homogeneous and spatially dependent ABMs and discuss an ecological niche-building phenomena that the spatially dependent model can exhibit.

6.1 Introduction

So far, each of the models we have discussed has been deterministic, meaning that they contain no random effects and will always produce the same output for a given input. By contrast, biological processes are inherently noisy and contain random effects. Here, we de-

velop a stochastic agent-based model (ABM) and use it to investigate the role of stochasticity in the CF community dynamics. Agent-based models often include spatial dynamics, which are of interest because ecological interactions between communities are complex and likely affected by the availability of oxygen and other biochemical resources within the spatial heterogeneity of the CF airway environment.

6.2 Model development

We develop an agent-based model to study the impact of spatial heterogeneity and stochasticity on the composition of bacterial communities in CF patients [109, 118]. In our agent-based framework, each individual microbe is an agent located in a spatial domain and a predetermined set of probabilistic rules govern the population dynamics. We consider a two-dimensional $n \times n$ grid as a domain. Each space in the grid can be occupied by an aerobe, c, and anaerobe, f, or be empty. Let N be the number of agents present in the grid at a given time. Each time step, the grid is randomly sampled until N agents have been selected. If an empty space in the grid is selected, a new space is sampled. When a space with a microbe is selected, the selected microbe can divide with a probability r_i or die with a probability d_i, where $r_i + d_i < 1$ and $i = c, f$. Like in the models of Chapters 4 and 5, the community growth probabilities are functions of oxygen $r_c(W)$ and $r_f(W)$.

We first developed a spatially homogeneous ABM which is a stochastic analog of the oxygen-based ODE model. In this case, a new space for a dividing microbe is randomly selected from the entire grid. If the newly selected space is empty, then the offspring cell is placed there; otherwise, the division event is aborted. For this spatially homogeneous ABM, we assume that the grid contains a global amount of oxygen which is governed by the ODE

$$\frac{dW}{dt} = \lambda - \mu W - \eta C W, \tag{6.1}$$

where C is the total amount of aerobic microbes present in the grid.

We introduced spatial dependence to our agent-based framework by restricting microbes to placing offspring cells nearby rather than selecting a location from the entire grid. In this case, when a bacteria is selected for reproduction the offspring is placed in one of the eight neighboring spaces of the parent, selected randomly. In addition, oxygen is only consumed by locally present aerobes as opposed to being consumed globally as in the spatially homogeneous model. The oxygen dynamics in position (i, j) of the grid are now governed by

$$\frac{dW_{i,j}}{dt} = \lambda - \mu W_{i,j} - \eta W_{i,j} C_{yn} - gmW_{i,j} + gW_{tot}, \tag{6.2}$$

where $C_{yn} = 1$ if a space contains an aerobic microbe and 0 otherwise. The parameter g is the migration rate of oxygen between neighboring spaces, m is the total number of neighbor spaces (for most spaces $m = 8$, $m = 5$ for boundary spaces, and $m = 3$ in the corners), and W_{tot} is the total amount of oxygen contained in the neighbor cells. These agent-based models were implemented in the Julia Programming Language [12, 89], and Figure 6.1 shows a flow-chart of the microbial selection procedure.

6.3 Model validation

We validated the spatially homogeneous ABM against the ODE model discussed in Chapter 4 and available patient data. The mean, 2.5^{th}, and 97.5^{th} percentiles of a 500-run ensemble are plotted in Figure 4.2 along with the patient data and best-fitting ODE simulation, and these simulations show that the spatially homogeneous model agrees very well with the ODE model. Additionally, Figure 6.2 shows spatial snapshots of a typical run of the spatially homogeneous ABM. The nine images of Figure 6.2 were taken at the time points for which

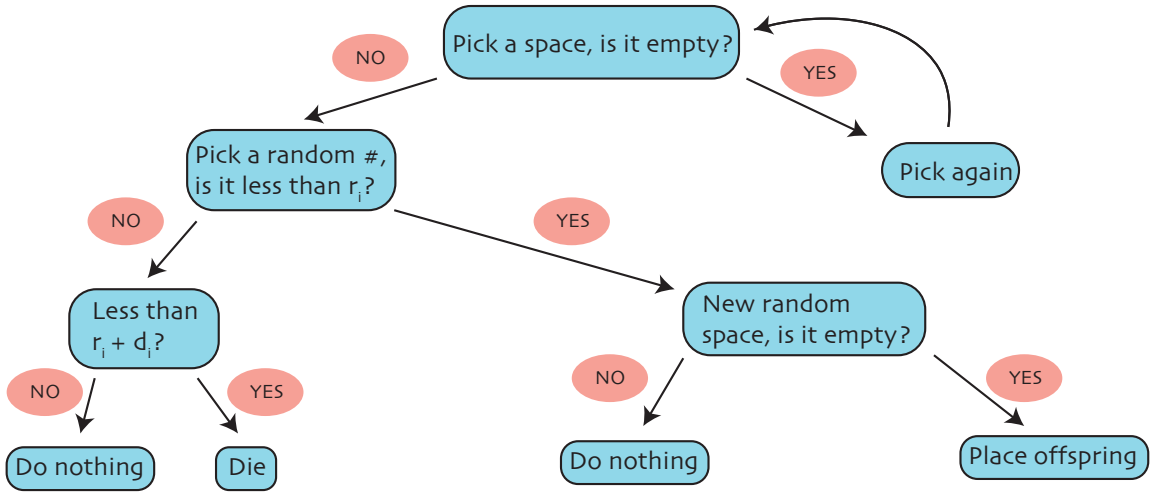

Figure 6.1: Flow-chart showing the procedure for microbial birth and death in the agent-based models.

data were available, i.e., $t = 0, 14, 19, 26, 28, 31, 33, 35$, and 38.

6.4 Role of spatial heterogeneity on aerobic-anaerobic bacterial dynamics

Microenvironments within CF airways are likely not homogeneous, and in fact, there are often steep gradients of nutrients and microbial densities [28]. Thus, we used our agent-based models to investigate the role spatial heterogeneity plays in the interaction of the aerobic and anaerobic communities. For local oxygen dynamics, we take $g = 0$ to exclude oxygen diffusion between neighboring spaces and emphasize local effects. Since $g = 0$ corresponds to the absence of oxygen diffusion, the oxygen ODE reduces to

$$\frac{dW}{dt} = \lambda - \mu W - \eta C_{yn} W, \tag{6.3}$$

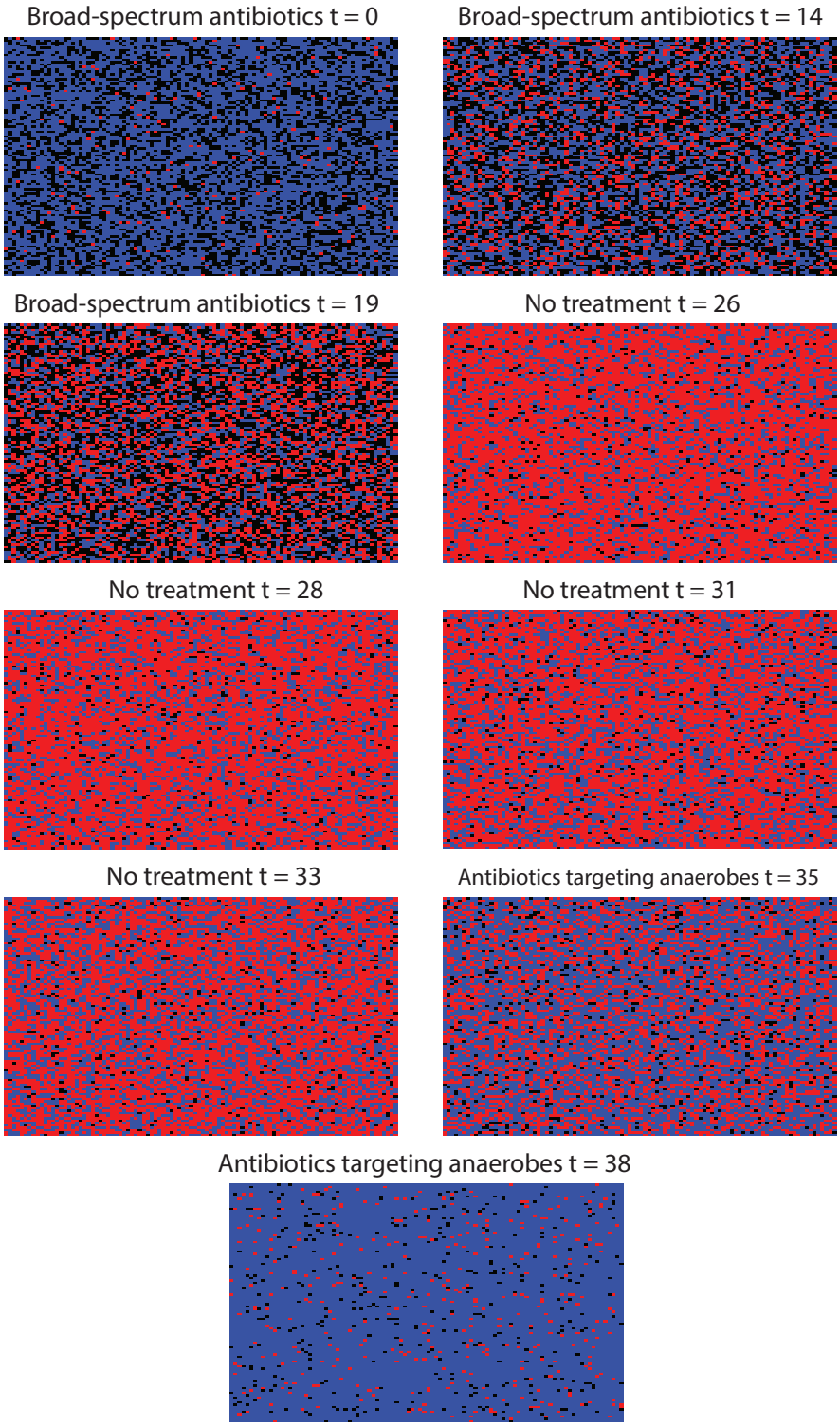

Figure 6.2: Snapshots of the spatially homogeneous agent-based model taken at the nine time points at which data were collected. In each image, black spaces are empty, blue spaces represent aerobes, and red spaces anaerobes. These images are a typical run of the model with the best-fitting ODE parameters and antibiotic treatment schedule.

so that the $n \times n$ ODE system is decoupled. Figure 6.3 shows a comparison of the population switch times between the spatially homogeneous and heterogeneous simulations. The top row of Figure 6.3 shows time series representations of typical runs of both models, as well as when the population switch occurs, the second and third rows show spatial snapshots pre- and post-population switch for the two models. The bottom row plots the switch time when varying the oxygen recruitment λ and broad-spectrum antibiotic efficacy d_{BS}.

Generally, including spatial heterogeneity increases the timeframe of the dynamics and time for a population switch to occur. To observe this, we ran simulations for $0 \leq d_{BS} \leq 10$ (Figure 6.3g) and $1.5 \times 10^5 \leq \lambda \leq 3.6 \times 10^5$ (Figure 6.3h). For both models, switch times decreased in proportion to d_{BS} and increased in proportion to λ. Small values of d_{BS} ($d_{BS} = 0$ being the base case) resulted in switch times of approximately 18 days for the homogeneous model and 80 days for the spatially dependent model. When varying λ switch times range from nearly 0 to approximately 18 and 70 days for the homogeneous and spatially dependent model, respectively.

6.5 Niche building

Our spatially dependent ABM is able to capture the niche-building phenomena seen in CF lung disease, in which certain microbial species take advantage of chemical gradients in an environment to occupy an ecological niche [84]. Our model is able to capture this dynamic, as the anaerobic community relies on the aerobic community to draw down oxygen concentrations via consumption, thereby creating a local environment favorable for anaerobic growth.

We explored a parameter space of the model in which aerobes persist in a stable equilibrium well under the carrying capacity of the system and anaerobes capitalize on low-oxygen regions

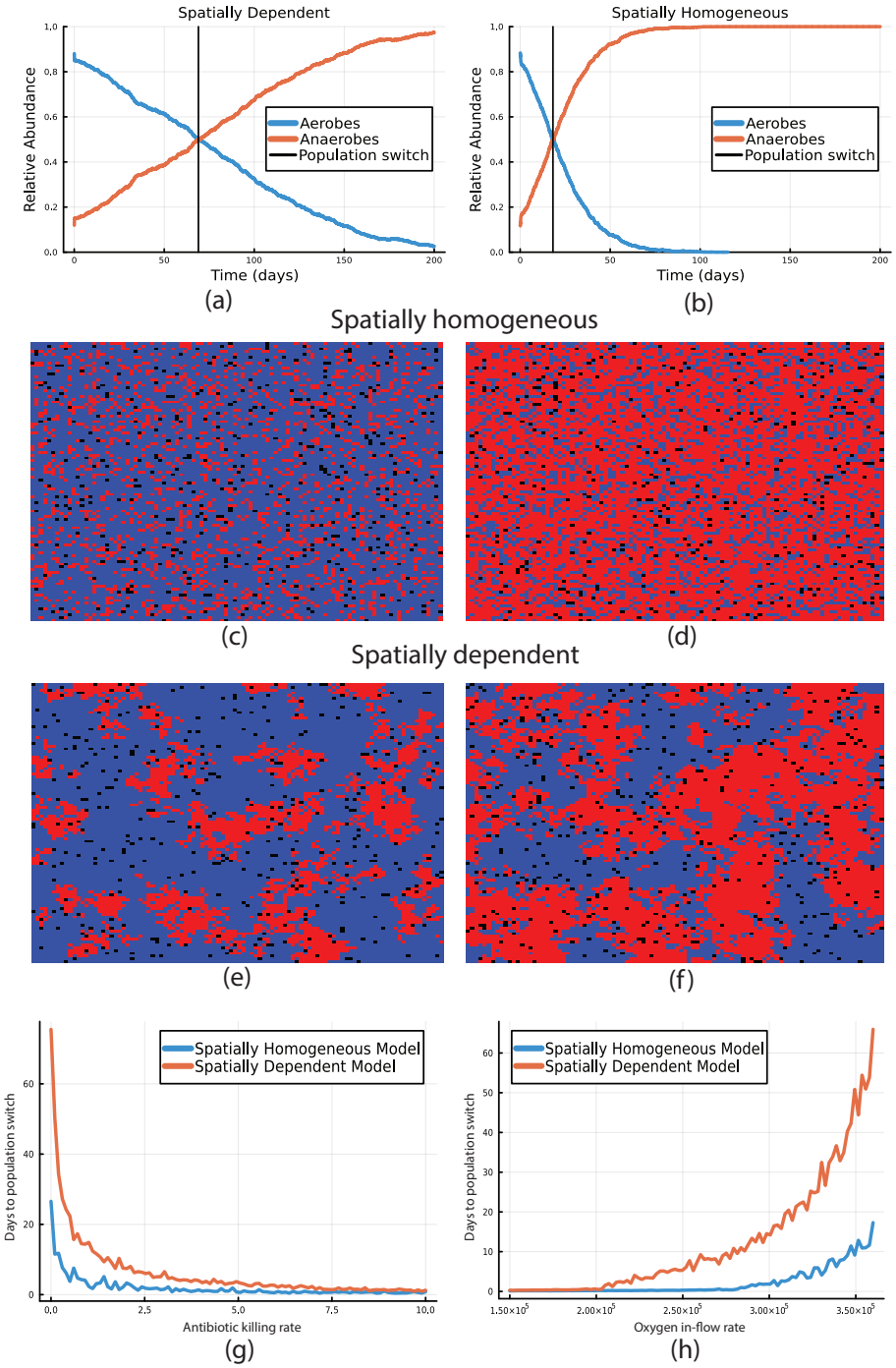

Figure 6.3: Comparison of spatially homogeneous and spatially dependent agent-based simulations. The top row shows time series of typical simulations of the spatially dependent (a) and homogeneous (b) models and population switch times. (c) and (d) show spatial snapshots for pre- and post-population switch for the homogeneous model, (e) and (f) show the same for the spatially dependent model. In (c-f), blue spaces represent aerobes and red anaerobes. (g) and (h) are parameter sweeps for d_{BS} and λ on the population switch time.

near groups of aerobes. Starting from randomized initial distributions, small groups of aerobes become distributed roughly uniformly throughout the grid. Anaerobes quickly begin to form clusters near the aerobes and can proliferate relatively quickly in the low-oxygen conditions. As the anaerobes reproduce, they start to reach higher oxygen regions and are killed so that high concentrations of anaerobes are always near groups of aerobes.

From time to time, a large group of anaerobes will suppress its supporting aerobe group via competitive exclusion and cause them to go extinct locally. When this happens, the resulting increase in oxygen concentration quickly eliminates the anaerobes as well and the region becomes uninhabited. This phenomena creates a global boom-bust cycle in which the anaerobic community sporadically bloom around groups of aerobes before suppressing the aerobes and crashing, seen in the time series plots of Figure 6.4. Figure 6.5 shows this dynamic in several snap shots taken at an arbitrary time during a simulation. From these simulations, this appears to be a form of stable coexistence of the two communities as the boom-bust cycle of the anaerobic community can continue potentially indefinitely and the aerobes are clearly in a steady-state regardless of the behavior of the anaerobes.

6.6 Conclusion

Airways are geometrically complex, so we developed a spatially heterogeneous agent-based model of the microbial community dynamics in CF airways. We first developed a spatially homogeneous version of our ABM and validated it against the ODE model and patient data discussed in Chapter 4, then incorporated spatial dynamics by restricting microbes to reproducing only in nearby spaces. For comparison purposes, we considered the case where no oxygen movement took place between neighboring spaces and observed that this restriction increased the time to exacerbation compared to the spatially homogeneous model. Future studies should focus on the effects of oxygen diffusion throughout the spatial domain, as

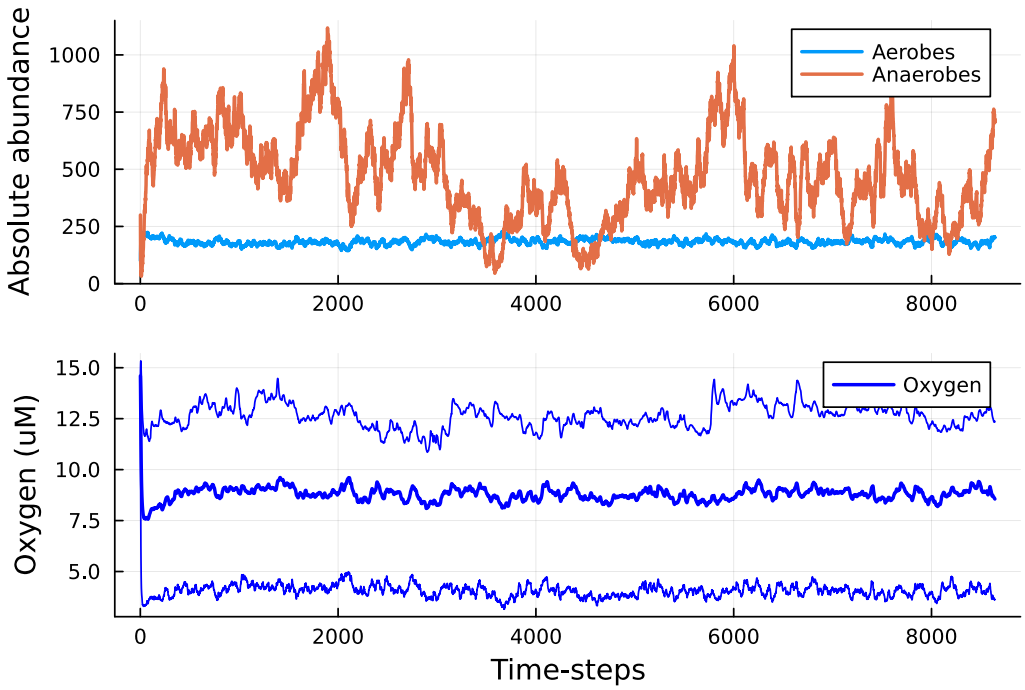

Figure 6.4: Time series plot of the spatially heterogeneous ABM with oxygen diffusion, the top figure shows community populations and the bottom oxygen concentrations with 2.5^{th} and 97.5^{th} percentiles. The top figure depicts the boom-bust cycle of the anaerobic community compared to the relatively stable aerobic population.

well as how local reproduction affects microbial growth rates. The results in this chapter indicated that the inclusion of spatial dependence increased the time scale for most aspects of the modeling. Further study into the dynamics of the two communities and their interactions with oxygen will improve a basic understanding of CF airway ecology. Such insights may inform clinical practices by identifying strategies to minimize the growth of more pathogenic bacteria, such as how oxygen dynamics can inhibit anaerobic bacteria, possibly with hyperbaric oxygen treatment.

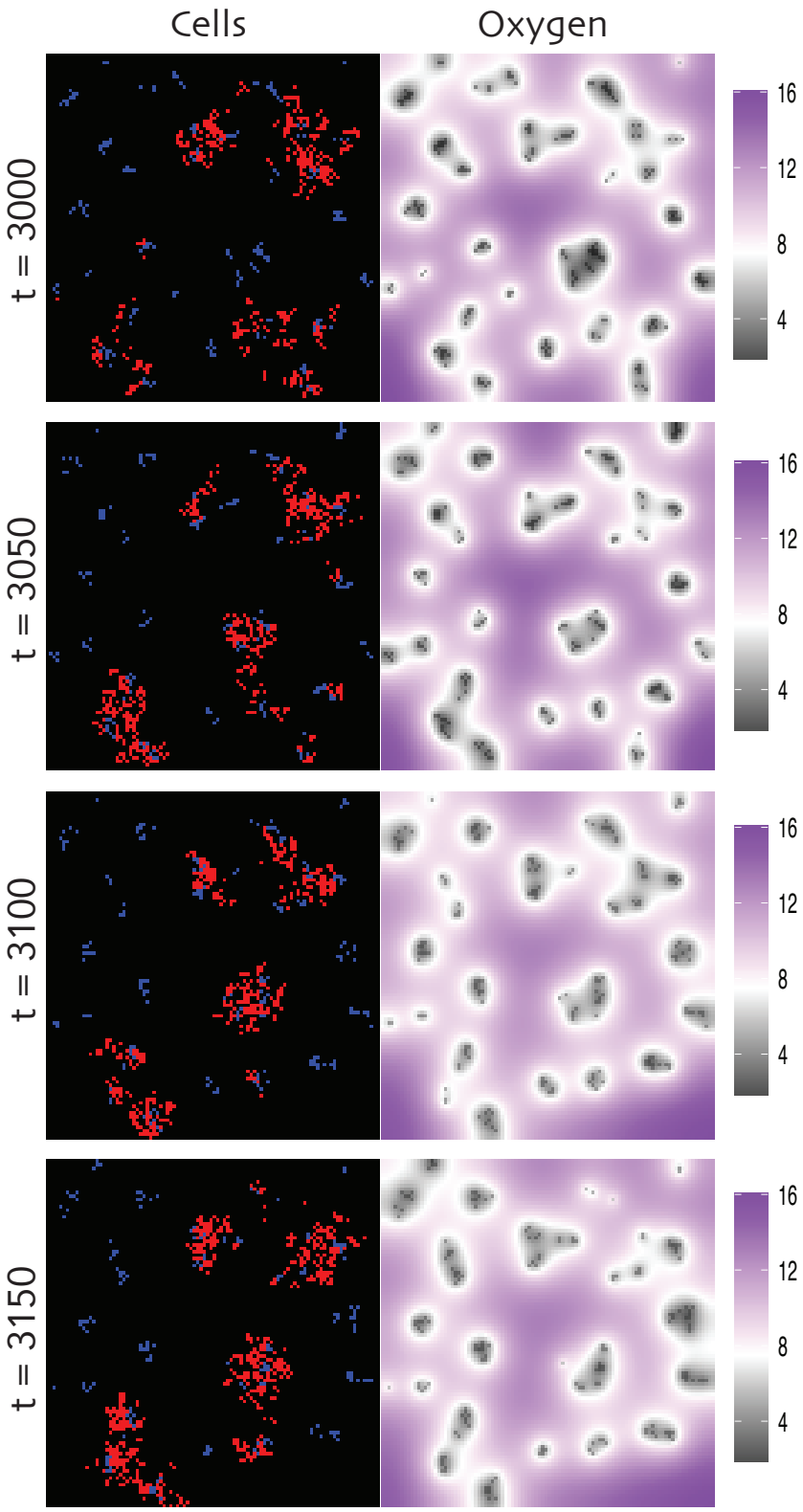

Figure 6.5: Spatial snapshots of the spatially dependent ABM with oxygen diffusion, cell locations are shown in the left-hand column, and corresponding oxygen concentrations in the right. Red squares represent anaerobes and blue aerobes, purple indicates high oxygen concentrations, and black low.

Chapter 7

Conclusions and Future Work

In this dissertation, we discussed a series of mathematical and computational models to investigate the role of oxygen in cystic fibrosis lung microbial dynamics. We first developed a model capable of quantifying the growth characteristics and estimating parameters of CF pathogens grown *in vitro* in various oxygen- and nutrient-dependent conditions. By fitting this model to experimental data, we identified a functional form of the most likely growth mechanism for nutrient-dependent growth. We then used this growth function to develop a model of competing aerobic and anaerobic microbial communities growing inside an airway of a person with CF. We validated this model against a clinical data set to determine baseline parameter values and performed numerical simulations to predict novel antibiotic therapies for CF pulmonary exacerbations and other basic insights of CF microbial dynamics. Next, we extended this model to include spatial effects via diffusion and investigated the role of oxygen gradients in accumulated mucus. Simulating our reaction-diffusion model allowed us to predict desirable pharmacodynamic properties for antibiotics in treating CF lung infections, as well as the minimum mucus plug size needed to support anaerobic growth. Finally, we presented a stochastic agent-based model to incorporate random effects to our modeling of CF microbial dynamics.

There are several potential directions for future work. A key assumption of the present work is the presence of only two microbial communities and one nutrient. While our goal here was to investigate the role of oxygen, the CF microbiome is a much more diverse and chemically complex than we considered and future modeling should consider including, e.g., facultative anaerobes or additional species and the addition of pH and/or sulfide-based dynamics. Similarly, there is room for additional analysis and discovery in the agent-based model and the effects of stochasticity in CF microbial dynamics. We also made several simplifying assumptions in our use of antibiotics and future modeling may benefit from the inclusion of more detailed pharmacokinetic and pharmacodynamic mechanisms. The data we had access to, while rich in some features, was limited in terms of quantity and some features such as spatial information. Access to additional data, specifically longitudinal data sets, would greatly increase the utility and potential for discovery of our modeling.

The long-term goal of this work is to develop improved treatments for CF lung infections, and we have presented several hypotheses that can be tested in laboratory settings. Questions that may be tested include: can anaerobic growth be minimized by increasing oxygen flow, such as in a hyperbaric chamber or by lowering the abundance of aerobes? What role does nutrient recycling play in biofilm formation and its relation to pulmonary function? Can model predictions of antibiotic timing and pharmacodynamics, minimum mucus plug size, and anaerobic spread be verified with *in vitro* assays? While there has been limited investigation into targeting anaerobic microbes for treatment, the case study in Chapter 4 provides evidence that this strategy warrants further study. Including more detailed pharmacokinetic and pharmacodynamic detail in future modeling may be beneficial in determining more effective clinical options, such as by using models to explore various methods of antibiotic administration.

The topic of this dissertation was cystic fibrosis associated lung infections, but the ecological principals are applicable to other polymicrobial infections and may be useful in combating

antibiotic resistance at large. Antibiotic resistance is a global health crisis requiring new approaches to treating bacterial infections and therapies that leverage ecological factors such as we have discussed here are a promising area to investigate [113, 114]. Phage therapy is another possible strategy and has seen some success in treating CF lung infections [21]. The modeling in this dissertation can be extended in a straightforward way to include bacteriophage to predict new potential therapies, target species for treatment, or phage strains that would be difficult to discover in a laboratory setting alone.

In summary, we discussed several models of microbial dynamics of cystic fibrosis lung infections. Each of these models are able to capture realistic features of CF lung infections and predict potential new therapies, while being simple enough to remain analytically tractable and computationally inexpensive. There are several logical steps forward for this work, including further modeling to further explore the effects of antibiotic, oxygen, or additional chemo-attractants, additional interactions between microbial species, and the development of *in vitro* experiments to test the hypotheses generated using such models.

Bibliography

[1] S. Abar, G. K. Theodoropoulos, P. Lemarinier, and G. M. P. O'Hare. Agent based modelling and simulation tools: A review of the state-of-art software. *Computer Science Review*, 24:13–33, 2017.

[2] H. Akaike. *Information theory and an extension of the maximum likelihood principle*. Akadémiai Kiadó, Budapest, Hungary, 1973.

[3] R. J. Allen and B. Waclaw. Bacterial growth: a statistical physicist's guide. *Rep. Prog. Phys.*, 82(1):016601, 2019.

[4] N. Allocati, M. Masulli, C. Di Ilio, and V. De Laurenzi. Die for the community: an overview of programmed cell death in bacteria. *Cell Death & Disease*, 6(1):e1609–e1609, 2015.

[5] M. Alnæs, J. Blechta, J. Hake, A. Johansson, B. Kehlet, A. Logg, C. Richardson, J. Ring, M. E. Rognes, and G. N. Wells. The fenics project version 1.5. *Archive of Numerical Software*, 3(100):9–23, 2015.

[6] H. Banks, K. Maxwell, L. Bociu, M. Noorman, and K. Tillman. The complex-step method for sensitivity analysis of non-smooth problems arising in biology. *Eurasian Journal of Mathematical and Computer Applications*, 3:16–68, 2015.

[7] H. T. Banks, K. Bekele-Maxwell, L. Bociu, and C. Wang. Sensitivity via the complex-step method for delay differential equations with non-smooth initial data. *Quarterly of Applied Mathematics*, 75(2):231–248, 2017.

[8] H. T. Banks, S. Hu, and W. C. Thompson. *Modeling and inverse problems in the presence of uncertainty*. CRC Press, 2014.

[9] H. T. Banks and C. Wang. Sensitivity via the complex-step method for delay differential equations with non-smooth initial data. Report, North Carolina State University. Center for Research in Scientific Computation, 2016.

[10] D. M. Bates and D. G. Watts. Nonlinear regression analysis and its applications. 2011.

[11] S. C. Bell, M. A. Mall, H. Gutierrez, M. Macek, S. Madge, J. C. Davies, P. R. Burgel, E. Tullis, C. Castaños, C. Castellani, C. A. Byrnes, F. Cathcart, S. H. Chotirmall, R. Cosgriff, I. Eichler, I. Fajac, C. H. Goss, P. Drevinek, P. M. Farrell, A. M. Gravelle,

T. Havermans, N. Mayer-Hamblett, N. Kashirskaya, E. Kerem, J. L. Mathew, E. F. McKone, L. Naehrlich, S. Z. Nasr, G. R. Oates, C. O'Neill, U. Pypops, K. S. Raraigh, S. M. Rowe, K. W. Southern, S. Sivam, A. L. Stephenson, M. Zampoli, and F. Ratjen. The future of cystic fibrosis care: a global perspective. *Lancet Respir Med*, 8(1):65–124, 2020.

[12] J. Bezanson, A. Edelman, S. Karpinski, and V. B. Shah. Julia: A fresh approach to numerical computing. *SIAM Review*, 59:65—98, 2017.

[13] A. Y. Bhagirath, Y. Li, D. Somayajula, M. Dadashi, S. Badr, and K. Duan. Cystic fibrosis lung environment and pseudomonas aeruginosa infection. *BMC Pulmonary Medicine*, 16(1):174, 2016.

[14] Z. Breijyeh, B. Jubeh, and R. Karaman. Resistance of gram-negative bacteria to current antibacterial agents and approaches to resolve it. *Molecules*, 25(6), 2020.

[15] T. D. Bui, A. K. Oppenheim, and D. T. Pratt. Recent advances in methods for numerical solution of o.d.e. initial value problems. *Journal of Computational and Applied Mathematics*, 11(3):283–296, 1984.

[16] X. M. Bustamante-Marin and L. E. Ostrowski. Cilia and mucociliary clearance. *Cold Spring Harbor perspectives in biology*, 9(4):a028241, 2017.

[17] R. S. Cantrell and C. Cosner. *Spatial ecology via reaction-diffusion equations*. John Wiley & Sons, 2004.

[18] L. M. Castner, M. Zimbric, S. Cahalan, C. Powell, and L. J. Caverly. Outcomes of cystic fibrosis pulmonary exacerbations treated with antibiotics with activity against anaerobic bacteria. *Journal of Cystic Fibrosis*, 20(6):926–931, 2021.

[19] L. J. Caverly and J. J. LiPuma. Good cop, bad cop: anaerobes in cystic fibrosis airways. *European Respiratory Journal*, 52(1):1801146, 2018.

[20] L. J. Caverly, J. Zhao, and J. J. LiPuma. Cystic fibrosis lung microbiome: Opportunities to reconsider management of airway infection. *Pediatric Pulmonology*, 50(S40):S31–S38, 2015.

[21] B. K. Chan, G. Stanley, M. Modak, J. L. Koff, and P. E. Turner. Bacteriophage therapy for infections in cf. *Pediatric Pulmonology*, 56(S1):S4–S9, 2021.

[22] Q. Chen, Y. Shen, and J. Zheng. A review of cystic fibrosis: Basic and clinical aspects. *Animal Model Exp Med*, 4(3):220–232, 2021.

[23] J. F. Chmiel, T. R. Aksamit, S. H. Chotirmall, E. C. Dasenbrook, J. S. Elborn, J. J. LiPuma, S. C. Ranganathan, V. J. Waters, and F. A. Ratjen. Antibiotic management of lung infections in cystic fibrosis. i. the microbiome, methicillin-resistant staphylococcus aureus, gram-negative bacteria, and multiple infections. *Ann Am Thorac Soc*, 11(7):1120–9, 2014.

[24] A. Cintrón-Arias, H. T. Banks, A. Capaldi, and A. L. Lloyd. A sensitivity matrix based methodology for inverse problem formulation. 2009.

[25] A. G. Cobián-Güemes, Y. W. Lim, R. A. Quinn, D. J. Conrad, S. Benler, H. Maughan, R. Edwards, T. Brettin, V. A. Cantú, D. Cuevas, R. Hamidi, P. Dorrestein, and F. Rohwer. Cystic fibrosis rapid response: Translating multi-omics data into clinically relevant information. *mBio*, 10(2):e00431–19, 2019.

[26] D. Conrad, M. Haynes, P. Salamon, P. B. Rainey, M. Youle, and F. Rohwer. Cystic fibrosis therapy: a community ecology perspective. *American journal of respiratory cell and molecular biology*, 48(2):150–156, 2013.

[27] A. Cornish-Bowden. One hundred years of michaelis–menten kinetics. *Perspectives in Science*, 4:3–9, 2015.

[28] E. S. Cowley, S. H. Kopf, A. Lariviere, W. Ziebis, and D. K. Newman. Pediatric cystic fibrosis sputum can be chemically dynamic, anoxic, and extremely reduced due to hydrogen sulfide formation. *mBio*, 6(4):e00767–15, 2015.

[29] P. B. Davis. Cystic fibrosis since 1938. *Am J Respir Crit Care Med*, 173(5):475–82, 2006.

[30] E. Delfino, F. Del Puente, F. Briano, C. Sepulcri, and D. R. Giacobbe. Respiratory fungal diseases in adult patients with cystic fibrosis. *Clin Med Insights Circ Respir Pulm Med*, 13:1179548419849939, 2019.

[31] V. K. Dixit and C. Rackauckas. Globalsensitivity. jl: Performant and parallel global sensitivity analysis with julia. *Journal of Open Source Software*, 7(76):4561, 2022.

[32] G. Domingue, J. W. Costerton, and M. R. Brown. Bacterial doubling time modulates the effects of opsonisation and available iron upon interactions between staphylococcus aureus and human neutrophils. *FEMS Immunol Med Microbiol*, 16(3-4):223–8, 1996.

[33] G. Döring, P. Flume, H. Heijerman, and J. S. Elborn. Treatment of lung infection in patients with cystic fibrosis: Current and future strategies. *Journal of Cystic Fibrosis*, 11(6):461–479, 2012.

[34] B. Efron and R. J. Tibshirani. *An introduction to the bootstrap*. Chapman & Hall, New York, N.Y.; London, 1993.

[35] M. El-Hachem, S. W. McCue, W. Jin, Y. Du, and M. J. Simpson. Revisiting the fisher-kolmogorov-petrovsky-piskunov equation to interpret the spreading-extinction dichotomy. *Proc Math Phys Eng Sci*, 475(2229):20190378, 2019.

[36] T. R. Field, C. D. Sibley, M. D. Parkins, H. R. Rabin, and M. G. Surette. The genus prevotella in cystic fibrosis airways. *Anaerobe*, 16(4):337–44, 2010.

[37] R. A. Fisher. The wave of advance of advantageous genes. *Ann. Eugen.*, 7(4):355–369, 1937.

[38] P. A. Flume, J. Mogayzel, P. J., K. A. Robinson, C. H. Goss, R. L. Rosenblatt, R. J. Kuhn, and B. C. Marshall. Cystic fibrosis pulmonary guidelines: treatment of pulmonary exacerbations. *Am J Respir Crit Care Med*, 180(9):802–8, 2009.

[39] J. M. Flynn, D. Niccum, J. M. Dunitz, and R. C. Hunter. Evidence and role for bacterial mucin degradation in cystic fibrosis airway disease. *PLOS Pathogens*, 12(8):e1005846, 2016.

[40] K. Gera and K. S. McIver. Laboratory growth and maintenance of streptococcus pyogenes (the group a streptococcus, gas). *Current protocols in microbiology*, 30:9D.2.1–9D.2.13, 2013.

[41] L. J. Ghuneim, R. Raghuvanshi, K. A. Neugebauer, D. V. Guzior, M. H. Christian, B. Schena, J. M. Feiner, A. Castillo-Bahena, J. Mielke, M. McClelland, D. Conrad, I. Klapper, T. Zhang, and R. A. Quinn. Complex and unexpected outcomes of antibiotic therapy against a polymicrobial infection. *Isme j*, 16(9):2065–2075, 2022.

[42] G. Glen and K. Isaacs. Estimating sobol sensitivity indices using correlations. *Environmental Modelling & Software*, 37:157–166, 2012.

[43] G. M. Green and E. H. Kass. Factors influencing the clearance of bacteria by the lung. *The Journal of clinical investigation*, 43(4):769–776, 1964.

[44] E. Hairer, S. Norsett, and G. Wanner. *Solving Ordinary Differential Equations I: Nonstiff Problems*, volume 8. 1993.

[45] E. Hairer and G. Wanner. *Solving ordinary differential equations II*, volume 375. Springer Berlin Heidelberg New York, 1996.

[46] W. Hao, K. Lam, and Y. Lou. Ecological and evolutionary dynamics in advective environments: Critical domain size and boundary conditions. *Discrete & Continuous Dynamical Systems-B*, 26(1):367, 2021.

[47] D. J. Hentges. *Anaerobes: General Characteristics*. University of Texas Medical Branch at Galveston Copyright © 1996, The University of Texas Medical Branch at Galveston., Galveston (TX), 1996.

[48] D. W. Jordan and P. Smith. *Nonlinear ordinary differential equations : an introduction for scientists and engineers*. New York : Oxford University Press, Oxford [England], 2007.

[49] C. P. Kempes, C. Okegbe, Z. Mears-Clarke, M. J. Follows, and L. E. P. Dietrich. Morphological optimization for access to dual oxidants in biofilms. *Proceedings of the National Academy of Sciences*, 111(1):208–213, 2014.

[50] V. M. Kenkre and M. N. Kuperman. Applicability of the fisher equation to bacterial population dynamics. *Phys Rev E Stat Nonlin Soft Matter Phys*, 67(5 Pt 1):051921, 2003.

[51] R. H. Keogh, R. Szczesniak, D. Taylor-Robinson, and D. Bilton. Up-to-date and projected estimates of survival for people with cystic fibrosis using baseline characteristics: A longitudinal study using uk patient registry data. *Journal of cystic fibrosis: official journal of the European Cystic Fibrosis Society*, 17(2):218–227, 2018.

[52] I. Kesisoglou, V. H. Tam, A. P. Tomaras, and M. Nikolaou. Discerning in vitro pharmacodynamics from od measurements: A model-based approach. *Computers & Chemical Engineering*, 158:107617, 2022.

[53] H. Kierstead and L. B. Slobodkin. The size of water masses containing plankton blooms. *J. mar. Res*, 12(1):141–147, 1953.

[54] M. R. Knowles and M. Drumm. The influence of genetics on cystic fibrosis phenotypes. *Cold Spring Harbor Perspectives in Medicine*, 2(12):a009548–a009548, 2012.

[55] C. Koerner-Rettberg and M. Ballmann. Colistimethate sodium for the treatment of chronic pulmonary infection in cystic fibrosis: an evidence-based review of its place in therapy. *Core Evidence*, page 99, 2014.

[56] A. Kolmogoroff, I. Petrovsky, and N. Piscounoff. Study of the diffusion equation with growth of the quantity of matter and its application to a biology problem. In P. Pelcé, editor, *Dynamics of Curved Fronts*, pages 105–130. Academic Press, San Diego, 1988.

[57] S. M. Kreda, C. W. Davis, and M. C. Rose. Cftr, mucins, and mucus obstruction in cystic fibrosis. *Cold Spring Harbor perspectives in medicine*, 2(9):a009589–a009589, 2012.

[58] A. E. LaBauve and M. J. Wargo. Growth and laboratory maintenance of pseudomonas aeruginosa. *Current protocols in microbiology*, Chapter 6:Unit–6E.1., 2012.

[59] C. Lamoureux, C. Guilloux, C. Beauruelle, S. Gouriou, S. Ramel, A. Dirou, J. Le Bihan, K. Revert, T. Ropars, R. Lagrafeuille, S. Vallet, R. Le Berre, E. Nowak, and G. Héry-Arnaud. An observational study of anaerobic bacteria in cystic fibrosis lung using culture dependant and independent approaches. *Scientific Reports*, 11(1):6845, 2021.

[60] J. J. Lee, H. Y. Lin, D. D. Liu, and M. Kong. Emax model and interaction index for assessing drug interaction in combination studies. *Frontiers in bioscience (Elite edition)*, 2:582–601, 2010.

[61] K. Lewis. Programmed death in bacteria. *Microbiol Mol Biol Rev*, 64(3):503–14, 2000.

[62] N. A. Licata, B. Mohari, C. Fuqua, and S. Setayeshgar. Diffusion of bacterial cells in porous media. *Biophys J*, 110(1):247–57, 2016.

[63] A. Logg, K. Mardal, and G. Wells. *Automated Solution of Differential Equations by the Finite Element Method: The FEniCS Book*. Springer Publishing Company, Incorporated, 2012.

[64] J. B. Lyczak, C. L. Cannon, and G. B. Pier. Lung infections associated with cystic fibrosis. *Clin Microbiol Rev*, 15(2):194–222, 2002.

[65] J. Macdougall. *Analysis of Dose–Response Studies—Emax Model*, pages 127–145. Springer New York, New York, NY, 2006.

[66] T. R. Martin and C. W. Frevert. Innate immunity in the lungs. *Proceedings of the American Thoracic Society*, 2(5):403–411, 2005.

[67] MATLAB:2021a. *9.10.0.1710957 (R2021a)*. The MathWorks Inc., 2021.

[68] E. J. McDade, J. L. Hewlett, S. P. Moonnumakal, and C. J. Baker. Evaluation of vancomycin dosing in pediatric cystic fibrosis patients. *The journal of pediatric pharmacology and therapeutics : JPPT : the official journal of PPAG*, 21(2):155–161, 2016.

[69] R. Mester, A. Landeros, C. Rackauckas, and K. Lange. Differential methods for assessing sensitivity in biological models. *PLOS Computational Biology*, 18(6):e1009598, 2022.

[70] J. K. Miller, J. S. Brantner, C. Clemons, K. L. Kreider, A. Milsted, P. Wilber, Y. H. Yun, W. J. Youngs, G. Young, H. T. Badawy, A. Milsted, C. Clemons, K. L. Kreider, P. Wilber, G. Young, Y. H. Yun, P. O. Wagers, and W. J. Youngs. Mathematical modelling of pseudomonas aeruginosa biofilm growth and treatment in the cystic fibrosis lung. *Mathematical Medicine and Biology: A Journal of the IMA*, 31(2):179–204, 2014.

[71] C. B. Morrison, M. R. Markovetz, and C. Ehre. Mucus, mucins, and cystic fibrosis. *Pediatr Pulmonol*, 54 Suppl 3(Suppl 3):S84–s96, 2019.

[72] C. Moser, S. Kjaergaard, T. Pressler, A. Kharazmi, C. Koch, and N. Høiby. The immune response to chronic pseudomonas aeruginosa lung infection in cystic fibrosis patients is predominantly of the th2 type. *APMIS*, 108(5):329–335, 2000.

[73] J. D. Murray. *Epidemic Models and the Dynamics of Infectious Diseases*, pages 610–650. Springer Berlin Heidelberg, Berlin, Heidelberg, 1993.

[74] J. M. Mutua, A. S. Perelson, A. Kumar, and N. K. Vaidya. Modeling the effects of morphine-altered virus specific antibody responses on hiv/siv dynamics. *Scientific Reports*, 9(1):5423, 2019.

[75] J. A. Myers, B. S. Curtis, and W. R. Curtis. Improving accuracy of cell and chromophore concentration measurements using optical density. *BMC Biophysics*, 6(1):4, 2013.

[76] A. V. Narla, J. Cremer, and T. Hwa. A traveling-wave solution for bacterial chemotaxis with growth. *Proceedings of the National Academy of Sciences*, 118(48):e2105138118, 2021.

[77] J. A. Nick, C. S. Chacon, S. J. Brayshaw, M. C. Jones, C. M. Barboa, C. G. St Clair, R. L. Young, D. P. Nichols, J. S. Janssen, G. A. Huitt, M. D. Iseman, C. L. Daley, J. L. Taylor-Cousar, F. J. Accurso, M. T. Saavedra, and M. K. Sontag. Effects of gender and age at diagnosis on disease progression in long-term survivors of cystic fibrosis. *Am J Respir Crit Care Med*, 182(5):614–26, 2010.

[78] F. Ou, C. McGoverin, S. Swift, and F. Vanholsbeeck. Near real-time enumeration of live and dead bacteria using a fibre-based spectroscopic device. *Sci Rep*, 9(1):4807, 2019.

[79] R. Pallett, L. J. Leslie, P. A. Lambert, I. Milic, A. Devitt, and L. J. Marshall. Anaerobiosis influences virulence properties of pseudomonas aeruginosa cystic fibrosis isolates and the interaction with staphylococcus aureus. *Scientific Reports*, 9(1):6748, 2019.

[80] L. Perko. *Differential equations and dynamical systems*. Springer-Verlag, 1991.

[81] G. Perpati, S. Nanas, E. Pouliou, V. Dionyssopoulou, E. Stefanatou, E. Armeniakou, A. Papamichalopoulos, and C. Roussos. Resting respiratory variables and exercise capacity in adult patients with cystic fibrosis. *Respiratory Medicine*, 104(10):1444–1449, 2010.

[82] N. Perry. Experimental validation of a critical domain size in reaction-diffusion systems with escherichia coli populations. *Journal of The Royal Society Interface*, 2(4):379–387, 2005.

[83] C. Pustelny, U. Komor, V. Pawar, A. Lorenz, A. Bielecka, A. Moter, B. Gocht, D. Eckweiler, M. Müsken, C. Grothe, H. Lünsdorf, S. Weiss, and S. Häussler. Contribution of veillonella parvula to pseudomonas aeruginosa-mediated pathogenicity in a murine tumor model system. *Infect Immun*, 83(1):417–29, 2015.

[84] R. Quinn, W. Comstock, T. Zhang, J. Morton, R. Silva, A. Tran, A. Aksenov, L. Nothias, D. Wangpraseurt, A. Melnik, G. Ackermann, D. Conrad, I. Klapper, R. Knight, and P. Dorrestein. Niche partitioning of a pathogenic microbiome driven by chemical gradients. *Science Advances*, 4:eaau1908, 2018.

[85] R. A. Quinn, S. Adem, R. H. Mills, W. Comstock, L. DeRight G., G. Humphrey, A. A. Aksenov, A. V. Melnik, R. da Silva, G. Ackermann, N. Bandeira, D. J. Gonzalez, D. Conrad, A. J. O'Donoghue, R. Knight, and P. C. Dorrestein. Neutrophilic proteolysis in the cystic fibrosis lung correlates with a pathogenic microbiome. *Microbiome*, 7(1):23, 2019.

[86] R. A. Quinn, Y. W. Lim, H. Maughan, D. Conrad, F. Rohwer, and K. L. Whiteson. Biogeochemical forces shape the composition and physiology of polymicrobial communities in the cystic fibrosis lung. *mBio*, 5(2):e00956–13, 2014.

[87] R. A. Quinn, K. Whiteson, Y. W. Lim, J. Zhao, D. Conrad, J. J. LiPuma, F. Rohwer, and S. Widder. Ecological networking of cystic fibrosis lung infections. *npj Biofilms and Microbiomes*, 2(1):4, 2016.

[88] R. A. Quinn, K. L. Whiteson, Y. W. Lim, P. Salamon, B. A. Bailey, S. Mienardi, S. E. Sanchez, D. Blake, D. J. Conrad, and F. Rohwer. A winogradsky-based culture system shows an association between microbial fermentation and cystic fibrosis exacerbation. *The ISME Journal*, 9:1024–1038, 2015.

[89] C. Rackauckas and Q. Nie. Differentialequations.jl – a performant and feature-rich ecosystem for solving differential equations in julia. *The Journal of Open Research Software*, 5, 2017.

[90] M. Rahman, K. Bekele-Maxwell, L. L. Cates, H. T. Banks, and N. K. Vaidya. Modeling zika virus transmission dynamics: Parameter estimates, disease characteristics, and prevention. *Scientific Reports*, 9(1):10575, 2019.

[91] K. Ren, Q. Wang, M. Hu, Y. Chen, R. Xing, J. You, M. Xu, X. Zhang, and Z. Rao. Research progress on the effect of autolysis to bacillus subtilis fermentation bioprocess. *Fermentation*, 8(12):685, 2022.

[92] T. E. Riedel, W. M. Berelson, K. H. Nealson, and S. E. Finkel. Oxygen consumption rates of bacteria under nutrient-limited conditions. *Applied and Environmental Microbiology*, 79(16):4921–4931, 2013.

[93] M. D. Rolfe, C. J. Rice, S. Lucchini, C. Pin, A. Thompson, A. D. S. Cameron, M. Alston, M. F. Stringer, R. P. Betts, J. Baranyi, M. W. Peck, and J. C. D. Hinton. Lag phase is a distinct growth phase that prepares bacteria for exponential growth and involves transient metal accumulation. *Journal of Bacteriology*, 194(3):686–701, 2012.

[94] A. Saltelli. Making best use of model evaluations to compute sensitivity indices. *Computer Physics Communications*, 145(2):280–297, 2002.

[95] E. J. Schwartz, K. R. Biggs, C. Bailes, K. A. Ferolito, and N. K. Vaidya. Hiv dynamics with immune responses: Perspectives from mathematical modeling. *Current Clinical Microbiology Reports*, 3:216–224, 2016.

[96] D. Sharma, L. Misba, and A. U. Khan. Antibiotics versus biofilm: an emerging battleground in microbial communities. *Antimicrobial Resistance & Infection Control*, 8(1):76, 2019.

[97] C. B. Silveira, A. G. Cobián-Güemes, C. Uranga, J. L. Baker, A. Edlund, F. Rohwer, and D. Conrad. Multi-omics study of keystone species in a cystic fibrosis microbiome. *International journal of molecular sciences*, 22(21):12050, 2021.

[98] M. Smieja. Current indications for the use of clindamycin: A critical review. *The Canadian journal of infectious diseases = Journal canadien des maladies infectieuses*, 9(1):22–28, 1998.

[99] I. M. Sobol. Global sensitivity indices for nonlinear mathematical models and their monte carlo estimates. *Mathematics and Computers in Simulation*, 55(1):271–280, 2001.

[100] A. M. Sousa and M. O. Pereira. Pseudomonas aeruginosa diversification during infection development in cystic fibrosis lungs—a review. *Pathogens*, 3(3):680–703, 2014.

[101] C. Spalding, E. Keen, D. J. Smith, A. M. Krachler, and S. Jabbari. Mathematical modeling of the antibiotic-induced morphological transition of pseudomonas aeruginosa. *PLoS Comput Biol*, 14(2):e1006012, 2018.

[102] K. Stevenson, A. F. McVey, I. B. N. Clark, P. S. Swain, and T. Pilizota. General calibration of microbial growth in microplate readers. *Scientific Reports*, 6(1):38828, 2016.

[103] F. A. Stressmann, G. B. Rogers, P. Marsh, A. K. Lilley, T. W. V. Daniels, M. P. Carroll, L. R. Hoffman, G. Jones, C. E. Allen, N. Patel, B. Forbes, A. Tuck, and K. D. Bruce. Does bacterial density in cystic fibrosis sputum increase prior to pulmonary exacerbation? *Journal of Cystic Fibrosis*, 10(5):357–365, 2011.

[104] X. Sun, A. K. Olivier, B. Liang, Y. Yi, H. Sui, T. I. Evans, Y. Zhang, W. Zhou, S. R. Tyler, J. T. Fisher, N. W. Keiser, X. Liu, Z. Yan, Y. Song, J. A. Goeken, J. M. Kinyon, D. Fligg, X. Wang, W. Xie, T. J. Lynch, P. M. Kaminsky, Z. A. Stewart, R. M. Pope, T. Frana, D. K. Meyerholz, K. Parekh, and J. F. Engelhardt. Lung phenotype of juvenile and adult cystic fibrosis transmembrane conductance regulator-knockout ferrets. *Am J Respir Cell Mol Biol*, 50(3):502–12, 2014.

[105] J. F. Sánchez-Pérez, M. Conesa, I. Alhama, F. Alhama, and M. Cánovas. Searching fundamental information in ordinary differential equations. nondimensionalization technique. *PLoS One*, 12(10):e0185477, 2017.

[106] J. F. Sánchez-Pérez, M. Conesa, I. Alhama, and M. Cánovas. Study of lotka–volterra biological or chemical oscillator problem using the normalization technique: Prediction of time and concentrations. *Mathematics*, 8(8):1324, 2020.

[107] J. L. Taylor-Cousar, M. A. Mall, B. W. Ramsey, E. F. McKone, E. Tullis, G. Marigowda, C. M. McKee, D. Waltz, S. M. Moskowitz, J. Savage, F. Xuan, and S. M. Rowe. Clinical development of triple-combination cftr modulators for cystic fibrosis patients with one or two f508del alleles. *ERJ Open Res*, 5(2), 2019.

[108] S. Trofimchuk and V. Volpert. Traveling waves in delayed reaction-diffusion equations in biology. *Mathematical Biosciences and Engineering*, 17(6):6487–6514, 2020.

[109] P. Uhl, J. Lowengrub, N. Komarova, and D. Wodarz. Spatial dynamics of feedback and feedforward regulation in cell lineages. *PLOS Computational Biology*, 18(5):e1010039, 2022.

[110] N. K. Vaidya, R. M. Ribeiro, A. S. Perelson, and A. Kumar. Modeling the effects of morphine on simian immunodeficiency virus dynamics. *PLoS Comput Biol*, 12(9):e1005127, 2016.

[111] N. K. Vaidya and L. M. Wahl. Avian influenza dynamics under periodic environmental conditions. *SIAM journal on applied mathematics*, 75(2):443–467, 2015.

[112] N. K. Vaidya and F.-B. Wang. Persistence of mosquito vector and dengue: Impact of seasonal and diurnal temperature variations. *Discrete & Continuous Dynamical Systems-B*, 2021.

[113] C. L. Ventola. The antibiotic resistance crisis: part 1: causes and threats. *P t*, 40(4):277–83, 2015.

[114] C. L. Ventola. The antibiotic resistance crisis: part 2: management strategies and new agents. *P t*, 40(5):344–52, 2015.

[115] V. E. Wagner and B. H. Iglewski. P. aeruginosa biofilms in cf infection. *Clinical Reviews in Allergy & Immunology*, 35(3):124–134, 2008.

[116] J. S. Webb, L. S. Thompson, S. James, T. Charlton, T. Tolker-Nielsen, B. Koch, M. Givskov, and S. Kjelleberg. Cell death in pseudomonas aeruginosa biofilm development. *J Bacteriol*, 185(15):4585–92, 2003.

[117] S. Wiggins. *Introduction to applied nonlinear dynamical systems and chaos*. Springer-Verlag, New York, NY, 1990.

[118] D. Wodarz. Computational modeling approaches to the dynamics of oncolytic viruses. *Wiley Interdiscip Rev Syst Biol Med*, 8(3):242–52, 2016.

[119] W. Yuan, Q. Chen, J. Qi, and Y. Li. The general traveling wave solutions of the fisher equation with degree three. *Advances in Mathematical Physics*, 2013:657918, 2013.

[120] S. Zarei, A. Mirtar, B. Andresen, and P. Salamon. Modeling the airflow in a lung with cystic fibrosis. *Journal of Non-Equilibrium Thermodynamics*, 38, 2013.

[121] S. Zarei, A. Mirtar, F. Rohwer, D. J. Conrad, R. J. Theilmann, and P. Salamon. Mucus distribution model in a lung with cystic fibrosis. *Computational and mathematical methods in medicine*, 2012:970809–970809, 2012.

[122] J. X. J. Zhang and K. Hoshino. *Chapter 5 - Optical transducers: Optical molecular sensing and spectroscopy*, pages 231–309. Academic Press, 2019.

[123] X. Y. Zhang, M. N. Trame, L. J. Lesko, and S. Schmidt. Sobol sensitivity analysis: A tool to guide the development and evaluation of systems pharmacology models. *CPT Pharmacometrics Syst Pharmacol*, 4(2):69–79, 2015.